NUTRIENT REGULATION OF AUTOPHAGY IN THE HEART

by

Purvi C. Trivedi

Submitted in partial fulfillment of requirements

for the degree of Master of Science

at

Dalhousie University

Halifax, Nova Scotia

August 2016

TABLE OF CONTENTS

LIST OF FIGURES

ABSTRACT

Impaired cardiac metabolism in the obese-diabetic heart leads to glucolipotoxicity and ensuing cardiomyopathy. Glucolipotoxicity causes cardiomyocyte injury by increasing energy insufficiency and by dysregulating proteolysis. Lysosomal signaling and function is governed by transcription factor EB (TFEB). However, limited studies have examined the impact of glucolipotoxicity on intra-lysosomal signaling proteins governing autophagy. Employing mouse models of diet-induced obesity, type-1 diabetes and ex-vivo model of glucolipotoxicity, we examined whether glucolipotoxicity negatively targets lysosomal proteins and TFEB to dysregulate autophagy and cause cardiac injury. Across *in-vivo* and *ex-vivo* glucolipotoxicity models, lysosomal autophagy was suppressed, which paralleled decreased cathepsin-B activity. Lysosome-associated membrane protein-2A (LAMP-2A), which is involved in chaperone-mediated autophagy (CMA), was reduced in obese-diabetic hearts and in glucolipotoxic *ex-vivo* models. Notably, diminished autophagy, induced by glucolipotoxicity, was highly associated with decreased CMA proteins content and cellular TFEB. Collectively, glucolipotoxicity renders cardiomyocytes susceptible to injury by depleting TFEB and impairing lysosomal proteolysis.

LIST OF ABBREVIATIONS USED

ACC, acetyl CoA carboxylase;

ACSL1, fatty acid acetyl CoA synthase;

AGE, advanced glycation end product;

AMPK, 5' AMP-activated protein kinase;

ARCM, adult rat cardiomyocyte;

ATG, autophagy related gene;

ATGL, adipose triglyceride lipase;

ATP, adenosine triphosphate;

bHLH, basic helix loop helix;

BMI, body mass index;

CD36, membrane of fatty acid translocase;

CHOP, CCAAT-enhancer-binding protein homologous protein;

CLEAR, coordinated lysosomal enhancement and regulation;

CMA, chaperone mediated autophagy;

CPT, carnitine palmitoyl transferase;

CQ, chloroquine;

CREB, cyclic AMP response element binding protein;

DAG, diacylglycerol;

eIF2α, eukaryotic translation initiation factor 2α;

ER, endoplasmic reticulum;

ERK1/2, extracellular receptor kinase 1/2;

ETC, electron transport chain;

FA, fatty acids;

FABP, fatty acid binding protein;

FAO, fatty acid oxidation;

FATP, fatty acid transport protein;

FXR, farnesoid X receptor;

GABARAP, GABAA receptor-associated protein;

GATE-16, golgi associated ATPase enhancer of 16kDa;

GFP, green fluorescent protein;

GLUT, glucose transporter;

GP, glucose/palmitate;

GPO, glucose/palmitate/oleate;

GS, glycogen synthase;

GSK, glycogen synthase kinase;

GTT, glucose tolerance test;

HBP, hexosamine biosynthetic pathway;

HDAC5, histone deacetylase 5;

HDL, high density lipoprotein;

HFHS, high fat high sucrose;

Hsc70, heat shock cognate protein 70;

HSL, hormone sensitive lipase;

Hsp90, heat shock protein 90;

InsR, insulin receptor;

IRS, insulin receptor substrate;

ITT, insulin tolerance test;

LAMP-1, lysosome associated membrane protein 1;

LAMP-2A, lysosome associated membrane protein 2A;

LC3B, microtubule associated protein light chain 3 subtype B;

LCFA, long-chain fatty acids;

LDL, low density lipoprotein;

LKB1, liver kinase B1;

LPL, lipoprotein lipase;

LSD, lysosomal storage disease;

LYNUS, lysosome nutrient sensing;

MCOLN1, mucolipin1;

MiTF, micropthalmia-associated transcription factor;

mRNA, messenger RNA;

MTCO1, mitochondrially encoded cytochrome C oxidase I;

mTOR, mammalian target of rapamycin;

NBR1, neighbour of BRCA1 gene;

NRCM, neonatal rat cardiomyocytes;

O, oleate;

P, palmitate;

PDH, pyruvate dehydrogenase;

PDHP, PDH phosphatase;

PDK, pyruvate dehydrogenase kinase;

PDK1, phosphoinositide-dependent kinase 1;

PE, phosphatidylethanolamine;

PGC1α, peroxisome proliferator-activated receptor gamma co-activator α;

PI3K, phosphoinositol-3-kinase;

PINK1, PTEN-induced putative kinase 1;

PIP2, phosphatidylinositol (4,5)-triphosphate;

PIP3, phosphatidylinositol (3,4,5)-triphosphate;

PKB, protein kinase B;

PP2B, protein phosphatase 2 B;

PPARα, peroxisome proliferator-activated receptor α;

PTP, protein tyrosine phosphatase;

RFP, red fluorescent protein;

RIP1, receptor interacting protein 1;

ROS, reactive oxygen species;

T1DM, type 1 diabetes mellitus;

T2DM, type 2 diabetes mellitus;

TAG, triacylglycerol;

TCA, tri carboxylic acid cycle;

TFE3, transcription factor E3;

TFEB, transcription factor EB;

TFEC, transcription factor EC;

ULK1/2, unc-51 like kinase 1/2;

UPS, ubiquitin proteasome system;

vATPase, vacuolar ATPase;

VLDL, very low density lipoprotein;

ACKNOWLEDGEMENTS

I take this opportunity to thank and regard the enormous support, encouragement and knowledge garnered from different minds during the course of this intensive training program. To begin with I would like to extend my deep sense of gratitude and respect to my research supervisor Dr. Thomas Pulinilkunnil. It has been a great privilege and honor to be mentored by Thomas especially for his meticulous thinking, constructive criticisms, perseverance and unflagging devotion towards research. As his first graduate student, he taught me the skills to pose significant research questions, achieve systematic solutions and helped me understand the philosophy of research. His painstaking efforts and untiring enthusiasm invested on me has yielded one full length manuscript and two book chapters out of this dissertation. I thank him for all the guidance, support, encouragement and friendship. I am also thankful to Dr. Petra Kienesberger for her patience, support and counsel in helping me move forward in my program.

I am also grateful to the members of my supervisory committee members Dr. T. Alexander Quinn and Dr. Aarnoud Van Der Spoel for their valuable suggestions and encouragement they provided me during the course of my academic and research training.

I sincerely acknowledge the friendship, support and encouragement of my colleagues from Pulinilkunnil and Kienesberger labs. Their intellect and brilliant presence provided a professionally stimulating atmosphere in the lab. I would also like to thank trainees and staff from Brunt and Reiman lab for their technical assistance and gracious collegiality during the course of my program. I also take pride in thanking DMNB, department of Biochemistry and Molecular Biology, Dalhousie University for providing an excellent graduate training program. I thank the faculty, technical and administrative staff for the help, support and encouragement during this program.

I would like to sincerely acknowledge the collaborative efforts of Drs. Jean Francois Legare, Ansar Hassan, Duncan Webster and Brian Rodrigues during the completion of this dissertation.

I would like to express my gratefulness to the Dalhousie Medicine New Brunswick for their graduate studentship support during my graduate program.

My special thanks to all my friends and well-wishers within and outside the faculty for their cheerful companionship and support.

Last but not the least, no words of esteem can suffice to express my love and appreciation for my loving parents. Without their moral, selfless support and sacrifice accomplishing my goal to acquire a MSC would have been impossible.

CHAPTER 1: INTRODUCTION

1.1. Obesity and Diabetes-related cardiomyopathy

Obesity is a worldwide phenomenon that is common among all age groups, sexes and cultures. Obesity is defined as a body mass index (BMI) higher than 30 and is further sub-divided into class 1 (BMI of 30-34.9), class 2 (BMI of 35-39.9) and class 3 (BMI ≥40) obesity (Muoio 2014, Twells, Gregory et al. 2014). Between the years of 1985 and 2011, the prevalence of obesity has increased in Canada from 6.1% to 18.3% (Twells, Gregory et al. 2014). Future projections are troubling; by 2019, it is estimated that more than half of all Canadians will be classified as overweight or obese and that the prevalence of obesity will be approximately 21-22% (Twells, Gregory et al. 2014). Obesity occurs due to positive energy imbalance, wherein nutrient and energy supply outweigh physiological demand and usage. During obesity excessive nutrient consumption leads to super-physiological levels of glucose and fatty acids which , renders cells insulin- resistant, leading to late-onset, type 2 diabetes mellitus (T2DM) (An and Rodrigues 2006). This form of chronic diabetes is a debilitating characterized by hyperglycemia, hyperlipidemia, and insulin resistance (Jaacks, Siegel et al. 2016). Numerous etiological factors that contribute to the onset of the T2DM and insulin resistance have been proposed including pancreatic beta cell dysfunction (Cerf 2013), increased inflammatory serum content (Kwak, Kim et al. 2016), and insulin signaling suppression through inflammation (Eguchi and Manabe 2014) and cell death pathways (Ghosh, An et al. 2004, Ghosh, Pulinilkunnil et al. 2005). Similarly, early-onset, type 1 diabetes mellitus (TIDM) is characterized by loss of pancreatic beta cell content and function, decreased insulin production and pancreatic release, and maladaptive fatty acid oxidation (Cnop, Welsh et al. 2005, Basu, Oudit et al. 2009). T1DM is insulin-dependent and is an autoimmune disease that appears to have a genetic basis (Pociot and Lernmark 2016). Obesity and diabetes are often comorbid with various types of diseases including osteoarthritis, gall bladder and gallstone disease, kidney failure, respiratory disorders, cancers such as pancreatic, colon and rectal cancers, and cardiovascular dysfunction (Must and McKeown 2000, Kolb, Sutterwala et al. 2016, Pepin, Timsit et al. 2016).

The primary cause of mortality in diabetics is cardiovascular disease (Hippisley-Cox and Coupland 2016). Despite glycemic control, diabetic patients exhibit left ventricular dysfunction that is commonly referred to as diabetic cardiomyopathy, which

occurs independently of vascular complications (An and Rodrigues 2006, Isfort, Stevens et al. 2014). Diabetic cardiomyopathy was first reported in 1972 by Rubler et al (Rubler, Dlugash et al. 1972). With increasing morbidity of both obesity and diabetes, the prevalence of diabetic cardiomyopathy has been significantly increasing worldwide over the last two decades (Miki, Yuda et al. 2013). The prevalence of diabetic cardiomyopathy is astoundingly high, with 40%-60% of diabetic patients exhibiting this disorder (Sharma and McNeill 2006). In fact, underdiagnoses of diabetic complications increases patient's susceptibility to heart failure by two-to-three fold compared to the general population. The prevalence and onset of cardiomyopathy was first convincingly demonstrated in the Framingham heart study (Kannel, Hjortland et al. 1974), STRONG (de Simone, Devereux et al. 2010) and SOLVD (Shindler, Kostis et al. 1996) clinical trials, and in genetic, dietary and pharmacological rodent models of obesity and diabetes (Asghar, Al-Sunni et al. 2009, Miki, Yuda et al. 2013). Although the etiology of type 1 and type 2 diabetes differs in many ways, increased risk of and pathological features of cardiomyopathy associated with both disorders are surprisingly similar (Boudina and Abel 2010). One of the early biochemical event that take place during diabetic cardiomyopathy include impaired cardiac energy metabolism, which has primarily been uncovered and studied in preclinical models (Bugger and Abel 2009). The pathological transformation of cardiac metabolism is followed by precipitation of pathological events such as left ventricular wall stiffness, deposition of collagen and impairment in calcium homeostasis (An and Rodrigues 2006). However, metabolic changes are underestimated due to rapidity of metabolic transformation, underdiagnoses and delayed detection in obese and diabetic humans showing signs of cardiomyopathy (Rodrigues, Cam et al. 1995). *Therefore, it stands to reason that reversal of altered cardiac substrate utilization or reversing the injurious effects of abnormal cardiac energy metabolism during obesity and diabetes will prevent the development of cardiomyopathy.* To achieve this goal, a thorough understanding of the mechanisms by which abnormalities in myocardial energy metabolism trigger disruptions in myocyte signaling and function is paramount.

1.2. Myocardial metabolism and function in health and disease

1.2.1. Cardiac metabolism

The heart is a striated and non-voluntary contractile muscle that maintains cellular health and function by delivering blood containing essential nutrients and oxygen to the body and receiving back cellular waste (Gavaghan 1998). Heart consists of several cell types including smooth muscle cells, endothelial cells, epicardial cells, fibroblasts, pacemaker cells, Purkinje fibres, and cardiomyocytes, all of which constitue the 'functional/contractile units' of the heart (Xin, Olson et al. 2013). The thick muscular walls of the myocardium comprising of cardiomyocytes that allow atrial and ventricular contraction (Miki, Yuda et al. 2013). The myocardium has a high demand for energy requiring continuous and incessant supply of 3.5 to 5 kg of ATP per day to maintain uninterrupted contraction (Randle 1980, Rodrigues, Cam et al. 1995). To achieve a high level of ATP production, the heart relies on multiple substrates such as fatty acids (FA), carbohydrate, amino acids and ketones, with FA and glucose being the principal fuels (Randle 1980).

In the healthy heart, long-chain FA (LCFA) are the preferred energy substrate accounts for approximately 60-70% of ATP production (An and Rodrigues 2006). Although FA is the most preferred substrate, the heart has a limited ability to synthesize this substrate and relies on continuous exogenous supply. FA can be made available to the heart from two systemic sources: 1) release from adipose tissue, bound to albumin and transport to the heart and 2) hydrolysis of triglyceride (TAG) rich lipoprotein to FA by the enzyme lipoprotein lipase (LPL) (An and Rodrigues 2006). Lipoprotein-derived FA enter cardiomyocytes by either passive diffusion or by protein-mediated transport, involving CD36 (member of fatty acid translocase), FA transport protein (FATP) and/or plasma membrane FA binding protein (FABP) **(Figure 1.1 A)** (An and Rodrigues 2006, Pulinilkunnil and Rodrigues 2006, Kienesberger, Pulinilkunnil et al. 2013). Once inside the cardiomyocyte, FA are esterified into fatty acyl-CoA via long chain fatty acyl-CoA synthase (ACSL1) in an ATP-dependent manner **(Figure 1.1 B)** (Mashek, Li et al. 2007). Fatty acyl-CoA is transported into mitochondrial matrix by an enzyme carnitine palmitoyl transferase (CPT) **(Figure 1.1 C)**. Within the mitochondrial matrix, fatty acyl-CoA molecules are progressively broken down by β-oxidation to liberate acetyl-CoA, which is

further metabolised into tri carboxylic acid cycle (TCA) to generate ATP **(Figure 1.1 D)** (Stanley, Recchia et al. 2005, An and Rodrigues 2006). The rate of β-oxidation is regulated by the intracellular levels of malonyl-CoA, which is synthesized from cytosolic acetyl-CoA via acetyl-CoA carboxylase (ACC), which is a potent inhibitor of CPT-1 **(Figure 1.1 E)** (Steinberg and Kemp 2009). Adenosine monophosphate activated protein kinase (AMPK), the "cellular fuel gauge", inhibits ACC activity and relieves ACC inhibition of CPT-1, thereby augmenting flux of long-chain fatty acyl CoA into β-oxidation **(Figure 1.1 F)** (Brownsey, Boone et al. 2006). Excess un-oxidized long-chain acyl CoA are incorporated into intracellular TAG, which can be hydrolyzed back to FA upon cellular requirement **(Figure 1.1 G)**. TAG hydrolysis represents a tightly regulated process and involves the concerted action of adipose triglyceride lipase (ATGL, producing diacylglyceral (DAG)), HSL (hormone sensitive lipase producing monoacylglycerol (MG)) and MGL (monoacylglycerol lipase producing FA) (Zechner, Kienesberger et al. 2009, Kienesberger, Pulinilkunnil et al. 2013).

In addition to FA, heart metabolizes approximately 25% of glucose and 15% of lactate, as well as smaller amounts of amino acids and ketones for ATP generation (Randle 1980). In an insulin-dependent process, glucose from the circulation is transported into the cardiomyocyte via glucose transporters (GLUTs), primarily through GLUT1 and GLUT4 isoforms, which are predominantly expressed in cardiac tissue **(Figure 1.1 H)**. (An and Rodrigues 2006). GLUT mediated glucose uptake could also be insulin-independent involving serine/threonine kinase, AMPK, which promote GLUT1 and GLUT4 translocation to sarcolemma (Samovski, Su et al. 2012). Once in the cytosolic compartment of sarcolemma, glucose is broken down to pyruvate via the process of glycolysis **(Figure 1.1 I)**. Pyruvate derived from glucose is transported into the mitochondria via monocarboxylate carrier **(Figure 1.1 J)**. Within the mitochondrial matrix, pyruvate is decarboxylated to acetyl-CoA through pyruvate dehydrogenase (PDH), a multienzyme complex **(Figure 1.1 K)**. PDH is regulated by either pyruvate dehydrogenase kinase (PDK) mediated inhibitory phosphorylation on the E1 subunit of PDH or by PDH phosphatase (PDHP) induced dephosphorylation of PDH leading to its activation **(Figure 1.1 L)**. Acetyl-CoA derived from pyruvate eventually enters the TCA cycle to undergo sequence of reactions to generate H_2O and CO_2 to synthesize ATP **(Figure 1.1 M)**. The flux of

acetyl-CoA into mitochondria derived from either glucose or FA acts as the nodal point for substrate metabolism as proposed by Randle (Randle 1980). During states of nutritional abundance, glucose utilization dominates, wherein pyruvate derived acetyl CoA is favored for oxidation by relieving the inhibition of PDH by PDK. However, negative feedback from high matrix acetyl-CoA concentrations stimulates PDK and reduces PDH activity. Indeed, in conditions where insulin levels are low such as during starvation, and during elevation in systemic and intramyocellular FA, PDK is activated, which inactivates PDH and inhibits glucose oxidation (Lee, Zhang et al. 2004), signifying the impact of insulin on substrate competition within the heart and the resultant remodeling of cardiac metabolism following loss of insulin or its action.

1.2.2. Loss of insulin or insulin action and metabolic inflexibility in the heart

Despite, FA is the most preferred energy substrate, heart exhibits extreme dependence on glucose consumption amounts 25-50 g in a 24 h period in humans (An and Rodrigues 2006). In the heart, insulin plays a very important role in metabolism, specifically, glucose transport, glycolysis, glucose oxidation, glycogen synthesis and protein synthesis. Circulating insulin binds to the insulin receptor (InsR) in the heart, which acts as a 'gate-keeper' of insulin-glucose communication between extra- and intra-cellular environments **(Figure 1.1 a)**. The insulin receptor is a hetero-tetrameric structure consisting of two extracellular α-subunits and two transmembrane β-subunits (Bertrand, Horman et al. 2008). The two β-subunits have tyrosine-kinase catalytic activity and facilitate an autophosphorylation cascade upon insulin binding on α-subunits (Bertrand, Horman et al. 2008). The β-subunit autophosphorylation results in phosphorylation of several tyrosine residues on one of the β-subunits **(Figure 1.1 b)** (Bertrand, Horman et al. 2008). The insulin signaling cascade is negatively regulated by protein tyrosine phosphatases (PTP) which dephosphorylate InsR **(Figure 1.1 c)**. Besides insulin receptor, downstream insulin signaling effectors also play an equally important role in governing cardiac metabolism and function. InsR activation following autophosphorylation leads to InsR mediated phosphorylation of two indispensable molecular targets: insulin-receptor substrate 1 & 2 (IRS-1/2) and Shc **(Figure 1.1 d)** (Bertrand, Horman et al. 2008). IRS-1 phosphorylation at several tyrosine residues induces IRS-1 activation. IRS activation leads to the association

of a subset of cellular proteins containing an SH2-domain including Grb2, Nck, and lipid kinase phosphoinositol-3-kinase (PI3K) (Frojdo, Vidal et al. 2009). Tyrosine phosphorylated residues on InsR and IRS-1 directly associates with PI3K's p85 subunit through this SH2-domain to mediate a wide array of cellular functions **(Figure 1.1 e)**. Recruitment of PI3K to the plasma membrane stimulates its catalytic phosphorylation of phosphatidylinositol (4,5)-diphosphate (PIP2) to phosphatidylinositol (3,4,5)-trisphosphate (PIP3) **(Figure 1.1 f)** (Frojdo, Vidal et al. 2009). Increases in PIP3 levels at the plasma membrane mediate further recruitment of protein kinase B (PKB)/Akt along with phosphoinositide-dependent kinase 1 (PDK1) **(Figure 1.1 g)** (Frojdo, Vidal et al. 2009). At the plasma membrane, PDK1 phosphorylates and activates Akt isoforms to further relay insulin's signal to downstream targets to facilitate glucose metabolism. Glucose entry into the cardiomyocyte is insulin dependent process, which is facilitated by GLUT1 and GLUT4. Prior studies on diabetic *db/db* mice and obese zucker rat have demonstrated that impaired insulin signaling reduced GLUT4 expression in the heart, leading to disruptions in glucose uptake and utilization, (Young, Guthrie et al. 2002, Carroll, Carley et al. 2005). Within the cardiomyocytes, glucose is further processed for storage as glycogen or is subjected to glycolysis and glucose oxidation for ATP generation. Insulin regulated glycogen synthesis is dependent on glycogen synthase enzyme, which is inactivated by glycogen synthase kinase α/β (GSK3α/β) through its inhibitory phosphorylation **(Figure 1.1 h)** (Shulman, Bloch et al. 1995). Insulin activates Akt which phosphorylates and inactivates GSK3α/β (Markou, Cullingford et al. 2008), retain glycogen synthase to be active, resulting in increased glycogen synthesis **(Figure 1.1 i)**. In addition to insulin's control over cardiac glycogen stores, insulin also promotes cardiac glycolysis. Indeed, reduced cardiac glycolysis due to impaired insulin signalling in the mouse heart resulted in hypertrophy, fibrosis and reduced cardiomyocyte function (Donthi, Ye et al. 2004). Furthermore, insulin augments glucose oxidation by inactivating PDK and activating PDHP and renders PDH active for facilitating conversion of pyruvate to acetyl-CoA.

In addition to insulin's effect on glucose metabolism, insulin is also an anti-lipolytic hormone, which inhibits FA metabolism by reducing FA entry into the cardiomyocytes. Exogenous FA importation is necessary to maintain optimal β-oxidative function which is

accomplished by concerted action of LPL and myocyte FA transporters (Yagyu, Chen et al. 2003). Insulin facilitates the "selectivity and usage" of substrates within the heart by inhibiting LPL activation and thereby promoting glucose utilization (Pulinilkunnil, An et al. 2004). Notably, cardiac specific knock-out of LPL switches the cardiac substrate selection preference to glucose (Augustus, Yagyu et al. 2004) signifying competing traits of different substrates. In the cardiac muscle, insulin can inhibit CPT-1 and subsequent FAO rates by increasing in expression of malonyl-CoA **(Figure 1.2 1)**. (Lopaschuk, Ussher et al. 2010). Indeed, in the absence of insulin action, FAs regulate cardiac function by transcriptional regulation of peroxisome proliferator-activated receptor α (PPARα), a nuclear receptor in the heart, which increases FA uptake, mitochondrial transport, and β-oxidation (Varga, Czimmerer et al. 2011). Overexpression of PPAR-α in mouse models have demonstrated an increase in FA uptake and oxidation and reduction in glucose utilization, producing a cardiac phenotype similar to a diabetic or an insulin-resistant heart (Finck, Han et al. 2003). Randle and his co-workers also demonstrated that excess FA supply in to the heart, impairs basal and insulin stimulated glucose uptake and oxidation, a pathway known as Randle cycle (Randle 1980).

Since insulin is central regulator of systemic and intracellular flux of glucose, FA and amino acids, any interruptions in insulin signaling leads to abnormal substrate utilization compromising the ability of heart to partition nutrients for metabolism. Insulin helps cardiomyocyte to maintain "metabolic flexibility", which is the ability of the heart to switch back and forth between glucose and FA to generate energy based on the demand and availability for contractile purposes (Larsen and Aasum 2008). However, during obesity and diabetes, lack of insulin or insulin action, triggers "metabolic inflexibility" which is the inability of cardiomyocyte to use glucose leading to an exclusive dependence on FA for energetic needs. Indeed, preclinical and clinical data have now confirmed that metabolic health deteriorates as mitochondria lose their capacity to switch freely between alternative forms of carbon energy (Muoio 2014). Chronic manifestation of this metabolic inflexibility is observed in the obese and diabetic heart independent of vascular complications, these include an imbalance in Ca^{2+} homeostasis, defects in contractility and increase in fibrosis. In addition to the above mentioned mechanisms, metabolic inflexibility

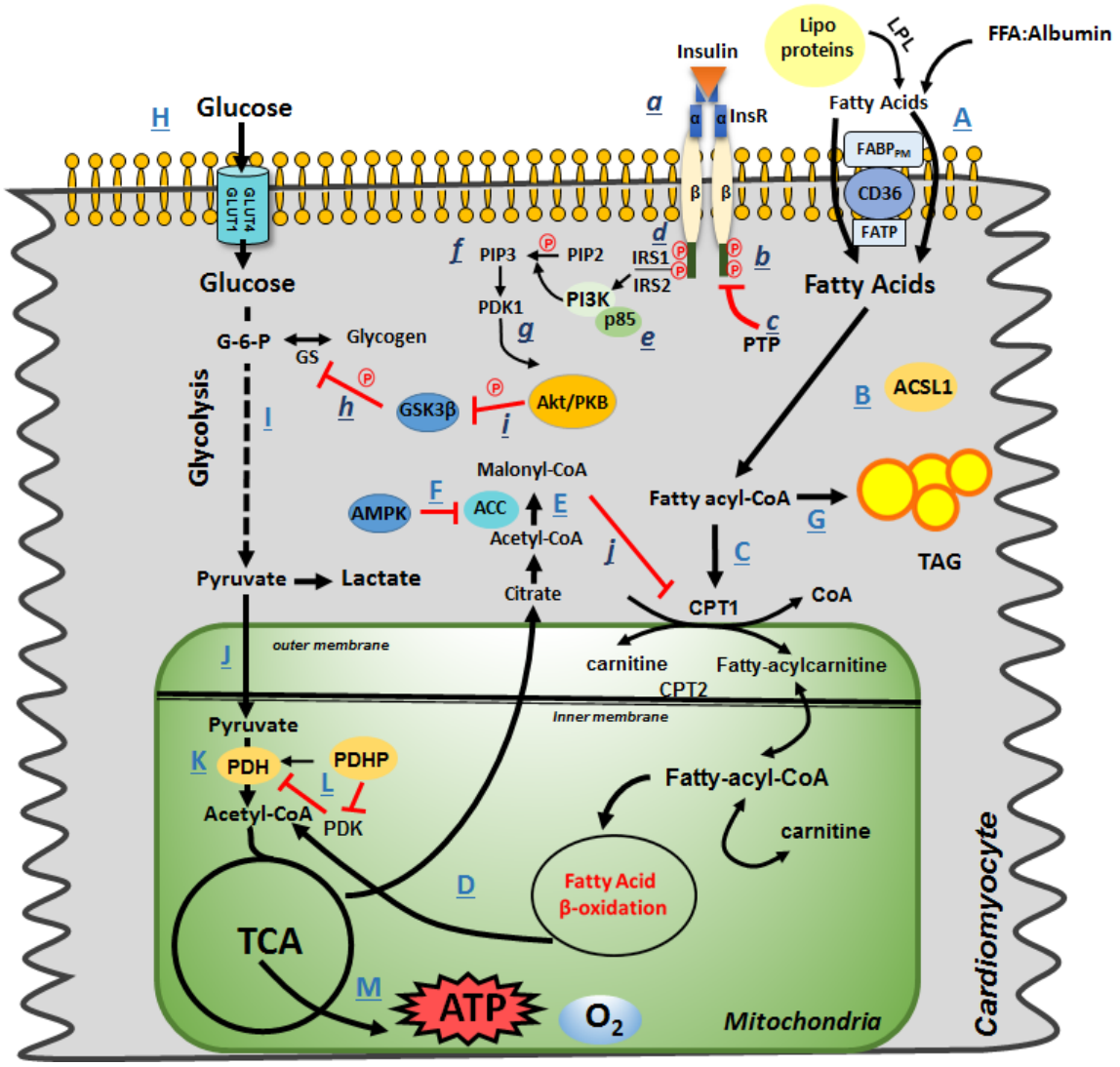

Figure 1.1. Role of insulin in regulating cardiac energy metabolism in healthy heart. Insulin regulates cardiac energy metabolism by activating metabolic pathways involving glucose and FA utilization. Insulin's binding to its transmembrane receptor initiates an intracellular autophosphorylation cascade that activates IRS-1 and promotes PI3K-phosphorylation of PIP2 to increase intracellular PIP3 concentrations. Increased PIP3 concentrations facilitates recruitment of PDK1 and Akt to the cardiomyocyte membrane whereby PDK1 phosphorylates Akt. GLUT4 facilitates transport of glucose through the cardiomyocyte sarcolemma. Insulin-induced GLUT4 translocation facilitates cellular glucose uptake and utilization. Intracellularly, glucose is processed to G-6-P that is either shunted into glycogen storage via glycogen synthase or processed further via glycolytic

pathway. The glycolytic end-product pyruvate is transported into the mitochondrial matrix and converted by PDH to form acetyl-CoA, which is processed via the TCA cycle to generate ATP. Within the mitochondria, citrate generated during the TCA cycle translocates into the cytosol to form acetyl-CoA that is further converted to malonyl-CoA by ACC action. The pumping ability of the heart requires uninterrupted ATP production that is garnered via reliance on fatty acid oxidation. LPL-derived FA enter into the myocardium via the concerted action of fatty acid translocase CD36 and FABP/FATP. Insulin inhibits FAO and directs the incorporation of fatty acids into TAG. Insulin increases malonyl-CoA levels which inhibits CPT-1 and the ensuing mitochondrial β-oxidation of FAs. Insulin limits the heart's reliance on fatty acid oxidation by augmenting glucose utilization rendering energetic homeostasis within the heart. Solid black arrow: indicate reaction is proceeding forward in a single-step; Dashed black arrow: indicate reaction is proceeding forward in multiple steps; Solid red line: indicate reaction is inhibited.

in the obese and diabetic heart results in underutilization of glucose and accumulation of FA metabolites leading to glucotoxicity and liptotoxicity together being referred to as glucolipotoxicity. Metabolic remodeling following glucolipotoxicity is manifested at the biochemical, structural and functional level in the cardiomyocyte that is hypothesized to be causative for inducing metabolic cardiomyopathy during obesity and diabetes.

1.2.3. Glucolipotoxicity and organelle stress

During obesity and diabetes, lack of insulin or insulin function impairs GLUT translocation leading to inadequate cardiac glucose transport, glucose oxidation, resulting in hyperglycemia **(Figure 1.2 A)**, which is a significant contributor to diabetic cardiomyopathy. Hyperglycemia in diabetic heart causes "glucotoxicity" by generating reactive oxygen species (ROS). Excess ROS also activates poly (ADP ribose) polymerase (PARP), which could divert glucose from glycolytic pathway into advanced glycation end product (AGE) formation, hexosamine biosynthetic pathway (HBP), polyol pathway and protein kinase C (PKC) activation, causing glucotoxic signalling cascade in obese-diabetic heart **(Figure 1.2 B)**; all of which could be ameliorated by normalizing levels of mitochondrial ROS (Wakasaki, Koya et al. 1997, Cai and Kang 2001, Du, Matsumura et al. 2003, An and Rodrigues 2006, Poornima, Parikh et al. 2006)

To maintain function in the diabetic heart, adaptive molecular events ensue to provide uninterrupted FA supply and oxidation. Enhanced lipolysis in adipose tissue and higher very low-density lipoprotein (VLDL) secretion from the liver dramatically increases systemic FA and lipoprotein TAG. This increase in systemic FA and TAG further enhances the uptake of FA by cardiomyocytes **(Figure 1.2 C)**, resulting in increase in the activity of TAG synthesizing enzymes and TAG accumulation, which is associated with lipotoxicity (Kienesberger, Pulinilkunnil et al. 2013). Elevated intracellular FA activates activate PPARα, which promotes the expression of genes involved in fatty acid oxidation (FAO) and concomitantly compromising glucose utilization during diabetes **(Figure 1.2 D)** (Lee and Kim 2015). Indeed cardiomyocyte-specific PPARα overexpressing mice, promote lipotoxicity and develop cardiac steatosis, systolic dysfunction and cardiomyopathy (Finck, Han et al. 2003). Accumulation of FA also enlarges the pool of intracellular FA derivatives, such as fatty acyl CoA **(Figure 1.2 E)**, ceramides, DAGs **(Figure 1.2 F)**, long chain acyl

CoAs and/or acylcarnitines **(Figure 1.2 G)** that are collectively referred to as "lipotoxic" intermediates (Brindley, Kok et al. 2010). Furthermore, uncontrolled FAO disrupts mitochondrial inner membrane, releases cytochrome *c*, leading to over production of reactive oxygen species (ROS) and mitochondrial dysfunction (Listenberger, Han et al. 2003).

Not only the amount of FA but also the type of FA has an influence on cardiac metabolism during health and disease (de Vries, Vork et al. 1997). In vivo, saturated (palmitate and stearate) and unsaturated (oleate and elaidate) FA are preferred substrates for oxidation to generate ATP due to their carbon chain length (de Vries, Vork et al. 1997). Prior studies on neonatal rat cardiomyocytes, have reported that saturated FA but not unsaturated FA, are lipotoxic to the cells (de Vries, Vork et al. 1997). Excess supply of palmitate are directed towards de novo ceramide synthesis, which eventually induces cell death in cardiomyocytes. Additionally, palmitate directly or indirectly interfere with insulin signaling via a variety of mechanisms including increased serine/threonine phosphorylation and decreased tyrosine phosphorylation of IRS1, impaired Akt phosphorylation and GLUT4 translocation to the sarcolemma **(Figure 1.2 H)** (An and Rodrigues 2006, van de Weijer, Schrauwen-Hinderling et al. 2011). On the other hand, unsaturated FA, oleate, serve to be protective against saturated FA-induced lipotoxicity. This protective effect of oleate against lipotoxicity was likely due to channelling palmitate in to the intracellular pool of TAG, suggesting that different FA exhibit different effects on cellular homeostasis. Indeed, palmitate-induced apoptosis in cardiomyocytes and pancreatic β cells was ameliorated when palmitate was co-supplemented with oleate (de Vries, Vork et al. 1997, Las, Serada et al. 2011).

In addition to mitochondrial dysfunction and cellular death, prior studies have also reported that palmitate-induced lipotoxicity causes alteration in endoplasmic reticulum (ER) membrane phospholipids resulting in ER swelling, compromising ER membrane structure and integrity (Borradaile, Han et al. 2006). Given the physical and functional interaction between mitochondria and the endoplasmic reticulum (ER), numerous studies have also examined the contribution of ER dysfunction towards diabetic cardiomyopathy (Yang, Zhao et al. 2015). Since the ER is the origin of secretory biosynthesis, luminal and transmembrane proteins, loss of ER function leads to an accumulation of misfolded or toxic

proteins a condition referred to as ER stress (Sano and Reed 2013). In response to stress, ER acutely activates unfolded protein response (UPR) to clear toxic protein accumulation (Groenendyk, Sreenivasaiah et al. 2010, Benbrook and Long 2012). Indeed dietary, pharmacological and genetic rodent models of diabetes and human diabetics exhibit up-regulation of unfolded protein response pathways in the heart (Liu and Dudley 2014). If the ER stress response pathway is inadequate and yields a terminally misfolded or irreparable protein, the protein binds to distinct chaperones depending on its localization and are retrogradely transported out of the ER and immediately subjected to proteasomal degradation or proteolysis (Benbrook and Long 2012). However, sustained ER stress results in insufficient proteasome function and can induce proteolysis by lysosomal autophagy (Benbrook and Long 2012). Therefore, it is plausible that if the pathway of lysosomal autophagy is incapable to overcome cellular stress, the accumulation of toxic protein aggregates results in "proteotoxicity". Furthermore, if proteotoxic stress continued, the pathway of cell death is triggered to destroy the cellular homeostasis. Indeed, clinical studies in obese and diabetic individuals, have reported elevated levels of circulating amylin protein results in amylin deposition in the heart. Accumulation of amylin oligomers lead to proteotoxic stress and apoptosis in many organs including heart, which was further associated with alteration of cardiomyocyte structure and function resulting in diabetic cardiomyopathy (Despa, Margulies et al. 2012). Therefore, it is plausible that cardiac glucolipotoxicity involve mitochondrial dysfunction, ROS overload, ER stress, and disruption in protein degradation leading to proteotoxicity, all of which contribute to the pathogenesis of cardiomyopathy observed in obesity and diabetes.

1.3. Protein degradation

Protein degradation is required for 1) protein recycling when amino acids are required for de novo protein synthesis; 2) quality control of incorrectly synthesized or misfolded proteins; 3) cellular defense by promoting proteolysis of invading pathogens; 4) cellular homeostasis wherein protein synthesis and degradation are precisely regulated in response to changes in physiological or pathological demand (Goldberg 2003). In the adult heart, protein degradation occurs through three different systems based on protein lifespan:

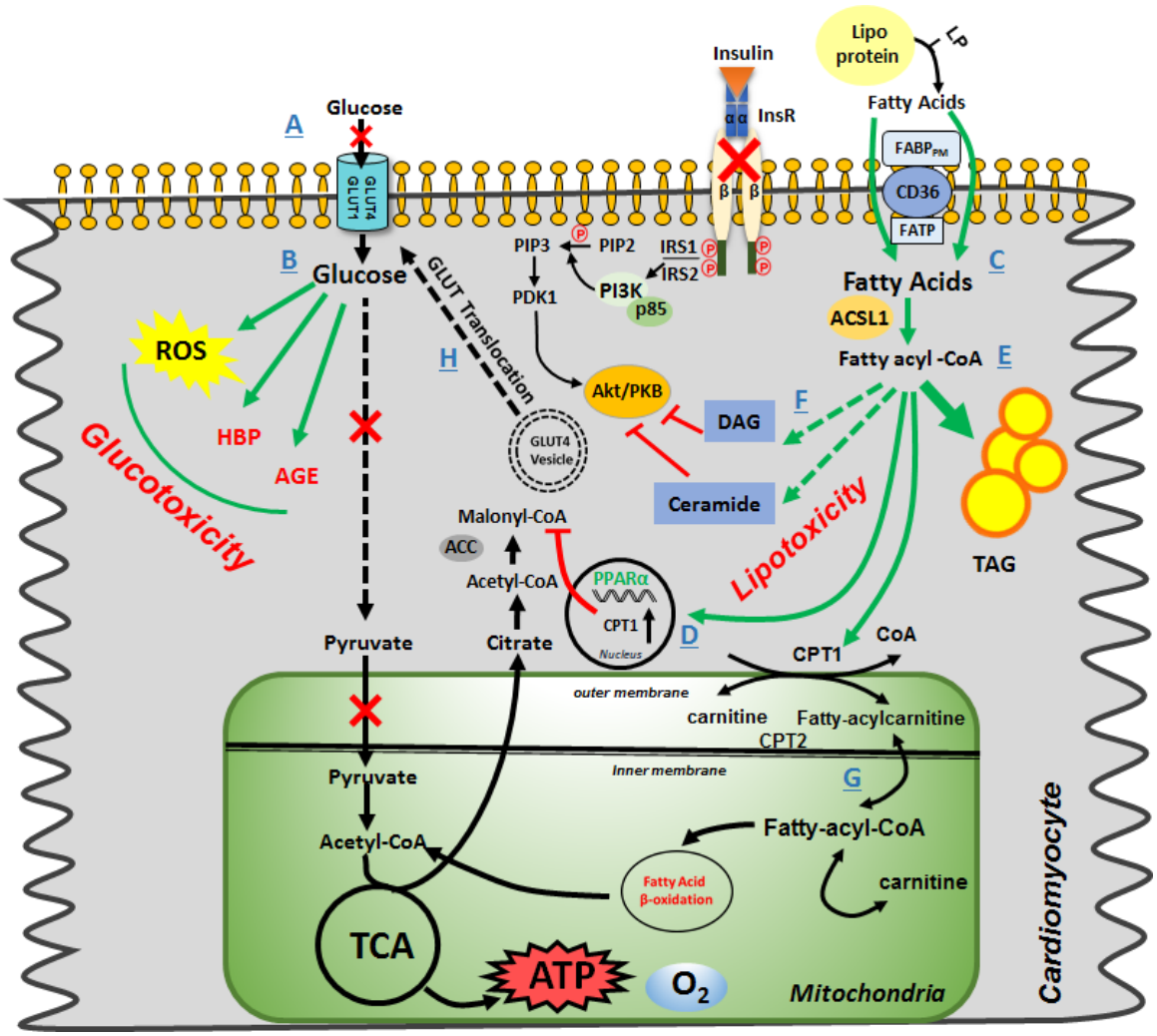

Figure 1.2: Altered cardiac energy metabolism and utilization in the obese and diabetic heart. During cardiac insulin resistance, impaired insulin signaling halts glycolytic flux redirecting glucose intermediates into the HBP. Decreased reliance on glucose is compensated by enhanced cardiac dependence on FAO via the Randle cycle. Intracellular FA is processed by ACSL1, generating intermediate fatty acyl-CoA that is further processed for mitochondrial β-oxidation pathway via CPT1 and CPT2 to generate ATP through TCA cycle. A part of the fatty acyl-CoA is stored as TAG and the remaining as lipotoxic intermediates; DAGs and ceramides. Following diabetes or diet-induced obesity, increased FA load within the cardiomyocyte activates PPARα which provokes further maladaptive use of β-oxidation pathway by increasing expression of CPT1, which depletes malonyl-CoA and releases its inhibition on FA oxidation. Additionally, the

lipotoxic DAGs and ceramides inhibit Akt function. Thus, when cardiac insulin signaling is dysfunctional, glucose oxidation is attenuated and fatty acid oxidation is augmented, leading to metabolic inflexibility within the cardiomyocyte and ensuing accumulation of lipotoxic intermediates. Solid black arrow: indicate reaction is proceeding forward in a single-step; Solid green arrow: indicate reaction is pathologically increased; Solid red line: indicate reaction is inhibited. Solid red X: indicates reaction is halted.

1) calcium-dependent calpain protease system (Patterson, Portbury et al. 2011); 2) ubiquitin proteasome system (UPS) (Pagan, Seto et al. 2013); and 3) more recently identified autophagy-lysosomal proteolytic pathway (Eskelinen and Saftig 2009, Guan, Mishra et al. 2014). The calpain protease system represents a small class of proteases known as calpains, along with regulatory calpain small subunit 1, also known as CAPN4 and endogenous regulatory inhibitor calpastatin. Calpains proteolytically cleave small individual proteins indiscriminate of amino acid sequence. Alternatively, the ubiquitin–proteasome system is a multi-subunit protease complex in the cytosol which is a major intracellular pathway for degradation of most if not all short lived proteins (Jung et al., 2008 and Wong and Cuervo, 2010). In this process substrate protein is covalently tagged with ubiquitin molecules via E1, E2 and E3 classes of ubiquitinating enzymes in response to a posttranslational modification (e.g., phosphorylation, sumoylation, chaperone binding). Subunits of the regulatory complex of the proteasome (26S proteasome) recognize the ubiquitin tag and degrade the protein (Powell, Herrmann et al. 2012). Recently, adaptive or causative changes in autophagic signaling pathways and impairment in lysosomal degradation of aggregated proteins have also been associated with ER stress, mitochondrial dysfunction, and cell death during myocardial ischemia reperfusion, atherosclerosis, aging and autoimmune disorders (Cuervo 2004, Czaja 2010, Choi, Ryter et al. 2013).

Lysosomes are single membrane acidic organelles containing luminal proteases, lipases, glycosidases, and nucleases that mediate complete breakdown of both intracellular and extracellular macromolecules (Singh and Cuervo 2011). Substrates are targeted to lysosomes for degradation via phagocytosis, endocytosis, and autophagy. Endocytosis results in endosomal degradation of plasma membrane-derived exogenous protein cargo following fusion of mature endosomes with a lysosome (Luzio, Gray et al. 2010). Autophagy (self-eating/digestion), is a proteolytic machinery resulting in degradation and clearance of both short- and long-lived proteins (Eskelinen and Saftig 2009), protein aggregates, midbody rings, mitochondria (mitophagy) (Jin and Youle 2012), nuclei (nucleophagy), endoplasmic reticulum (reticulopathy) (Nakatogawa and Mochida 2015), lipid droplets (lipophagy) (Singh and Cuervo 2012), and peroxisomes (pexophagy) (Oku and Sakai 2010) within the lysosomes to maintain energetic balance and organelle homeostasis. Two primary types of autophagy have been described in mammalian cells,

macroautophagy, and chaperone-mediated autophagy (CMA). A third, comparably less important type of autophagy does exist termed as microautophagy (MIA) which involves the pinocytosis of cytosolic regions surrounding lysosomes resulting in engulfment and degradation of cytosolic materials (Choi, Ryter et al. 2013).

1.3.1. Macroautophagy

Macroautophagy involves the partially-selective bulk sequestration of proteotoxic load within an ER-derived double membrane-bound organelle known as an autophagosome (Tanida 2011), which allows delivery of protein and organelle cargo to lysosomes for proteolysis. Macroautophagy is classically described in four steps: initiation, nucleation, elongation and maturation, and fusion with a lysosome (Singh and Cuervo 2011, Appelqvist, Waster et al. 2013). The process of macroautophagy is under the direct control of autophagy related gene (Atg) proteins, which form functional complexes that mediate individual steps of autophagy. Earlier studies on yeast have uncovered approximately 30 of these Atg proteins that organize and regulate various steps of autophagy (Mizushima, Levine et al. 2008, Mizushima 2009, Singh and Cuervo 2011, Tanida 2011, Yamada and Singh 2012). Under conditions of nutrient excess, insulin activates serine/threonine kinase mTOR (mammalian target of rapamycin) (Jung et al. 2009) phosphorylates and inactivates Unc-51-like kinase-1 and -2 (ULK) the initiator of autophagy (**Figure 1.3. A**) (Jung, Jun et al. 2009). However, following nutritional deprivation, inactivation of mTOR relives inhibition of ULK to associate with and activate Atg13 and FIP200 (focal adhesion kinase family-interacting protein of 200 kDa) leading to the induction of autophagy (Jung, Jun et al. 2009). Furthermore, increased AMP:ATP ratio, signifying nutritional depletion, activates AMPK via liver kinase B1 (LKB1)-mediated phosphorylation at threonine 172, allowing AMPK to phosphorylate and activate ULK1 at serine 777 and inhibit mTOR by phosphorylation at serine 2446 (**Figure 1.3. B**) (Alers, Loffler et al. 2012). Induction of autophagy starts with the formation of ER-associated omegasome leading to de novo synthesis of isolation membrane (preautophagosome or phagophore) (**Figure 1.3. C**) (Tanida 2011). This process requires induction complex comprising of Beclin 1 (Atg6 in yeast), and vacuolar sorting protein 34 (Vps34)-Vps15 which when activated by class III phosphatidylinositol-3-kinase (PI3K) gets co-ordinately mobilized to isolation membrane

(**Figure 1.3. D**) (Singh and Cuervo 2011, Tanida 2011, Yamada and Singh 2012, Shen and Mizushima 2014). Following the formation of the isolation membrane, it elongates to engulf cytoplasmic components by recruiting two parallel ubiquitin-like conjugation cascades involving the microtubule associated protein 1 light chain 3 (LC3) or Atg8 and the Atg7 mediated Atg5/Atg12/Atg16 complex formation. In mammals, Atg12-Atg5 conjugate interacts with Atg16L1 to form multimeric complex of Atg12-Atg5-Atg16L1, which localizes to the outer membrane of preautophagosomal structure (Tanida 2011). Furthermore, Atg12-Atg5-Atg16L1 is essential for Atg8/LC3 conjugation and formation, maturation and closure of the isolation membrane to form a mature autophagosome. Four mammalian Atg8 homologs have been described; microtubule-associated protein 1 light chain 3 (LC3/MAP1), GABAA receptor-associated protein (GABARAP) and golgi-associated ATPase enhancer of 16kDa (GATE-16) (Singh and Cuervo 2011, Tanida 2011). LC3, GABARAP and GATE-16 are ubiquitin-like proteins with LC3 being the most characterised functional homolog of yeast Atg8. LC3 is synthesized as proLC3, which is cleaved by cysteine protease Atg4B to form LC3I, thus exposing its C terminal glycine residue. LC3I is then activated by Atg7 (an E1 like enzyme), transferred to Atg3 (an E2 like enzyme) and eventually conjugated to phosphatidylethanolamine (PE) to form LC3-PE conjugation, also referred to as LC3II (**Figure 1.3. E**). LC3I is primarily localized in the cytosol whereas LC3II is localized to both cytosolic side (outer) and inner membrane of autophagosome (Tanida 2011). LC3II on the cytosolic side of autophagosome is de-lipidated by Atg4B to form LC3I which is recycled to be used again in autophagosomal formation. Therefore, Atg4B acts as de-conjugating enzyme and aid in regulating free LC3 levels. LC3II is primarily localized to the autophagosomal membrane is essential for maturation of autophagosome and therefore, used as an index of autophagosomal content. Additionally, adaptor proteins such as ubiquitin-binding protein p62 (also known as sequestosome 1) and NBR1 (Neighbor of BRCA1 gene) are recruited to the developing autophagosomal membrane through an LC3-interaction binding domain, enabling partial selectivity of the autophagic process (**Figure 1.3. F**) (Yamada and Singh 2012). Upon completion and closure, the mature autophagosome eventually fuses with a lysosome to form an autolysosome (**Figure 1.3. G**). Since autophagosomes lacks proteases for degrading engulfed content, autolysosomal formation is required for degradation of protein

cargo. Following autolysosome formation, the lysosomal hydrolases degrade LC3-II and the intra-autophagosomal contents (Mindell 2012, Shen and Mizushima 2014). The dynamic kinetics of autophagosome production and clearance by lysosomes is known as autophagic flux (Barth, Glick et al. 2010, Yang, Carra et al. 2013).

Lipophagy involves autophagosomal targeting of lipid droplets, allowing cardiomyocytes to release and modulate usage of fatty acid reservoirs. Degradation of lipid droplets releases free triglycerides that are utilized for mitochondrial β-oxidation (Czaja 2010, Singh and Cuervo 2012, Settembre and Ballabio 2014). Lipophagy was first described in hepatocytes and was shown to be indispensable for regulating TAG storage as Atg7 -/- mice were found to harbor vast accumulations of hepatic TG. Lipid droplets are recognized by autophagosomes through LC3-mediated detection. TG accumulation during fatty liver disease has also been found to be associated with robust downregulation of Atg7 expression (**Figure 1.3. H**) (Yang, Li et al. 2010).

In addition to lipophagy, mitophagic functioning is a critical process in cells that contain vast numbers of mitochondria, such as cardiomyocytes (Tong and Sadoshima 2016). Mitophagy ensures mitochondrial quality control by pruning the myocyte environment of dysfunctional mitochondria and promoting production of functional ATP-producing mitochondria. Mitochondrial redox reactions generate ROS, which (Moyzis, Sadoshima et al. 2015)indispensably relies on adequate mitophagic activity, allowing cells to expunge ROS load. Dysfunctional mitochondria that are unable to handle ROS overload are targeted for mitophagy by a PTEN-induced putative kinase 1 (PINK1)-Parkin mediated mechanism (Moyzis, Sadoshima et al. 2015, Saito and Sadoshima 2015). Specifically, PINK1 protein content is increased on the mitochondrial outer membrane, which signals Parkin-mediated ubiquitination of PINK1 molecules **(Figure 1.3. I)**. Ubiquitinated PINK1 molecules are then targeted by ubiquitin cargo receptors p62/SQSTM1 and NBR1 (Moyzis, Sadoshima et al. 2015). Autophagy function is also crucial during organismal development, which is highlighted by the fact that autophagy is acutely upregulated shortly after birth, when nutrient supply from the placenta ceases (Kuma, Hatano et al. 2004). Mice lacking Atg5, critical for autophagosomal formation, die within 12 h of birth. Due to compromised autophagy in these mice, the amino acid levels start decreasing immediately after the birth, underscoring the importance of autophagy as a source of amino acids and energy at the

time of nutrient deprivation (Kuma, Hatano et al. 2004, Mizushima 2009). Autophagy also plays an important role in maintaining cellular protein quality control. Depending on the cellular condition, there is a continuous protein turnover within the cell (Lecker, Goldberg et al. 2006, Mizushima and Klionsky 2007) that is proteins are being broken down in to amino acids and re-synthesized into proteins.

1.3.2. Chaperone mediated autophagy

Physiological activation of autophagy is initiated approximately 30 min into the starvation and does not last more than 8–10 hr. However, CMA begins after 10 h of starvation and unlike macroautophagy, CMA promotes individual and selective degradation of the protein (Kaushik and Cuervo 2012, Kaushik and Cuervo 2012). The concept of macroautophagy has been investigated over the last few years in different tissues and diseases, with major focus being to elucidate the signaling pathways surrounding the formation of autophagosome, autophagolysosomes, and fusion of autophagosomes to lysosomes. However, limited studies have examined inter and- intra-lysosomal events that govern cargo protein binding, uptake, translocation and degradation within the lysosomal matrix, specifically those mediated by CMA (Kaushik and Cuervo 2012, Kaushik and Cuervo 2012). Furthermore, very little is known about whether metabolic changes influence these lysosomal CMA processes in the heart and cause progressive deterioration of mitochondrial and contractile function in a setting of insulin resistance and diabetes.

CMA is a highly organized and selective process for degrading ~ 35% of soluble cytosolic proteins (Kon and Cuervo 2010) harboring a consensus KFERQ motif in their amino acid sequence, that targets them for recognition and lysosomal degradation (Dice, 1990). Cytosolic chaperone, the heat-shock cognate protein of 70 kDa (hsc70, distinct from hsp70, but belongs to the same family) recognizes the KFERQ motif and using ATP delivers protein cargo to the lysosomal surface. Following lysosomal targeting, substrate-Hsc70 complex binds to a CMA receptor, lysosome-associated membrane protein-type2A (LAMP-2A) **(Figure 1.3. J)** (Cuervo and Dice, 1996). LAMP-2A is the only receptor capable of binding to and translocating proteins, and undergo multimerization, a characteristic absent in other LAMP isoforms (Saftig, Schroder et al. 2010, Kaushik and Cuervo 2012). Notably, protein cargo binding to LAMP-2A and hence the lysosomal

membrane content of LAMP-2A correlates stringently with CMA activation. Binding of the targeted protein-chaperone complex to monomeric LAMP-2A promotes its multimeric assembly into high molecular weight complexes at the lysosomal membrane that is a prerequisite for substrate translocation into the lysosomal lumen (Kaushik and Cuervo 2012). Following which the substrate protein is unfolded, and then translocated across the lysosomal membrane in an ATP-dependent manner, to be rapidly degraded by a mixture of lysosomal proteases (Agarraberes et al., 1997). Impairment in multimerization of LAMP-2A prohibits substrate translocation. Following the substrate transport into the lysosomal lumen, LAMP-2A translocation complex disintegrates. The lysosomal degradation of membrane LAMP-2A involves its protease specific truncation and subsequent degradation in the lysosomal matrix which is inhibited in the presence of substrates for CMA (Kaushik and Cuervo 2012). Furthermore, intra-lysosomal hsc70 (lys-hsc70) is also required for protein translocation through LAMP-2A and disassembly of LAMP-2A from its multimeric complex (Kaushik and Cuervo 2012). Indeed, levels of LAMP-2A at the lysosomal membrane are tightly regulated and directly correlate with CMA activity (Cuervo and Dice, 2000). Uptake of proteins that are targeted for degradation also promotes redistribution of LAMP-2A from the matrix into the lysosomal membrane. Thus LAMP-2A levels at the lysosomal membrane is primarily regulated by alterations in its half-life and its redistribution between the lysosomal membrane and the lysosomal matrix. However recent studies also demonstrated that LAMP protein could be recycled by increases in lysosomal number also termed as lysosomal biogenesis which is transcriptionally regulated by the basic helix-loop-helix-leucine zipper (bHLH-LZ) transcription factor EB (TFEB) (Sardiello et al., 2009) that positively regulate genes part of coordinated lysosomal expression and regulation (CLEAR) network. Given that the proteins undergoing degradation through CMA exhibit diverse role in a myriad of intracellular processes, it is plausible that changes in LAMP-2A function and lysosomal biogenesis could have significant impact on CMA degradation of these proteins and significantly impact cellular metabolism and function.

1.4. The Lysosome: Cellular garbage can or a therapeutically targetable organelle?

Lysosomes are single membrane-bound organelles that are formed and ultimately derived from the Golgi apparatus. Lysosomes were first discovered in 1955 by Belgian biologist Christian de Duve by electron microscopic analysis (De Duve 1958). First deemed as the cell's "suicide bags" and eventually the cell's "garbage can", recent discoveries in lysosomal physiology, functioning and the critical involvement of lysosomes in cellular homeostasis, have revolutionized the lysosome research paradigm (Appelqvist, Waster et al. 2013). Furthermore, continued discoveries and characterizations of lysosomal storage diseases (LSD) have highlighted the critical involvement of lysosomes in maintaining cellular health and have garnered increased interest in lysosomes as therapeutic targets. At present, approximately 50 types of lysosomal storage diseases have been described, each of which involve genetic mutations in proteins involved in lysosomal functioning and/or degradation (Platt, Boland et al. 2012).

Lysosomes contain large numbers of transmembrane and membrane-bound proteins that regulate and maintain lysosomal physiology and function (Xu and Ren 2015). Lysosomal membrane is mainly composed of the lysosome-associated membrane glycoproteins, LAMP-1 and LAMP-2 respectively (Cuervo and Dice 2000, Eskelinen, Illert et al. 2002, Appelqvist, Waster et al. 2013). LAMP-1 and LAMP-2 consist of a short carboxyl terminal region containing a lysosomal membrane-targeting signal facing the cytosolic side, one transmembrane domain and a heavily glycosylated domain facing the matrix. LAMP-1 is the most abundant lysosomal membrane protein (~50%) that helps maintain lysosomal membrane integrity and is used as an index of lysosomal content (Eskelinen 2006) **(Figure. 1.3. K)**. LAMP-1 deficiency induces a very subtle phenotype in mice, however global deletion or loss of function mutation of LAMP-2 in mice and humans (genetic condition known as Danon disease) results in autophagosome and glycogen accumulation (Nishino, Fu et al. 2000, Stypmann, Janssen et al. 2006).

The ability of lysosomes to clear proteotoxic load is contingent on sufficient lysosomal functioning. Lysosomes are acidified by proton transportation across the lysosomal membrane to the lumen through the vacuolar ATPase (vATPase) proton pump **(Figure. 1.3. L)** (Xu and Ren 2015). The inner lysosomal membrane is lined with a carbohydrate-protein complex known as the glycocalyx, which protects the lysosomal membrane from

the acidic lumen (Settembre, Fraldi et al. 2013). The lysosomal lumen is maintained at a pH of 4.5, which is required for optimal protease functioning. At least 60 different proteolytic enzymes are known to reside within the lysosome (Appelqvist, Waster et al. 2013, Settembre, Fraldi et al. 2013) **(Figure. 1.3 M)**. An important class of proteases, known as cathepsins, are essential for autophagic clearance of proteotoxic cargo. Approximately a dozen cathepsins have been characterized in mammalian cells, each of which enzymatically cleave specific residues on targeted protein waste. There are nearly eleven members of the cathepsin family, out of which chathepsin B, L and S are known to be expressed in the heart (Cheng, Shi et al. 2012). Cathepsin function is undoubtedly reliant on the acidic lysosomal lumen. Lysosomal proteolytic activity is transcriptionally regulated by master regulator of lysosome biogenesis and function, TFEB (Sardiello, Palmieri et al. 2009).

1.5. Transcriptional regulation of autophagy and lysosomal function

In recent decades, several key proteins have been identified as critical transcriptional effectors and inhibitors of autophagy function. Particular transcription factors have been shown to be key regulators of specific proteins in the autophagy process such as FOXO3a being a regulator of LC3 and Nrf2 being a regulator of p62 (Jiang, Harder et al. 2015). Other transcription factors which has been implicated in autophagy regulation include hypoxia inducible factor-1α (HIF-1 α) and p53, which induce the expression of various genes involved in lysosomal autophagy (Bellot, Garcia-Medina et al. 2009, Obacz, Pastorekova et al. 2013). Most importantly, two major transcription factor families have been found to be critically involved in regulating a network of proteins indispensable for autophagic functioning; the zing finger family DNA-binding protein ZKSCAN3 (Chauhan, Goodwin et al. 2013), as the major repressor of lysosomal and autophagic functioning, and micropthalmia-associated transcription factor (MiTF) superfamily comprised of TFEB and TFE3, as the major activator and regulator of genes critical for autophagosomal and lysosomal functioning and biogenesis (Martina, Chen et al. 2012). ZKSCAN3 has been found to be a negative regulator of lysosomal autophagy, biogenesis and function and was found to be sensitive to nutrient status. Particularly, nutrient deprivation has been found to result in ZKSCAN3 cytoplasmic accumulation, leading to inhibition of activity, whereas

nutrient availability promotes mTOR-dependent nuclear translocation of ZKSCAN3, allowing ZKSCAN3 inhibition over autophagy (Chauhan, Goodwin et al. 2013). However, MiTF superfamily of transcription factors, particularly TFEB, has been implicated and characterized to be the most important transcriptional influence over autophagy and lysosomal functioning (Martina, Diab et al. 2014).

TFEB, is a master transcriptional regulator of proteins involved in autophagosomal assembly, autophagosomal maturation, autophagosome-lysosome fusion, and lysosomal biogenesis and function (Settembre, Di Malta et al. 2011). TFEB is a member of the MiTF, which also includes MiTF, TFE3 and TFEC. TFEB is a bHLH transcription factor with E-box binding elements that was first identified in 1990 by Carr and Sharp (Carr and Sharp 1990). However, TFEB was not fully described until 2009 when (Ballabio's group) Sardiello et al. elegantly characterized TFEB's ability and capacity to regulate cellular degradation processes, particularly those involving autophagy and lysosomal proteolysis. Sardiello et al. characterized an intricate genetic network, entitled CLEAR network, that involved the regulations of 471 gene targets that contained CLEAR promoter elements, allowing cells to rapidly regulate these targets at the same time (Sardiello, Palmieri et al. 2009, Palmieri, Impey et al. 2011, Settembre, Fraldi et al. 2013). CLEAR promoter elements are repetitions of ten base pair motif (GTCACGTGAC) located within the first 200 base pair of many lysosomal genes. CLEAR elements forms a type of E Box (CANNTG), which is recognized by TFEB and/or other bHLH/LZ family members. TFEB-signaling not only generates more autophagosomes, but also accelerates their delivery to lysosomes by increasing lysosomal number, thereby facilitating protein degradation (Settembre, Fraldi et al. 2013).

TFEB activity is nutritionally regulated. During conditions of nutrient surplus, intra-lysosomal amino acid content is retained within the lysosomal lumen, resulting in increased amino acid concentration and activating the lysosomal membrane protein ragulator in a vATPase-dependent manner (Mony, Benjamin et al. 2016) **(Figure. 1.3. N)**. Intra-lysosomal amino acid and other nutrient content are sensed by various lysosomal membrane proteins, such as vATPase, Ragulator, RagA/B, RagC/D, vATPase, lysosome Na ATP, mTOR and DEP domain-containing mTOR-interacting protein (DEPTOR), which are critical components of an intricate nutrient monitoring system known as the

lysosome nutrient sensing (LYNUS) machinery **(Figure. 1.3. O)** (Settembre, Fraldi et al. 2013, Mony, Benjamin et al. 2016). Activation of ragulator induces its guanine nucleotide exchange factor activity, loading Rag isoforms A, B, C, and D with GTP. GTP loaded Rag A and B form heterodimer complexes with isoforms C and D (RagA/B-C/D), which promote mTOR and TFEB localization and tethering to the lysosomal membrane (Settembre, Zoncu et al. 2012) **(Figure. 1.3 P)**. Lysosomal membrane bound mTOR stimulates inhibitory phosphorylation of TFEB at serine residues 142 and 211 (Settembre, Zoncu et al. 2012, Settembre, Fraldi et al. 2013). Additionally, extracellular receptor kinase (ERK), a mitogen activated protein kinase (MAPK), is activated during nutritional replete conditions and also negatively targets TFEB by phosphorylation at serine residue 142 **(Figure. 1.3. P)** (Settembre, Zoncu et al. 2012). Furthermore, the serine/threonine kinase receptor interacting protein 1 (RIP1) is also known to inhibit TFEB through its ability to upregulate ERK and ERK-mediated phosphorylation of TFEB at serine 142 (Yonekawa, Gamez et al. 2015). TFEB phosphorylation at serine 142 and 211 promotes binding to YWHA (14-3-3) cytosolic adaptor proteins, which restrict TFEB mobilization to the nucleus and retain TFEB to the cytosolic compartment. 14-3-3 proteins retain TFEB to the cytosol by masking TFEB's nuclear localization sequence (Martina, Chen et al. 2012, Yonekawa, Gamez et al. 2015).

However, during nutrient deplete conditions, intra-lysosomal amino acid reservoirs are mobilized and translocated to the cytosol through lysosomal amino acid transporters such as member of the solute carrier family 38 (SLC38), for utilization as energy substrates in mitochondrial oxidative pathways (Rebsamen, Pochini et al. 2015). Decreasing lysosomal concentrations of amino acids leads to inactivation of ragulator and associated Rag proteins, which triggers the dislodging of mTOR and TFEB from the lysosomal membrane. Furthermore, low levels of intra-lysosomal nutrients elicit release of calcium through lysosomal calcium transporter mucolipin 1, which activates the phosphatase calcineurin (protein phosphatase 2b) (Medina, Di Paola et al. 2015) **(Figure 1.3 Q)**. Calcineurin activation is essential for dephosphorylation and activation of TFEB. Recently, it has been reported that not only lysosomal nutrient levels, but also ROS overload can induce lysosomal calcium release and activate TFEB in a calcineurin-dependent manner. Upon dephosphorylation, TFEB is released from cytosolic containment and migrates into the

nucleus through nuclear transporters importin 7 and 8 **(Figure. 1.3 R)** (Raben and Puertollano 2016). Upon nuclear entry, TFEB binds to CLEAR promoter sequences of various genes involved in autophagosomal and lysosomal function such as UVRAG, WIPI, MAP1LC3B, SQSTM1, VPS11, VPS18, Atg9B and vATPase. (Sardiello, Palmieri et al. 2009, Shen and Mizushima 2014). TFEB-mediated action ultimately dictates autophagosomal assembly and degradation and lysosomal biosynthesis and function by directly regulating proteins involved in lysosomal acidification and autophagy.

Nuclear TFEB activity is dependent on heterodimeric interactions with other MiTF family members, specifically TFE3. The functions of TFEB and TFE3 appear to be redundant as both TFEB and TFE3 regulate proteins involved in autophagy and lysosomal functioning by activating the CLEAR network (Raben and Puertollano 2016). However, TFEB and TFE3 are distinguished in many types of disease states, including cancer and autoimmune disorders (Raben and Puertollano 2016). Nuclear TFEB is also potently inhibited by histone deacetylase 5 (HDAC5), through binding and inhibition of TFEB's transcription. However, PKD1 phosphorylation of HDAC5 induces HDAC5 nuclear export, which relieves HDAC5-mediated inhibition on TFEB, allowing TFEB to activate the CLEAR network (Du Bois, Pablo Tortola et al. 2015).

In a recent ground-breaking paper, TFEB was found to not only be regulated by phosphorylation, but also by acetylation at lysine residue 116, acting analogously to phosphorylation by confining TFEB to the cytosol (Bao, Zheng et al. 2016). Interestingly, TFEB was also found to be activated through deacetylation by sirtuin 1 (SIRT1), promoting nuclear TFEB intrusion **(Figure. 1.3 S)**. Notably, a myriad of studies have shown that the stilbenoid phenol resveratrol is cardio-protective under numerous conditions, and it has been found that this cardio-protection is mediated through resveratrol's ability to potently upregulate SIRT1 activity, which is now known to facilitate TFEB activity (Bao, Zheng et al. 2016). TFEB also ensures its own inactivation through transcriptionally regulating folliculin. Folliculin is a lysosomal membrane-tethered protein that functions to rapidly reactivate mTOR and inactivate TFEB upon restoring cellular nutrients (Petit, Roczniak-Ferguson et al. 2013). Thus, TFEB not only promotes autophagosomal and lysosomal processes, but also ensures that these processes are rapidly inactivated during fed states. TFEB expression is regulated by transcriptional effectors through the recently described

FXR/CREB transcription axis **(Figure. 1.3 T)** (Sardiello 2016). During states of fasting, the transcription factor c-AMP response element binding (CREB) protein becomes activated and moves to the nucleus to regulate various proteins involved in autophagy including ULK1 and TFEB. However, during fed states, the protein farnesoid X receptor (FXR) becomes active and potently antagonizes CREB transcriptional activities, suppressing general autophagic functioning (Sardiello 2016). Post-transcriptionally, TFEB mRNA is regulated by micro-RNA 128, which targets TFEB mRNA for Argonaut-mediated degradation (Decressac, Mattsson et al. 2013). Furthermore, it has also been recently found that TFEB regulates peroxisome proliferator-activated receptor gamma coactivator (PGC1α), a master regulator of mitochondrial biogenesis. Interestingly, PGC-1α is known to activate TFEB, modulating TFEB expression and action. Surprisingly, it has been discovered that TFEB can transcriptionally regulate its own genetic expression (*Tfeb*), since it houses a CLEAR promoter region as well (Sardiello 2016).

1.6. Role of TFEB in diseases

Recently, a plethora of research has reported that dysregulation of TFEB activity accompanies various pathologies including obesity (Guan, Mishra et al. 2014), insulin resistance, fatty liver disease, and ischemia-reperfusion injury. The extent of ischemia-reperfusion injury was shown to be sensitive to TFEB action as viral overexpression of TFEB in NRCMs protected against hypoxia-induced BNIP3 cell death (Ma, Liu et al. 2015). It has also been elegantly demonstrated that TFEB is highly suppressed during amyloidogenic heart failure and that restoring TFEB activity protects against cardiac injury and improves contractility (Guan, Mishra et al. 2014). In this study, authors thoroughly examined TFEB in zebrafish, mice and human hearts following amyloid deposition and found that forced viral overexpression improved cardiac outcomes in zebrafish and mice hearts. Indeed, lysosomal dysfunction during ischemia and lipid loading is associated with abnormalities in TFEB function (Godar, Ma et al. 2015). Despite these findings it remains to be investigated if glucolipotoxicity during obesity and diabetes induces lysosomal stress by negatively targeting TFEB to suppress autophagy causing proteotoxicity and cardiomyopathy.

1.7. Summary and rationale

Heart is a metabolically demanding organ due to its uninterrupted contractility, which requires a constant supply of energy to maintain its function. High energy demand to generate ATP is primarily derived from two important substrates, glucose and FA oxidation. Depending on the energy demand and substrate availability, heart is highly flexible in switch over between glucose and FA to generate energy. However, in certain pathological outcomes such as during obesity and diabetes, insulin deficiency or insulin resistance results in loss of metabolic flexibility leading to FA over-utilization, whereas glucose remains unused. FA over-utilization and loss of glucose utilization resulting in glucotoxicity and lipotoxicity, together referred to as "glucolipotoxicity". Furthermore, glucolipotoxicity in the obese and diabetic heart, causes mitochondrial dysfunction and ER stress. Loss of insulin level and function, triggers uncontrolled proteolysis within the ER, leading to impairment in protein quality control machinery. The defect in ER protein quality control machinery, results in accumulation of misfolded proteins, which if not subjected to timely protein degradation process generates ROS and cell death. Indeed, functional defects in diabetic muscle, liver and islets are strongly associated with impaired ubiquitin-mediated proteasomal degradation leading to cytotoxic protein aggregation termed as "proteotoxicity" (Balasubramanyam, Sampathkumar et al. 2005, Costes, Huang et al. 2011, Willis and Patterson 2013). Interestingly, significant accumulation of amylin proteins were observed in lipid-laden failing hearts of obese patients, which exacerbated with diabetes (Despa, Margulies et al. 2012). Therefore, it is plausible that glucolipotoxicity induces proteotoxic stress predisposing the obese and diabetic heart to failure. Physiological reduction of proteotoxic load can be relieved by proteolysis via lysosomal autophagy. At baseline, lysosomal autophagy is upregulated for constantly removing of damaged or misfolded proteins and also damaged organelles to maintain protein quality control. Whereas, under nutrient deprived condition or during stress, autophagy acts as a guard by providing substrate essential for energy production to maintain cellular homeostasis. Macroautophagy and CMA, are the two most described autophagy in mammals. Role of macroautophagy has been characterized in most of the cardiac pathologies such as ischemia/reperfusion injury, hypertension and cardiomyopathy. However, precise role of macroautophagy in cardiac adaptation to nutrient overload during

obesity and diabetes is not known. Current data on role of macroautophagy in maintaining cardiac function have reported inconsistency in different models of obesity and diabetes. This inconsistency in data could be due to the absence of data on the molecular mechanisms regulating lysosome signaling, biogenesis and function in the obese and diabetic heart. In addition, role of CMA in regulating cardiac autophagy during obesity and diabetes is not known. Notably, humans and mice with loss of function of LAMP-2 showed impaired autophagosome clearance, lysosomal dysfunction, and cardiomyopathy, suggesting that lysosomal CMA is critical for cardiac function. Expression of numerous lysosomal proteins responsible for autophagic processes are under the direct control of TFEB, a transcriptional regulator of lysosome autophagy and biogenesis. TFEB-action not only generates autophagosomes, but also accelerates their delivery and clearance by lysosomes via increases in lysosomal biogenesis (Sardiello, Palmieri et al. 2009, Settembre, Di Malta et al. 2011). It is plausible that changes in lysosome function and biogenesis could significantly impact cellular function in the setting of obesity, insulin resistance and diabetes, however, limited studies have examined impact of glucolipotoxicity on TFEB and its downstream functions.

In this study we examined the hypothesis that glucolipotoxicity negatively targets TFEB, a transcriptional regulator of lysosome function, to impair autophagy thereby rendering cardiomyocyte susceptible to proteotoxicity and cell death. This hypothesis will be examined by systematically addressing the four specific aims listed below:

1. To characterize and validate the ex-vivo glucolipotoxicity model by utilizing H9C2 cardiomyoblast, neonatal rat cardiomyocytes (NRCM) and adult rat cardiomyocytes (ARCM) and examine the effect of glucolipotoxicity on cell death and lipid utilization pathways.
2. In ex-vivo models, examine the effect of glucolipotoxicity on proteins involved in macroautophagy, CMA and that regulating lysosome function such as TFEB.
3. To recapitulate the ex-vivo data, in mouse model of diet induced obesity (DIO) and type-1 diabetes (Akita mice).
4. To examine the status of lysosome content, signaling and proteolytic activity in the cardiomyocyte using both in-vivo mouse model and ex-vivo models of glucolipotoxicity.

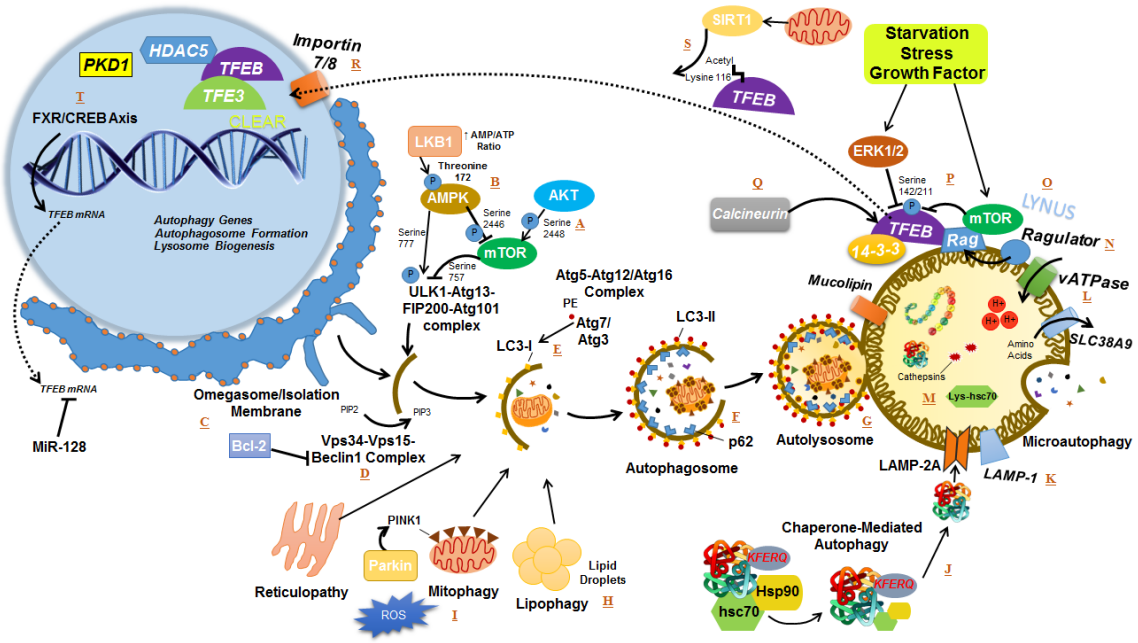

Figure 1.3. Physiological regulation of autophagic recycling of proteins and organelles ensures myocyte homeostasis. Macroautophagy initiation occurs by de novo synthesis of a preautophagosome from the ER with the aid of ULK1-Atg13-Fip200-Atg101 protein complex. During nutrient deprivation, ULK1 is activated by AMPK-mediated phosphorylation at serine 777, but during nutritional surplus, ULK1 is inhibited by mTOR-mediated phosphorylation at serine 757. Macroautophagy is propagated forward by Beclin1-Vps34-Vps15 protein complex, which has PI3K catalytic activity, but is suppressed by Bcl-2 binding to Beclin1. Recruitment and PE lipidation of LC3B on the developing autophagosomal membrane promotes autophagosomal maturation, elongation and closure. Cargo receptor P62 mediates autophagosomal targeting of proteotoxic and organelle load. Autophagosomes fuses with a lysosome to form an autolysosome, where proteolysis occurs. Lysosomal membrane vATPase ensures acidification of the lysosomal lumen for proper functioning of proteases such as cathepsin B. CMA targets intracellular KFERQ-proteins utilizing Hsc70-Hsp90 chaperone complex. Targeted protein cargo is transported to the lysosomal lumen through LAMP2A. LAMP1 is the most abundant lysosomal membrane protein and is important for lysosomal integrity. Microautophagy involves sequestration of protein and cytosol by lysosomal membrane invagination. LYNUS machinery senses intra-lysosomal amino acid content and relays nutritional status to Rag isoforms, which bind to mTOR and TFEB during nutrient deprivation. ERK- and

mTOR-mediated phosphorylation of TFEB at serine residues 142 and 211 retain TFEB to the cytosol. Calcineurin dephosphorylation and SIRT1 deacetylation of TFEB promote TFEB nuclear transport through importin 7/8, allowing TFEB/TFE3 activation of CLEAR genes to regulate lysosomal biogenesis and function.

CHAPTER 2: EXPERIMENTAL METHODS

2.1. Animal models

All protocols involving rodents were approved by the Dalhousie University, Institutional Animal Care and Use Committee (Protocol # 14-077).

2.1.1. Diet-induced obesity

Male C57BL/6J mice were procured from the Jackson laboratory (stock numbers: 000664). Mice were housed on a 12 h light and 12 h dark cycle with ad libitum access to water and chow diet (5001; Lab diet, St Louis, MO, USA; with 13.5 kcal% from fat) or high-fat high-sucrose (HFHS) diet (12451; Research Diets, New Brunswick, NJ, USA; with 45kcal% from fat and 17 kcal% from sucrose). Nine to ten weeks old male mice were randomly assigned to cohorts fed either chow or HFHS diet for 16 weeks. Body weight gain was recorded weekly by calculating the difference in body weight before starting the diet and every week after starting the diet. The weight gain was recorded every week for 16 weeks. After 16 weeks, mice were injected three times with either saline or chloroquine (CQ, C6628; Sigma) for the last 48 h (30 mg/kg), 24 h (30 mg/kg) and 2 h (50 mg/kg) prior to euthanasia to assess autophagic flux (Jaishy, Zhang et al. 2015). All the mice were subjected to one hour food withdrawal before euthanasia. Tissues were collected and stored at - 80°C for further analysis.

2.1.2. Akita mice

Male C57BL/6J wild-type (WT; *Ins2*$^{WT/WT}$) and type 1 diabetic Akita (*Ins2*$^{WT/C96Y}$) mice were purchased from Jackson Laboratory (stock numbers: WT, 000664; *Ins2*$^{WT/C96Y}$, 003548). Akita mice exhibit mutation in insulin 2 (*Ins2*) gene wherein cysteine 96 residue at 7th amino acid of A chain is replace by tyrosine (C96Y) resulting in the misfolding of mutant insulin protein. Ins2 gene mutation on the C57BL/6J mice background, have resulted in the progressive loss of β cell density and function, leading to severe hyperglycemia at 4 weeks of age. Akita mice were housed on a 12 h light and12 h dark cycle with ad libitum access to chow diet (5001; Lab diet, St Louis, MO, USA; with 13.5 kcal% from fat) and water. Body weight was recorded every week. After 12 weeks, mice

were euthanized after 12 h of overnight fasting and tissues were collected and stored at -80°C for further analysis.

2.1.3. Glucose tolerance test

Glucose tolerance was assessed in 15 h fasted non-anesthetized mice following intraperitoneal (i.p.) administration of 20% D-glucose in saline at 2 g per kg of body weight. Blood glucose was measured at 0, 15, 30, 60 and 120 min after glucose administration using Accu-Check Aviva glucometers (Roche, Basel, CH).

2.1.4. Insulin tolerance test

Systemic insulin tolerance was assessed in 5 h-fasted non-anesthetized mice following intraperitoneal (i.p.) administration of human insulin (Novo Nordisk, Bagsvaerd, DK) at 0.8 units/kg body weight. Blood glucose was measured at 0, 15, 30, 60, 90 and 120 min after insulin administration using Accu-Check Aviva glucometers (Roche, Basel, CH).

2.1.5. Tissue homogenization

Frozen heart was powdered using pestle and mortar, followed by homogenization using polytron homogenizer in ice-cold buffer containing 20 mM Tris-HCl, pH 7.4, 5 mM EDTA, 10 mM $Na_4P_2O_7$ (567540; Calbiochem, EMD Chemicals, Gibbstown, NJ, USA), 100 mM NaF, 1% Nonidet P-40, 2 mM Na_3VO_4, 10 µl/ml of protease inhibitor (P8340, Sigma, St Louis, MO, USA; contains AEBSF - [4-(2-Aminoethyl)benzenesulfonyl fluoride hydrochloride], aprotinin, bestatin hydrochloride, E-64 – [N-(trans-Epoxysuccinyl)-L-leucine-4-guanidinobutylamide], leupeptin hemisulfate salf and pepstatin A) and 10 µl/ml of phosphatase inhibitor (524628, Calbiochem; contains bromotetramisole oxalate, cantharidin and calyculin A, *Discodermia calyx*). Homogenate was centrifuged at 1000 x *g* for 10 min at 4℃ to obtain a '1000 x *g* pellet" which is composed of nuclear membrane proteins. The supernatant was then transferred to another microfuge tube and centrifuged at 20,000 x *g* for 20 min at 4℃. The resulting pellet after 20,000 x *g* centrifugation was resuspended using 1X extraction buffer (LYSISO1; Lysosome isolation kit; Sigma) and referred to as '20,000 x *g* pellet' composed of membrane proteins from lysosome, mitochondria, peroxisome and endoplasmic reticulum. The supernatant obtained after

20,000 x *g* centrifugation, consist of soluble proteins in the cytosolic compartment. The 1000 x *g* pellet was sonicated using nucleus extraction buffer containing 1 mM EGTA, 1 mM EDTA, 10 mM HEPES, 1.25 g glycerol, 412 mM NaCl, 1.5 mM $MgCl_2$, 1mM DTT (0281; Amresco, OH, USA), protease inhibitor (P8340, Sigma, St Louis, MO, USA; 10 µl/ml) and phosphatase inhibitor (524628, Calbiochem, EMD Chemicals, Gibbstown, NJ, USA; 20 µg/ml) and pH was adjusted to 7.5. The obtained lysate was then centrifuged at 10,000 x *g* for 10 min at 4℃ and supernatant (consisting of nuclear membrane proteins) was collected in a microfuge tube. Protein concentrations were determined using the BCA protein assay kit (23255; Pierce, Thermo Fisher Scientific, Waltham, MA, USA) and protein concentration from nuclear membrane was determined using Bradford protein assay reagent (500205; Quick Start Bradford Dye Reagent, BioRad, Mississauga, Ontario, Canada). Lysates were stored at -80℃ for subsequent biochemical analysis.

2.2. Immunoblot analysis

Heart lysates were subjected to sodium dodecyl sulfate-polyacrylamide (SDS) gel electrophoresis and proteins were transferred onto a nitrocellulose membrane. Blotted proteins were visualized using reversible Coomassie stain (24580; MemCode Reversible protein Stain, Pierce, Thermo Fisher Scientific, Waltham, MA, USA) and targets probed using the primary antibodies: anti-LC3B (2775S; Cell Signaling, Beverly, MA, USA), anti-LAMP-2A (18528; Abcam, Toronto, ON, Canada), anti-Cleaved Caspase-3 (9664; Cell Signaling), anti-pmTOR Ser^{2448} (2971; Cell Signaling), anti-TFEB (A303-673a-T; Bethyl Labs), anti-mTOR (2972; Cell Signaling), anti-pP70S6K Thr^{389} (9234; Cell Signaling), anti-P70S6K (9202; Cell Signaling), anti-Hsp90 (ADI-SPA-830-D; Enzolife), anti-p62 (03-GP62-C; American Research Products, Belmont, MA, USA), anti-pS6 $Ser^{240/244}$ (2215; Cell Signaling), anti-Hsc70 (AB2788; Abcam, Toronto, ON, Canada), anti-pTFEB Ser^{142} (GIFT from Dr. Gerard Karsenty, Columbia University), anti-ATGL (2138; Cell Signaling), anti-Beclin (3495; Cell Signaling), anti-Pan Actin (sc-1616; Santa Cruz Biotechnology, TX, USA), anti-Pan Calcineurin (2614; Cell Signaling), anti-MTCO1 (14705; abcam), anti-AMPKα (SC-1913; Santa Cruz), anti-AMPKα Thr^{172} (2531; Cell Signaling) and anti-CHOP (SC-7351; Santa Cruz Biotechnology, TX, USA). Immunoblots were developed using the Western Lightning Plus-ECL enhance chemiluminescence substrate (Perkin

Elmer, Waltham, MA). Densitometric analysis was performed using Image lab software (Bio-Rad) and protein levels were corrected to protein stain.

2.3. Cathepsin B activity assay

Cathepsin B is a lysosomal cysteine proteinase enzyme which hydrolyzes proteins and cleave at the carboxyl side of Arg-Arg bonds in small molecule substrates. The substrate N-Suc-Leu-Leu-Val-Tyr-7-AMC (S6510; Sigma, MA, USA) was used for the fluorometric detection of cathepsin B activity. The fluorescence of the free aminomethyl coumarin released was measured. Cathepsin B activity was measured in tissue or cellular lysates. Standard curve was prepared in the range of 300 nM to 12.5 nM using 7-Amino-4-Methylcoumarin (26093-31-2; Enzo, Alfa Aesar). Briefly, standards, samples and cathepsin B enzyme (BML-SE198-0025; Enzo life sciences, NY, USA) were added into96 well plate. Following addition of standards, samples and cathepsin B, activation buffer L-Cysteine (prepared in a buffer containing 352 mM potassium phosphate monobasic, 48 mM sodium phosphate dibasic and 4.0 mM EDTA at 40° C, pH 6.0) was added to get the final concentration of 8.0 mM. The volume of each well was made up to 150 µl by adding 0.1% of Brij 35 solution (0281; Amresco, OH, USA, 0.1% V/V of 30% w/v Brij solution in water). Lastly, the fluorogenic substrate at a final concentration of 0.006 mM was added into the sample and control wells and the plate was mixed immediately using thermo mixture. Intensity of fluorescence was measured in triplicate at the excitation wavelength of 360 nm and the emission wavelength of 440 nm at 0 min time point. The plate was then incubated at 37°C and fluorescence was measured again at the 60 min time point. Data are presented as RFU/min/µg of proteins.

2.4. Cell Culture

2.4.1. H9C2 cardiomyoblast culture

H9C2 rat embryonic cardiomyoblast (CRL-1446; ATCC) cells were cultured at a cell density of 4 $x10^5$ in 60 mm plates and maintained in Dulbecco's modified Eagle's high-glucose medium (SH30243.01; DMEM-HG; Hyclone Laboratories, UT, USA) supplemented with 10% fetal bovine serum (1400-500; FBS, Seradigm) for 48 hr. H9C2 cardiomyoblasts were allowed to differentiate for 48 hr in DMEM-1X medium (11966025;

Thermo Fisher Scientific, MA, USA) supplemented with 0.5% FBS and 5 mM glucose. After 48 hr of differentiation, cells were exposed to either low or high concentrations of different substrates as mentioned in section 2.4.5. Cells were then harvested in phosphate-buffered saline (0780; Amresco), followed by centrifugation at 10,000g for 10 min at 4˚C to pellet down the cells. Cell pellets were sonicated using lysis buffer (composition as described in tissue homogenization section), followed by centrifugation at 1500 x *g* for 10 min at 4˚C. Supernatant was transferred to another microfuge tube and protein concentrations were determined using the BCA protein assay kit (23255; Pierce, Thermo Fisher Scientific, Waltham, MA, USA). Lysates were stored at -80˚C for subsequent analysis.

2.4.2. Neonatal rat ventricular cardiomyocyte isolation

Neonatal rat ventricular cardiomyocytes (NRCMs) were isolated from 2 day old Sprague-Dawley rat pups. Briefly, hearts were excised to collect the ventricles and RBC and atria were removed to collect the ventricles. Ventricles were then minced in to small pieces and thoroughly washed with ice cold 1X PBS. Minced ventricles then digested repeatedly using proteolytic enzymes collagenase- type 2 (2% W/V), DNase (0.5% W/V) and trypsin (2% W/V) (Worthington Biochemical Corporation) with gentle stirring to dissociate tissues into single cells. Following digestion, cells were collected and centrifuged to obtain a cell pellet. The cell pellet after the digestion was then re-suspended using plating media which composed of DMEM/F12 HAM (D6421; Sigma), 10% FBS, 15 % horse serum, 1% penicillin-streptomycin (30-002-CI, Corning, NY, USA) and 50 µg/ml gentamycin (30-005-CR; Corning) and subjected to differential plating for 2 h to eliminate non-cardiomyocytes. Supernatant from differential plating containing cardiomyocytes was collected and suspended in growth medium containing DMEM/F12 HAM (D6421; Sigma), 10% FBS, 10 µM cytosine-β-D-arabinofuranoside (C1768; ARAC, Sigma), Insulin-Transferrin-Selenium (25800-CR, ITS, Corning), 1% penicillin-streptomycin (30-002-CI, Corning, NY, USA) and 50 µg/ml gentamycin (30-005-CR; Corning) and plated at a density of 5 x10^4 using 35 mm primaria cell culture plates. The following day, cells were washed in DMEM 1X media and cultured in serum-free DMEM-1X medium containing 10 µM ARAC, 50 µg/ml gentamycin, 1% penicillin-streptomycin and 10 mM glucose for

24 h. After 24 h, cells were treated with low and high concentrations of different substrates as described in section 2.4.5.

2.4.3. Adult rat cardiomyocyte isolation

Adult rat cardiomyocytes (ARCM) were isolated from hearts of adult Sprague dawley rats. Rats were anaesthetized using sodium pentobarbital at 65 mg/kg. Heart was isolated and immersed in cold Tyrode buffer containing 11.69 mM NaCl, 1.49 mM KCl, 0.33 mM KH_2PO_4, 1.206 mM $MgSO_4$, 12.51 mM taurine, 3.604 mM dextrose, 4.766 mM HEPES and 0.396 mM L-carnitine at pH 7.4 in 5% CO_2-95% air at 37℃. Following excision, the heart was perfused via the aorta in a retrograde manner by the Langendorff technique. Heart was subjected to collagenase (60 mg collagenase, 25 µM $CaCl_2$ in 75 ml Tyrode buffer) digestion using a recirculating mode for 30 min. Thereafter, the heart was taken out from the perfusion system, ventricles were cut off and minced into small pieces. The minced ventricles were made calcium tolerant by exposing the cells to an increasing physiological concentrations of calcium at 200 µM, 500 µM and 1 mM. After exposing to each calcium concentrations, the cells were allowed to settle by gravity and non-pelleted (floating dead cells) cells were separated from the pelleted viable cardiomyocytes. The cell pellet was then re-suspended in plating media 199 (M5017; Sigma) containing 26.2 mM $NaHCO_3$, 25 mM HEPES, 1.24 mM L-carnitine, 137 µM streptomycin (S9137; Sigma), 280.6 µM penicillin (P3032; Sigma), 10 mM taurine (T0625; Sigma) and 1 % BSA Fraction V (10735094001; Roche) at pH 7.4. Cells were then plated on laminin (11243217001; Roche) coated 35 mm plates at a density of 50-75x10^3 cells/plate. After 4 hr, plating medium was replaced with fresh media and cells were subjected to low and high concentrations of different substrates as mentioned in section 2.4.5.

2.4.4. Preparation of bovine serum albumin complexed fatty acid

Bovine serum albumin (BSA) complexed FA solution was prepared in DMEM 1X medium. 120 mM stock solution of sodium oleate (O7501; Sigma) and sodium palmitate (P9767; Sigma) were prepared in DMEM-1X media. The stock solution of palmitate and oleate were prepared in DMEM-1X media, pre warmed at 90℃. The resulting stock solution was then mixed in a 4% fatty acid free BSA solution, prepared in DMEM 1X media, pre

warmed at 50℃. The resulting FA and BSA solution was then allowed to complex at 37℃ for 30 min. After 30 min, the media was sterile filtered using 2 μm sterile filter. The sterile medium was immediately used to treat the cells.

2.4.5. Experimental design for cell culture

H9C2, NRCM and ARCM cells were incubated with different substrates such as glucose (G; 5 mM and 30 mM; DX0145; EMD Chemicals), oleate (O; 0.4 mM and 1.2 mM); palmitate (P; 0.4 mM and 1.2 mM); or a combination of glucose/oleate (GO; 5/0.4 mM and 30/1.2 mM), glucose/palmitate (GP; 5/0.4 mM and 30/1.2 mM) and glucose/palmitate/oleate (GPO; 5/0.4/0.4 mM and 30/1.2/1.2 mM) for 17 h. Following 17 h of exposure to different substrates, autophagic flux was determined by treating cells with either vehicle or 200 μM chloroquine (CQ, C6628; Sigma) for 3 h in nutrient deprived medium, Earle's Balanced Salt Solution (EBSS;14155-063; Thermo Fisher Scientific) buffered with 25 mM HEPES (15630-080; Thermo Fisher Scientific). Subsequently, cells were harvested in ice cold PBS, sonicated and subjected to SDS gel electrophoresis. Autophagic flux was assessed by measuring LC3B-II via immunoblotting.

2.4.6. Presto blue cell viability assay

H9C2 rat cardiomyoblasts were seeded in a 96-well plate at a density of 10 x 10^3 cells per well in 200 μL of DMEM-HG + 10% FBS. H9C2 cells were differentiated as previously described. Following treatment with higher concentrations of glucose (G; 30 mM), palmitate (P; 1.2 mM); or a combination of glucose/palmitate (GP; 30/1.2 mM) and glucose/palmitate/oleate (GPO; 30/1.2/1.2 mM) for 17 h, presto blue reagent (A13261; Invitrogen) was added according to manufacturer's specifications. Plate was read at time points ranging from 0.5-2 h in a Synergy H4 plate reader at a wavelength of 570nM.

2.4.7. Fluorescence microscopy

2.4.7.1. Lysotracker

H9C2 and NRCM cells were exposed to different substrates for 17 h, followed by incubation with 75 nM of lysotracker (L7526; LysoTracker Green DND-26; Thermo Fisher Scientific) for 3 h in the presence of nutrient deprived medium, EBSS. After 3 h incubation

with lysotracker, cells were counter stained for nuclei with Hoechst 33342 stain (62249; Thermo Fisher Scientific) for 7 min and live cell images were obtained using ZEISS microscope. Lysotracker probes are fluorophore linked to a weakly basic amines that accumulate in an acidic organelles in live cells such as lysosome with low internal pH and can be used to examine the lysosome biosynthesis by measuring green fluorescence intensity. Cells were imaged at excitation/emission maxima of approximately 504/511 nm for EGFP using fluorescence microscope with 20 x objectives digital camera. Fluorescence intensity was measured from five images per group using ZEN Pro software.

2.4.7.2. GFP-RFP-LC3

Differentiated H9C2 cells were transduced with GFP-RFP-LC3 Premo autophagy sensor (P36239; Thermo Fisher Scientific) for 48 h followed by exposure to different substrates for 17 h. After 17 h, cells were treated with 200 μM chloroquine in the presence of nutrient deprived medium, EBSS to assess autophagic flux. The cells were counter stained for nuclei using Hoechst 33342 stain for 7 min. Live cell images were obtained using ZEISS microscope. Autophagosome abundance using microscopy was by measuring red fluorescence (RFP) indicator of autolysosome accumulation, quenching of pH sensitive GFP fluorescence (green) highlighting autophagosome fusion with lysosomes, and GFP merge with RFP (Yellow) demonstrating an accumulation of autophagosomes. Cells were imaged at excitation/emission maxima of approximately 504/511 nm for EGFP and 555/584 nm for TagRFP using fluorescence microscope with 20 x objective digital camera. Fluorescence intensity was measured from a selected sections of five images using ZEN Pro software.

2.5. Statistical analysis

Results are expressed as mean ± SEM. Pairwise comparison between groups was performed using unpaired two-tailed Student's t test and comparison between multiple groups was performed using analysis of variance one-way ANOVA or Two-way ANOVA followed by Tukey test using GraphPad Prism software. P values of less than 0.05 were considered statistically significant.

CHAPTER 3: RESULTS

3.1. Palmitate alone or a combination of glucose and palmitate upregulate pathways of cell death and lipid utilization in H9C2 cells.

To ascertain the individual contribution of different substrates on cellular autophagy, we employed an *in-vitro* model of differentiated H9C2 cardiomyoblast cells. H9C2 cells are derived from embryonic rat heart, which simulates functionality of an intact cardiac muscle (Pagano, Naviglio et al. 2004). In these cells, we first screened different substrates such as glucose (G), oleate (O), palmitate (P), and also a combination of glucose/palmitate (GP), glucose/oleate (GO), glucose/palmitate/oleate (GPO), to confirm if H9C2 cells are tolerant to low and high concentrations of these substrates and furthermore whether induction of autophagy by nutrient deprivation impacts cell viability. Glucose was used at a concentration of 5 mM representing physiological (low) levels and 30 mM representing pathological (high) levels. Palmitate and oleate were used at low and high concentration of 0.4 mM and 1.2 mM respectively. These concentrations are clinically relevant and frequently observed in healthy and diseased (Ni, Zhao et al. 2015) individuals. Glucose (G) and oleate (O) at low and high concentrations alone or in combination did not affect the viability of H9C2 cells **(Figure 3.1. A-D)**. However, H9C2 cells were susceptible to a loss of cellular viability following incubation with a combination of glucose/palmitate (GP) at both low and high concentrations **(Figure 3.1. I-J)**. Notably, both low and high concentrations of palmitate (P) alone reduced cell viability **(Figure 3.1. E-F)**, a consequence of toxicity from elevated lipotoxic intermediate. The decrease in cell viability in response to high palmitate (P) alone or in combination with glucose (GP) was further recapitulated by performing cell viability assay using presto blue assay **(Figure 3.1. M)**. Therefore glucotoxicity and lipotoxicity adversely affected the myocyte viability.

Changes in cellular viability were also associated with a strong induction of cleaved caspase-3 levels, a surrogate marker for apoptosis (Orrenius, Zhivotovsky et al. 2003). Low and high concentrations of oleate (O) did not augment cleaved caspase-3 levels in H9C2 cells compared to glucose alone **(Figure 3.2. A-D)**. In response to the high concentration of palmitate, the cleavage of caspase-3 was significantly increased compared to high glucose alone **(Figure 3.2. C-D)**, an effect not observed with low concentration of palmitate **(Figure 3.2. A-B)**. However, exposure to a combination of glucose/palmitate

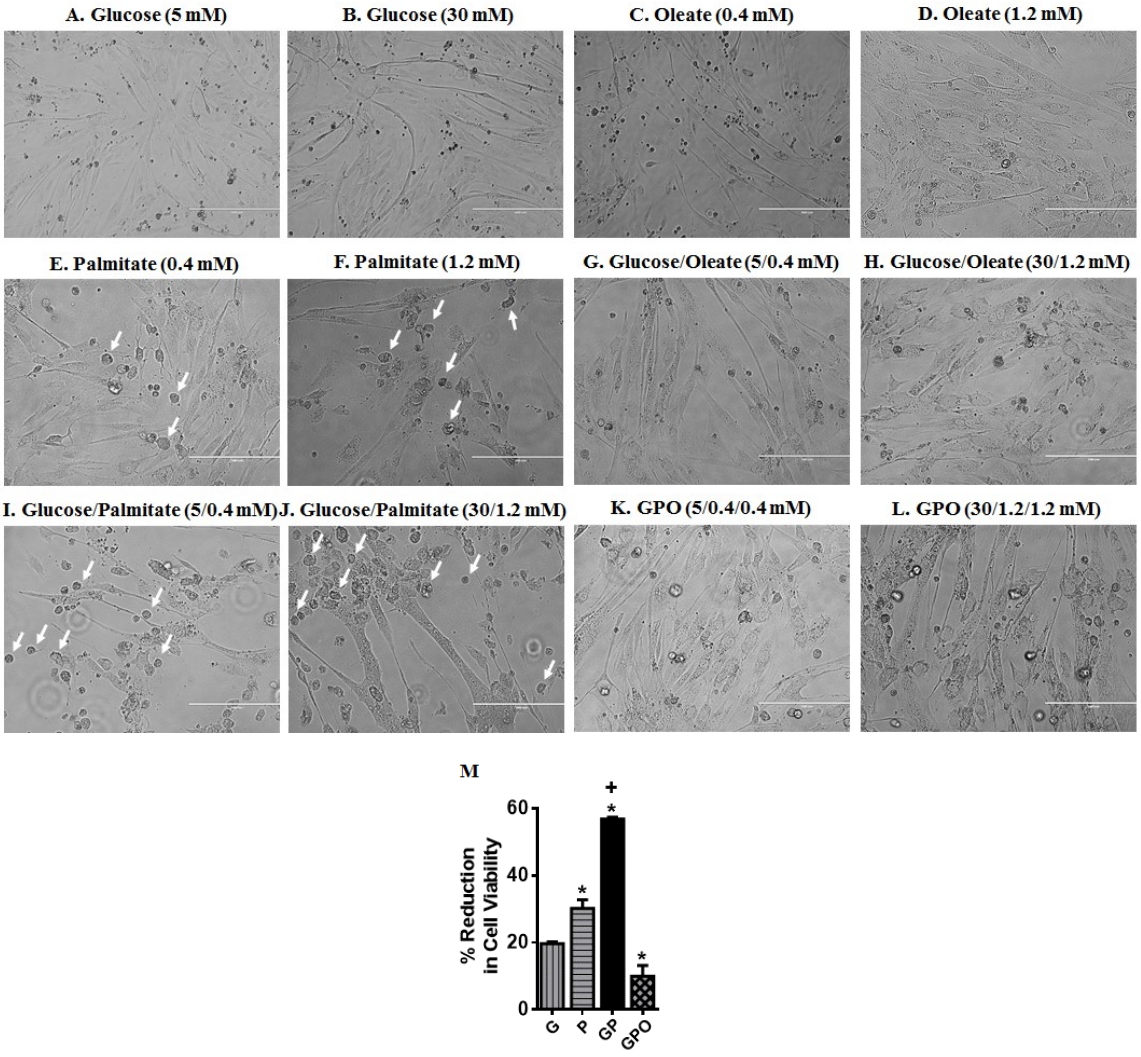

Figure 3.1. Exposure to low and high palmitate alone or in combination with glucose decreases cell viability in H9C2 rat cardiomyoblast. H9C2 cells were incubated with (A-B) glucose (G; 5 or 30 mM), (C-D) oleate (O; 0.4 or 1.2 mM), (E-F) palmitate (P; 0.4 or 1.2 mM), (G-H) glucose/oelate (GO; 5/0.4 or 30/1.2 mM), (I-J) glucose/palmitate (GP; 5/0.4 or 30/1.2 mM) and (K-L) glucose/palmitate/oleate (GPO; 5/0.4/0.4 or 30/1.2/1.2 mM) for 17 h, followed by 3 h starvation in EBSS medium and imaged for morphological aberrations. (M) Presto blue cell viability determination in H9C2 cells treated with higher concentrations of glucose, palmitate, and combination of glucose/palmitate or glucose/palmitate/oleate 17 h. White arrow signifies de-differentiated non-viable cells. Graph represents mean ± S.E.M., *P<0.05 vs glucose and +P<0.05 vs palmitate; one-way ANOVA, n = 3, A.U.; arbitrary unit.

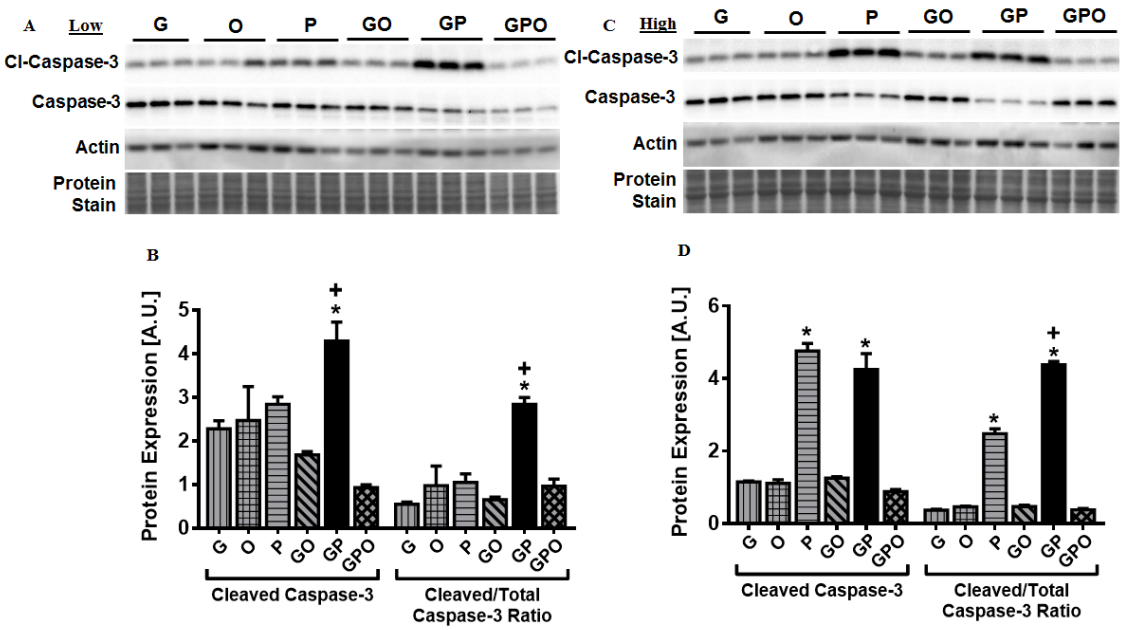

Figure 3.2. Palmitate-induced upregulation in cell death pathway in H9C2 cells, is exacerbated in the presence of glucose. H9C2 cells were incubated with glucose (G; 5 or 30 mM), oleate (O; 0.4 or 1.2 mM), palmitate (P; 0.4 or 1.2 mM), glucose/palmitate (GP; 5/0.4 or 30/1.2 mM) and glucose/palmitate/oleate (GPO; 5/0.4/0.4 or 30/1.2/1.2 mM) for 17 h, followed by 3 h starvation in EBSS medium prior to cell harvest. (A, C) Immunoblot and (B, D) densitometric analysis were performed to examine the protein levels of (A, B, C and D) cleaved caspase-3 and total caspase-3 normalized to protein stain in total cell lysates and actin was used as a loading control. Graph represents mean ± S.E.M., *P<0.05 vs glucose and +P<0.05 vs palmitate; one-way ANOVA, n = 3, A.U.; arbitrary unit. **Note:** All the presented lanes are from the same membranes. All the experiments were repeated three times. First two times experiments were performed with n=1 and the final experiment was performed with n=3 technical replicates on which statistical analysis was performed.

(GP) at both low and high concentrations, induced a robust increase in cleaved caspase-3 levels in H9C2 cells **(Figure 3.2. A-D)**. Notably, in H9C2 cells, palmitate-induced cleaved to total caspase-3 ratio was further increased when palmitate was co-incubated with high glucose, signifying glucolipotoxicity mediated activation of cell death pathway Interestingly, a combination of oleate, glucose and palmitate (GPO) at low and high concentrations did not augment cleaved caspase-3 levels suggesting that oleate offered resistance to glucose/palmitate (GP)-mediated caspase-3 cleavage and cell death **(Figure 3.2. A, B, C and D)**, likely by sequestering toxic FA into TG pool (Listenberger, Han et al. 2003, Kienesberger, Pulinilkunnil et al. 2013).

We further examined if the observed remodelling of stress pathways was associated with changes in lipid utilization. We examined the effect of different substrates on the ATGL level, a lipase that catalyses the first step of TG hydrolysis in to diacylglycerol and free FA (Kienesberger, Pulinilkunnil et al. 2013). Low concentrations of glucose (G) and oleate (O) had no effect on ATGL level in H9C2 cells **(Figure 3.3. A-B)**. However, ATGL levels were robustly induced in response to low palmitate (P), combination of glucose/oleate (GO), glucose/palmitate (GP) and glucose/palmitate/oleate (GPO) when compared to glucose alone **(Figure 3.3. A-B)**. Interestingly, exposure of H9C2 cells to high concentrations of oleate (O) or palmitate, significantly augmented ATGL level, when compared to glucose alone **(Figure 3.3. C-D)**. Oleate-induced increase in ATGL level was further potentiated by co-incubation with glucose **(Figure 3.3. A-D)**, suggesting that when supplemented in excess, oleate is preferentially used over glucose through its effects on ATGL. In contrast, a combination of high glucose/palmitate (GP) did not result in increase in ATGL level, suggesting that glucose suppressed palmitate-induced increase in ATGL level **(Figure 3.3. C-D)**, an effect that was reversed by co-incubation with oleate **(Figure 3.3. C-D)**. Our findings from H9C2 cells, suggest that a combination of high glucose and high oleate represented a milder form of lipid overload that did not compromise cellular viability and lipid turnover, whereas combination of high glucose and high palmitate simulated a severe form of glucolipotoxicity decreasing TG hydrolase levels, with a robust induction of cleavage of caspase-3, both of which were sensitive to oleate inhibition.

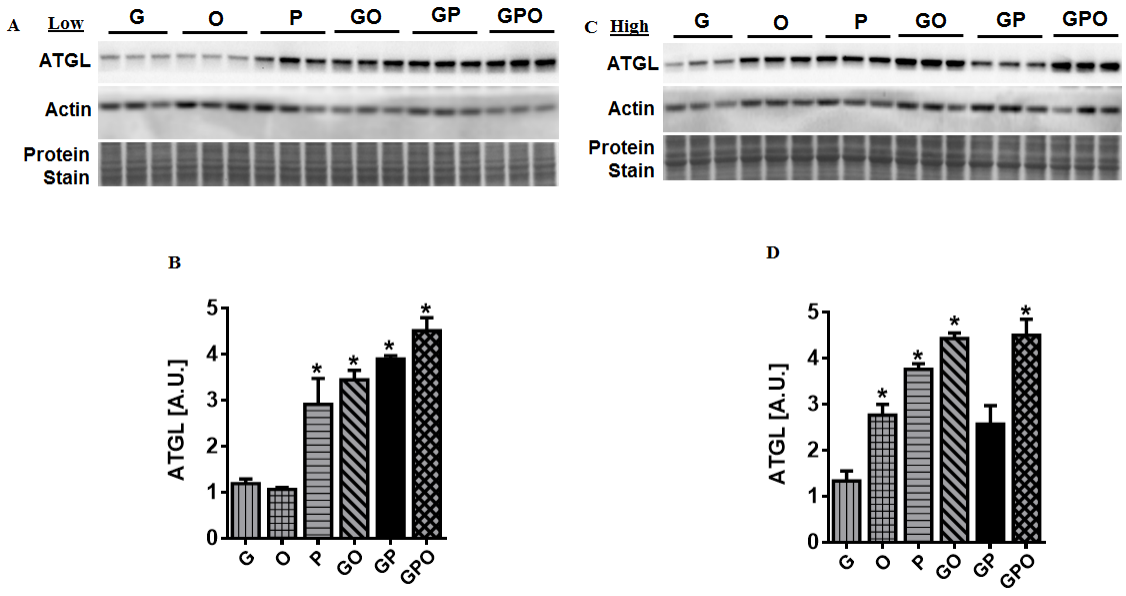

Figure 3.3. High palmitate mediated increase in lipid utilization is suppressed in the presence of high glucose. H9C2 cells were incubated with glucose (G; 5 or 30 mM), oleate (O; 0.4 or 1.2 mM), palmitate (P; 0.4 or 1.2 mM), glucose/palmitate (GP; 5/0.4 or 30/1.2 mM) and glucose/palmitate/oleate (GPO; 5/0.4/0.4 or 30/1.2/1.2 mM) for 17 h, followed by 3 h starvation in EBSS medium prior to cell harvest. (A, C) Immunoblot and (B, D) densitometric analysis were performed to examine the protein levels of (A, B, C and D) ATGL normalized to protein stain in total cell lysates and actin was used as a loading control. Graph represents mean ± S.E.M., *P<0.05 vs glucose and +P<0.05 vs palmitate; one-way ANOVA, n = 3, A.U.; arbitrary unit. **Note:** All the presented lanes are from the same membranes. All the experiments were repeated three times. First two times experiments were performed with n=1 and the final experiment was performed with n=3 technical replicates on which statistical analysis was performed.

3.2. Cell death pathway is activated in neonatal rat cardiomyocytes (NRCM) exposed to palmitate alone or when co-incubated with glucose

In addition to H9C2 cells, we also employed NRCM cells in our studies, since H9C2 cells are non-contractile in nature and their utility is only limited to studying cellular signalling pathways and not cardiomyocyte function (Parameswaran, Kumar et al. 2013). However, NRCM cells beat and are terminally differentiated, representing a more robust cardiac muscle phenotype. Therefore, we substantiated our H9C2 data using, NRCMs. Morphological assessment of NRCMs revealed that low and high palmitate alone (P) or in combination with glucose decreased cardiomyocyte viability **(Figure 3.4. E, F, I and J)**. Similar to H9C2 cells, exposure of NRCMs to low and high concentration of glucose (G) or oleate (O) and a combination of glucose/oleate (GO) and glucose/oleate/palmitate (GPO) did not affect cell viability **(Figure 3.4. A, B, C, D, G, H, K and L)**. Furthermore, loss of cell viability **(Figure 3.4. E, F, I and J)** and increases in cleavage of caspase-3 **(Figure 3.5. A-D)** were observed in NRCMs incubated with low and high palmitate (P) alone or in combination with glucose (GP), an effect that was sensitive to oleate co-incubation **(Figure 3.5. A-D)**.

In addition to cell death, ATGL levels were affected in NRCMs, similar to that observed in H9C2 cells. Low concentration of FA alone or in combination with glucose, upregulated ATGL level compared to glucose (G) alone **(Figure 3.6. A-B)**. Specifically, high concentration of oleate (O) alone or in the presence of either glucose (GO) or a combination of glucose/palmitate/oleate (GPO) augmented ATGL level **(Figure 3.6. C-D),** an effect similar to that observed in H9C2 cells. Surprisingly, unlike H9C2 cells, incubation with high concentration of palmitate (P) alone or in combination with glucose (GP), did not elicit increase in ATGL protein in NRCM cells **(Figure 3.6. C-D)**. Collectively, these findings validate the utility of H9C2 and NRCM cells for glucolipotoxic studies ex-vivo. Our data show that a combination of glucose and palmitate (GP) at both low and high concentrations simulated the most severe form of glucolipotoxicity and palmitate (P) alone at both low and high concentrations represented a moderate form of palmitotoxicity.

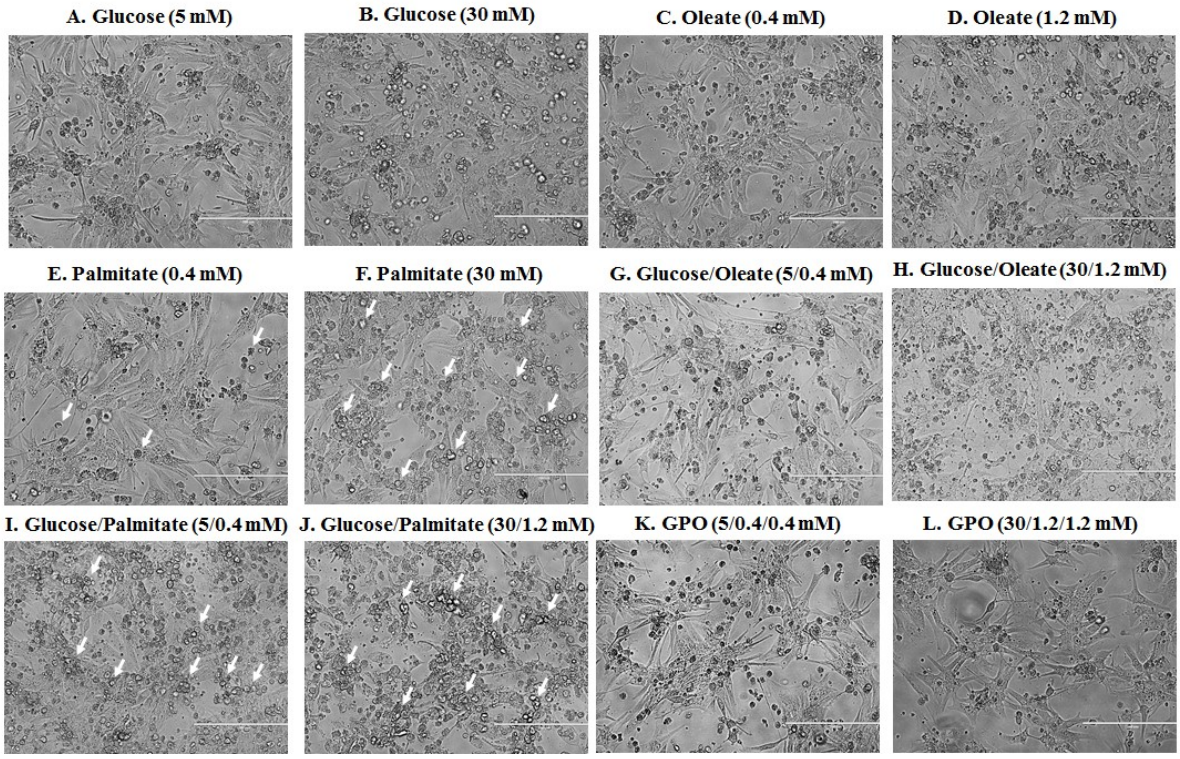

Figure 3.4. Treatment of NRCMs with low or high palmitate alone or in combination with glucose results in loss of cell viability. NRCM cells were incubated with glucose (G; 5 or 30 mM), oleate (O; 0.4 or 1.2 mM), palmitate (P; 0.4 or 1.2 mM), glucose/palmitate (GP; 5/0.4 or 30/1.2 mM) and glucose/palmitate/oleate (GPO; 5/0.4/0.4 or 30/1.2/1.2 mM) for 17 h, followed by 3 h starvation in the presence of EBSS medium and imaged for morphological aberrations. White arrow signifies de-differentiated non-viable cells.

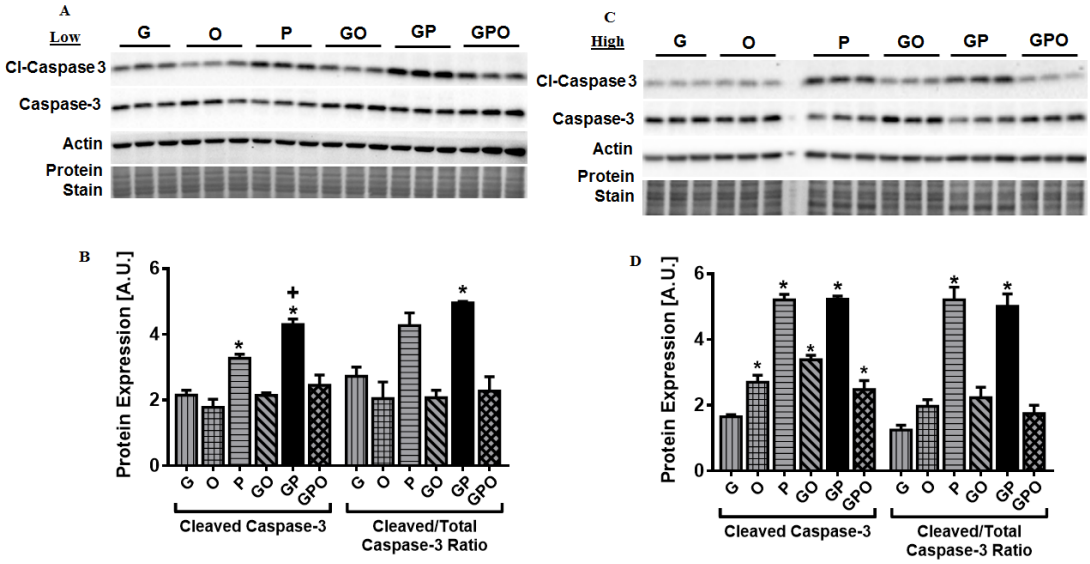

Figure 3.5. Low and high palmitate alone or in combination with glucose increases cleaved caspase-3 levels in NRCM cells. NRCM cells were incubated with glucose (G; 5 and 30 mM), oleate (O; 0.4 and 1.2 mM), palmitate (P; 0.4 and 1.2 mM), glucose/palmitate (GP; 5/0.4 and 30/1.2 mM) and glucose/palmitate/oleate (GPO; 5/0.4/0.4 and 30/1.2/1.2 mM) for 17 h, followed by 3 h starvation in the presence of EBSS media prior to cell harvest. (A, C) Immunoblot and (B, D) densitometric analysis were performed to examine the protein levels of (A, B, C and D) cleaved caspase-3 and total caspase-3 normalized to protein stain in total cell lysates and actin was used as a loading control. Graph represents mean ± S.E.M., *P<0.05 vs glucose and +P<0.05 vs palmitate; one-way ANOVA, n = 3, A.U.; arbitrary unit. **Note:** All the presented lanes are from the same membranes. All the experiments were repeated three times. First two times experiments were performed with n=1 and the final experiment was performed with n=3 technical replicates on which statistical analysis was performed.

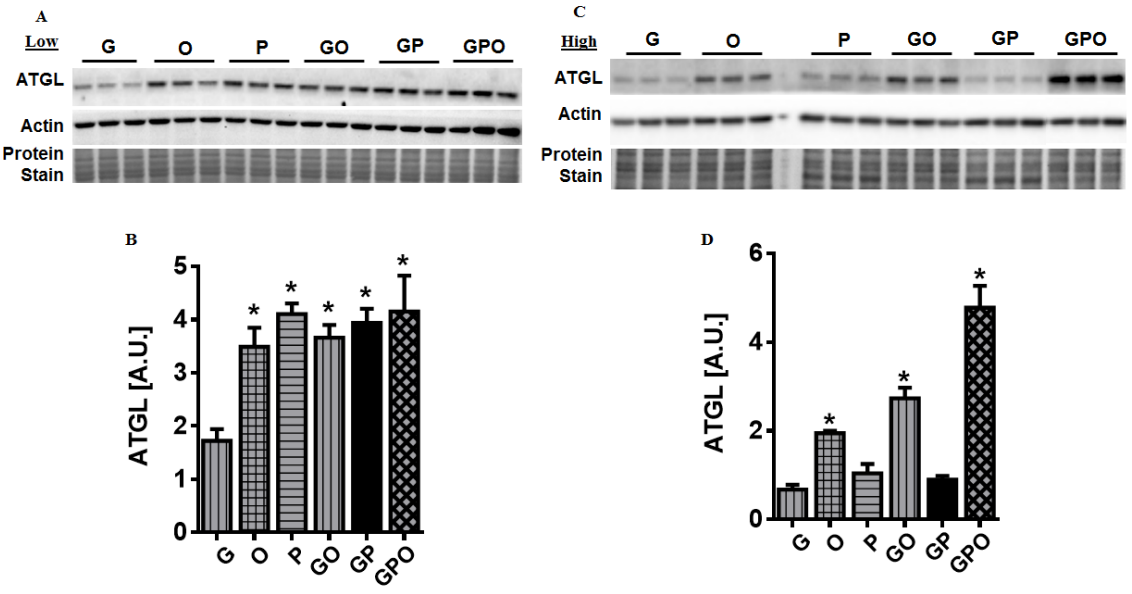

Figure 3.6. Unlike oleate, high palmitate and a combination of high glucose/palmitate fail to upregulate ATGL protein in NRCM cells. NRCM cells were incubated with glucose (G; 5 or 30 mM), oleate (O; 0.4 or 1.2 mM), palmitate (P; 0.4 or 1.2 mM), glucose/palmitate (GP; 5/0.4 or 30/1.2 mM) and glucose/palmitate/oleate (GPO; 5/0.4/0.4 or 30/1.2/1.2 mM) for 17 h, followed by 3 h starvation in the presence of EBSS media prior to cell harvest. (A, C) Immunoblot and (B, D) densitometric analysis were performed to examined the protein levels of (A, B, C and D) ATGL normalized to protein stain in total cell lysates and actin was used as a loading control. Graph represents mean ± S.E.M., *P<0.05 vs glucose and +P<0.05 vs palmitate; one-way ANOVA, n = 3, A.U.; arbitrary unit. **Note:** All the presented lanes are from the same membranes. All the experiments were repeated three times. First two times experiments were performed with n=1 and the final experiment was performed with n=3 technical replicates on which statistical analysis was performed.

Therefore, to dissect the contribution of individual substrates on autophagy, for all subsequent experiments, glucose (G), oleate (O), palmitate (P) and a combination of glucose/palmitate (GP) were employed with glucose and oleate serving as a control for carbohydrates and lipids respectively.

3.3. Exposure to palmitate alone or a combination of glucose and palmitate suppresses macroautophagic flux in H9C2 and NRCM cells

We investigated whether the proteins involved in the macroautophagy process is impacted distinctly by different substrates. Utilizing immunoblotting and immunofluorescence methodologies, we examined the conversion of pre-autophagosome bound microtubule protein LC3B-I to the autophagosome bound lipidated form of LC3B-II in the presence or absence of lysosomal de-acidifier, CQ. Baseline LC3B-II protein level reflects the content of matured autophagosomes and signifies a combined effect of autophagosome synthesis and clearance, which encompasses lysosomal function. However, conclusions drawn on autophagic status of a cell from absolute measure of baseline LC3B-II level is incomplete, since changes in LC3B-II could not only due to defects in autophagosome clearance within the lysosome (lysosome function) but also could be due to changes in autophagosome biosynthesis. Therefore, we measured autophagic flux or autophagosome turnover in H9C2 **(Figure 3.7.)** and NRCM **(Figure 3.9.)** cells. Autophagic flux was assessed in the presence of vehicle or autophagy inhibitor, CQ, by measuring LC3B-II protein levels via immunoblotting or by imaging fluorescently labeled LC3B-II puncta in cells incubated with different substrates. In H9C2 cells, exposed to low concentration of different substrates, baseline LC3B-II levels remained unchanged **(Figure 3.7. A-B)**. H9C2 cells incubated with high concentration of different substrates did not alter LC3B-I level **(Figure 3.7. D-E)**. However, exposure of H9C2 cells to a combination of high glucose/palmitate (GP) concentration augmented baseline LC3B-II levels when compared to palmitate (P) alone **(Figure. 3.7. D-E).** Autophagosome abundance using microscopy was also assessed by measuring red fluorescence (RFP) indicator of autolysosome accumulation, quenching of pH sensitive GFP fluorescence (green) highlighting autophagosome fusion with lysosomes, and finally GFP merge with

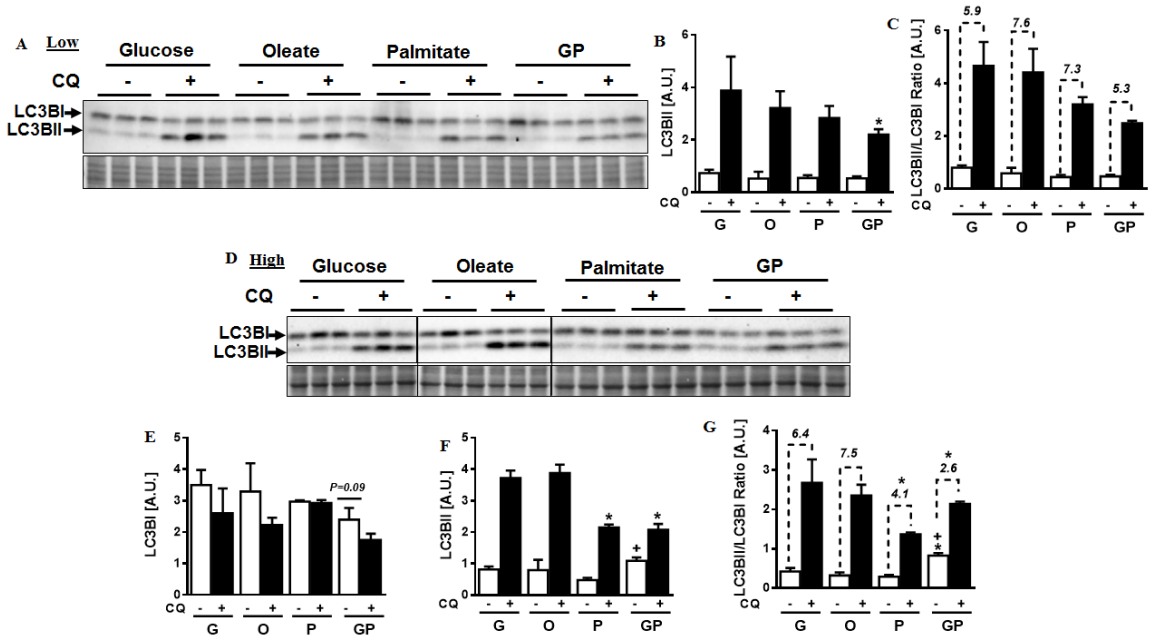

Figure 3.7. High palmitate and high glucose/palmitate combination impairs autophagic flux in H9C2 cardiomyoblast. H9C2 cells were incubated with glucose (G; 5 or 30 mM), oleate (O; 0.4 or 1.2 mM), palmitate (P; 0.4 or 1.2 mM) and glucose/palmitate (GP; 5/0.4 or 30/1.2 mM) for 17 h. After 17 h, cells were treated with either vehicle or CQ (200 μM) for 3 h in the presence of nutrient deprived media, EBSS to assess autophagic flux prior to cell harvest. (A and D) Immunoblot and (B, C, E and F) densitometric analysis were performed to examine the protein levels of (A-F) LC3B-I and LC3B-II normalized to protein stain in total cell lysates and actin was used as a loading control. Graph represents mean ± S.E.M., *P<0.05 vs glucose and +P<0.05 vs palmitate; one-way ANOVA, (E) *P<0.05; two way ANOVA, n = 3, A.U.; arbitrary unit. The values above dotted lines represent the fold change of LC3B-II/LC3B-I ratio in the presence and absence of CQ. **Note:** (A) the presented lanes are from the same membranes. (D) The presented lanes are from different membranes separated by a black line between the lanes. All the experiments were repeated three times. First two times experiments were performed with n=1 and the final experiment was performed with n=3 technical replicates on which statistical analysis was performed.

RFP (Yellow) demonstrating an accumulation of autophagosomes (Barth, Glick et al. 2010). A combination of high glucose/palmitate (GP) concentration augmented LC3B-II puncta **(Figure 3.8 D-E)** when compared to glucose (G) or oleate (O) alone. This finding suggested that glucolipotoxic milieu is promoting autophagosome accumulation at baseline in the absence of CQ, likely an outcome of inhibited autophagosome clearance or due to accelerated autophagosome biosynthesis. To clarify this issue, we examined LC3B-II levels via immunoblotting and immunofluorescence in presence of CQ in H9C2 cells exposed to different substrates. Interestingly, H9C2 cells incubated with a combination of low glucose and palmitate (GP) and subsequently challenged with CQ, displayed no change in LC3B-II levels compared to glucose (G) alone **(Figure 3.7. A-B)**, which was unable to influence changes in autophagosome turnover as indicated by unchanged LCB-II to LC3B-I ratio **(Figure 3.7. A and C)**. Notably H9C2 cells incubated with high palmitate (P) or a combination of high glucose/palmitate (GP) and challenged with CQ, exhibited a significant decrease in LC3B-II levels when compared to glucose (G) alone **(Figure 3.7. D-E)**. However, the magnitude of autophagosome turnover as measured by LC3B-II/LC3B-I ratio was unaffected with glucose (G, 6.4 fold) and oleate (O, 7.5 fold) incubations but was significantly declined in high palmitate (P, 4.1 fold) and high glucose/palmitate combination groups (GP, 2.6 fold, **Figure 3.7. D and F**) compared go glucose alone, which was further substantiated by decreases in LC3B-II puncta in the respective groups **(Figure 3.8. D-F)**. Interestingly, NRCM cells exposed to either low or high concentrations of oleate (O), palmitate (P) and a combination of glucose/palmitate (GP) did not alter baseline LC3B-II level when compared to glucose alone (G) **(Figure 3.9. A-F)**, an effect that was distinct from H9C2 cells. Notably, exposure of NRCM cells with high palmitate or a combination of glucose/palmitate significantly decreased baseline LC3B-I level **(Figure 3.9. D-E).** Furthermore, this decrease in LC3B-I level in response to high palmitate or glucose/palmitate could be a major contributor to the high baseline level of LC3B-II/LC3B-I ratio in these cells **(Figure 3.9. D, F).** However, following CQ challenge, LC3B-II levels significantly lower in NRCMs incubated with low or high concentrations of palmitate (P) alone or with a combination of glucose/palmitate (G/P) **(Figure 3.9. A, B, D and E)**. The changes in the level of LC3B-II also reflected in autophagosome turnover (GP, 2.6 fold) groups compared to glucose alone.

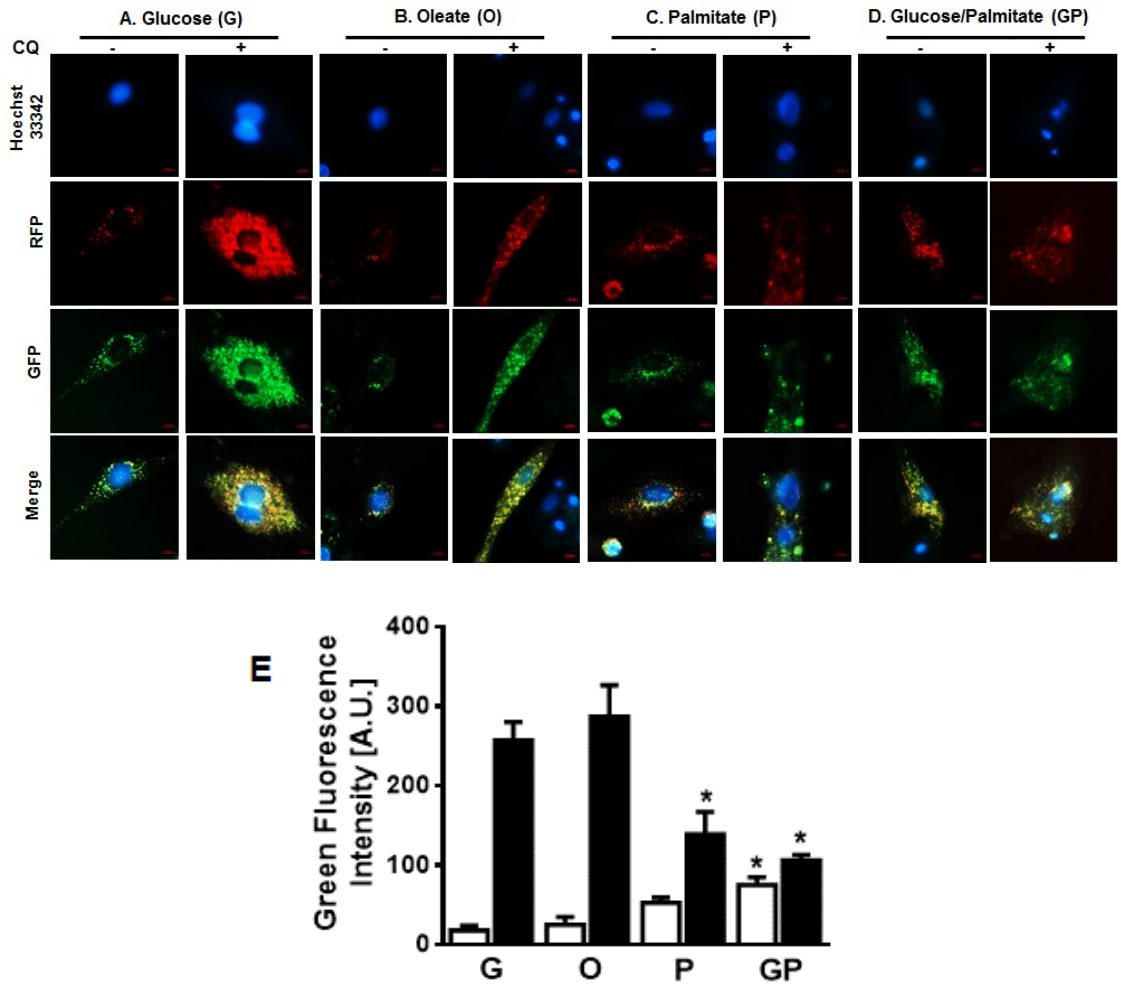

Figure 3.8. High palmitate and high glucose/palmitate combination causes autophagosome accumulation and impairs autophagosome turnover in H9C2 cardiomyoblast. H9C2 cells were transduced with premo autophagy sensor GFP-RFP-LC3 for 48 h. After 48 h, cells were incubated with glucose (G; 5 or 30 mM), oleate (O; 0.4 or 1.2 mM), palmitate (P; 0.4 or 1.2 mM) and glucose/palmitate (GP; 5/0.4 or 30/1.2 mM) for 17 h, followed by treatment with either vehicle or CQ (200 μM) for 3 h in the presence of nutrient deprived medium, EBSS. (A-D) Fluorescence image showing GFP (Green) and RFP (Red) and GFP-RFP-LC3 (Yellow) and nuclei stained with Hoechst 33342 (Blue). (E) Graphical representation of fluorescence intensity measured from 3 images per group. Graph represents mean ± S.E.M., *P<0.05 vs glucose and +P<0.05 vs palmitate; one-way ANOVA, n = 3 images were analysed per group. A.U.; arbitrary unit.

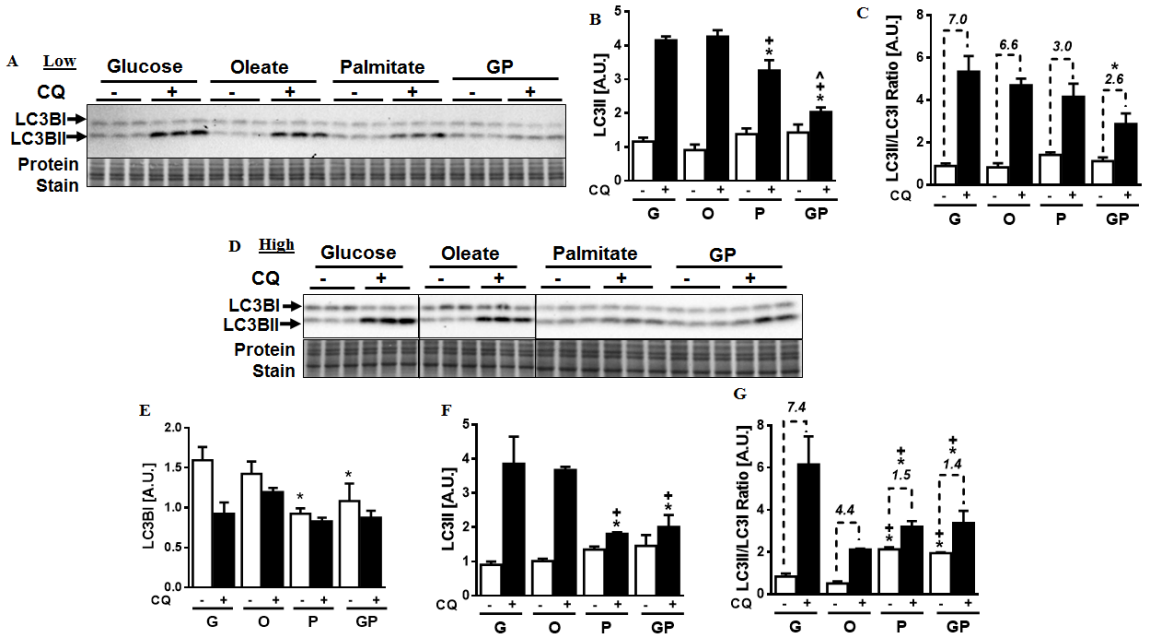

Figure 3.9. High palmitate and high glucose/palmitate combination impairs autophagic flux in NRCM cells. NRCMs were incubated with glucose (G; 5 or 30 mM), oleate (O; 0.4 or 1.2 mM), palmitate (P; 0.4 or 1.2 mM) and glucose/palmitate (GP; 5/0.4 or 30/1.2 mM) for 17 h. After 17 h, cells were treated with either vehicle or CQ (200 µM) for 3 h in the presence of nutrient deprived medium, EBSS to assess autophagic flux prior to cell harvest. (A) Immunoblot and (B) densitometric analysis was performed to examine the protein levels of (A-F) LC3B-I and LC3B-II normalized to protein stain in total cell lysates and actin was used as a loading control. Graph represents mean ± S.E.M., *P<0.05 vs glucose and +P<0.05 vs palmitate; one-way ANOVA, (E) *P<0.05; two way ANOVA, n = 3, A.U.; arbitrary unit. The values above dotted lines represent the fold change of LC3B-II/LC3B-I ratio in the presence and absence of CQ. **Note:** (A) the presented lanes are from the same membranes. (D) The presented lanes are from different membranes separated by a black line between the lanes. All the experiments were repeated three times. First two times experiments were performed with n=1 and the final experiment was performed with n=3 technical replicates on which statistical analysis was performed.

Furthermore, impairment in autophagic flux observed with low concentrations were exacerbated by high oleate (O, 4.4 fold), palmitate (P, 1.5 fold) and combination of glucose/palmitate (GP, 1.4 fold) **(Figure 3.9. A, C, D and F)**. Overall our findings suggest that NRCM but not H9C2 cells, are more sensitive to autophagy inhibition by either low palmitate (P) alone or a combination of glucose palmitate (GP). Regardless of the cell type, high palmitate alone (lipotoxicity) or in combination with high glucose (glucolipotoxicity) significantly suppressed autophagic flux signifying an effect of nutrient overload on myocyte autophagy. Therefore, to simulate pathological conditions of obesity and diabetes, for all subsequent ex vivo experiments, we only examined the effects of high concentration of substrates on lysosomal CMA and function, which plausibly explains the observed inhibition of macroautophagy.

3.4. Palmitotoxicity and glucolipotoxicity in H9C2 and NRCM cells deplete cellular TFEB, decrease CMA protein content, with concomitant reduction of lysosome abundance and proteolysis

We speculated that palmitate and a combination of glucose and palmitate compromises lysosome function. To address this query, we first examined the direct effect of nutrient overload on lysosomal content in live H9C2 cells incubated with lysotracker, a green fluorescent acidotropic probe, which label and stain the acidic lysosomes. In response to high oleate (O), decrease in lysosome staining was observed compared to glucose alone **(Figure 3.10 B and E)**. However, following exposure to palmitate alone, lysosomal staining was completely blunted compared to glucose alone **(Figure 3.10 C and E)**, an effect further exacerbated in the presence of high glucose (GP) **(Figure 3.10 D-E)**, suggesting a plausible decrease in lysosomal number, lysosomal de-acidification and/or loss of lysosome membrane integrity. To complement the imaging data, we measured the activity of cathepsin B, a cysteine protease enzyme that is stable in acidic environment of the lysosome and plays an important role in degrading lysosomal cargo and hence can be used as a measure for lysosome function (Appelqvist, Waster et al. 2013). Indeed, a loss of

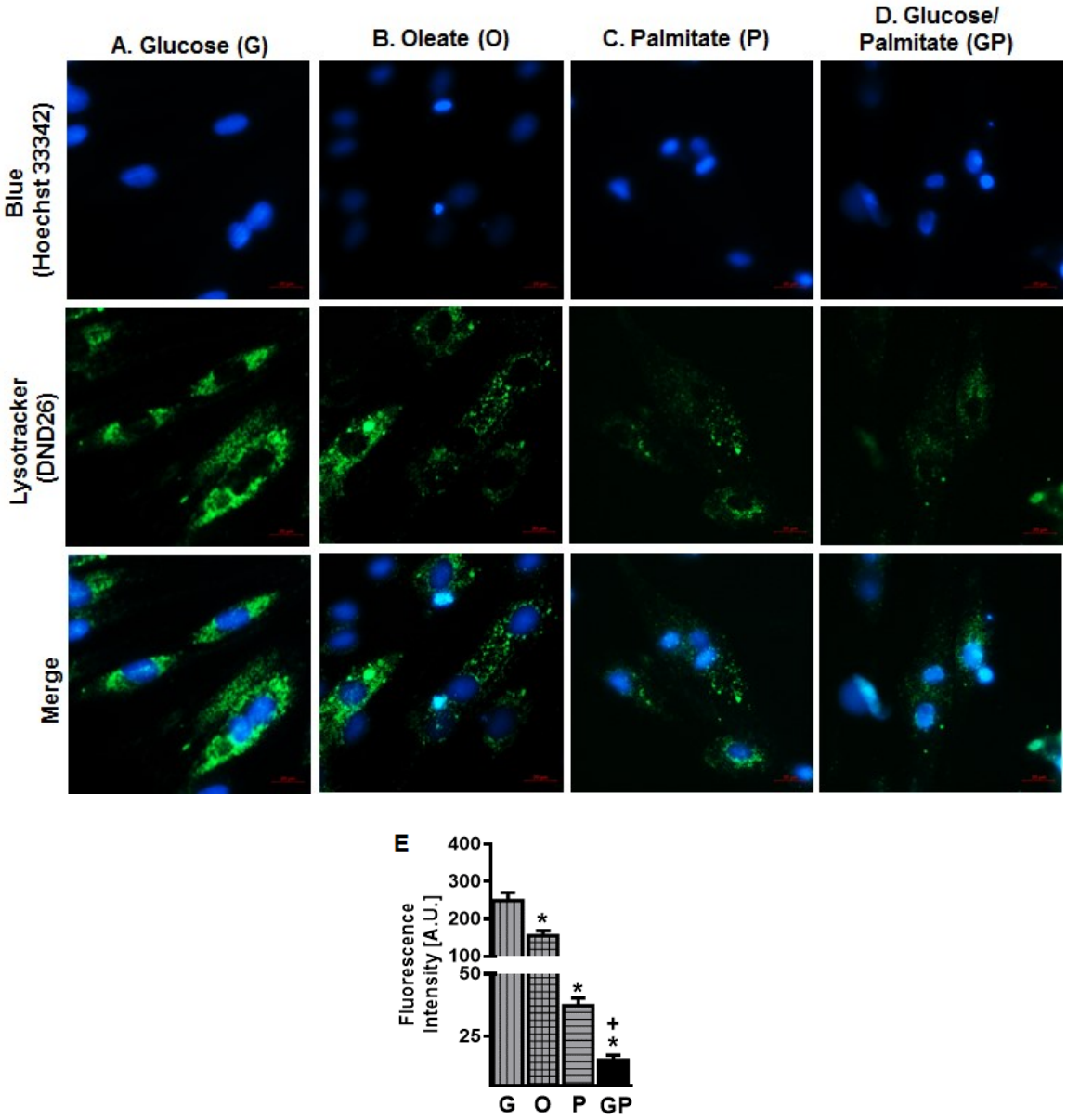

Figure 3.10. High palmitate and high glucose/palmitate combination treatment decreases lysosomal content in H9C2 cardiomyoblast. H9C2 cells were exposed to (A) glucose (30 mM), (B) oleate (1.2 mM), (C) palmitate (1.2 mM) and (D) glucose/palmitate (30/1.2 mM) for 17 h. After 17 h, cells were incubated with lysotracker DND-26 dye in the presence of nutrient deprivation medium, EBSS for 3 h. (A-D) Fluorescence image showing GFP (Green) and nuclei stained with Hoechst 33342 (Blue). (E) Graphical representation of fluorescence intensity measured from 7 to 8 images per group. Graph represents mean ± S.E.M., *P<0.05 vs glucose, +P<0.05 vs palmitate; one-way ANOVA, A.U.; arbitrary unit.

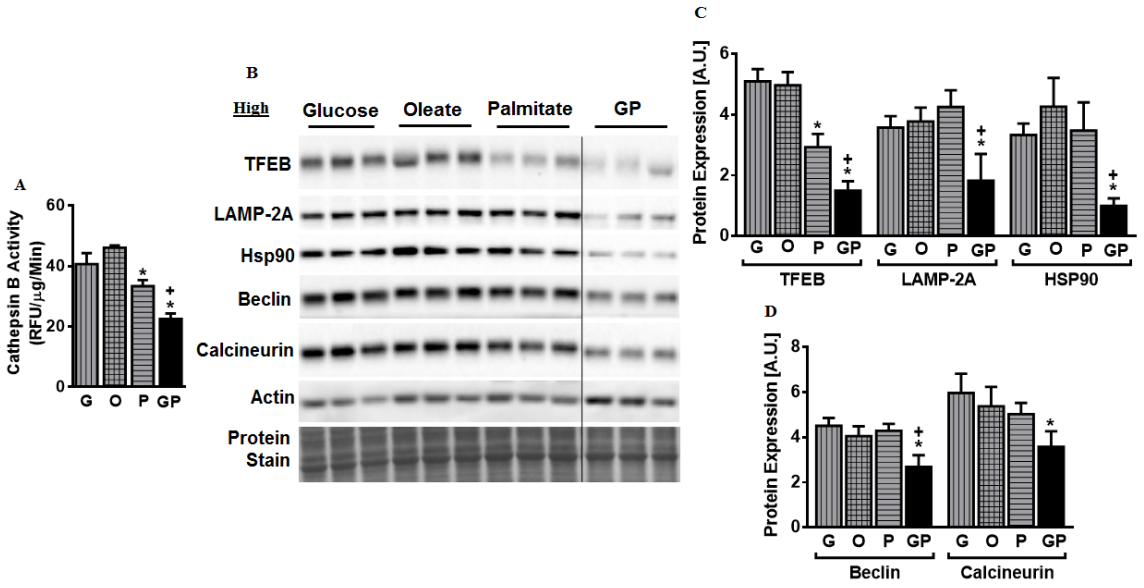

Figure 3.11. High palmitate or high glucose/palmitate combination decreases proteolytic activity and CMA protein levels, which is associated with loss of cellular TFEB content in H9C2 cells. H9C2 cells were incubated with glucose (G; 30 mM), oleate (O; 1.2 mM), palmitate (P; 1.2 mM) or glucose/palmitate (GP; 30/1.2 mM) for 17 h, followed by 3 h starvation in the presence of EBSS media prior to cell harvest. (A) Cathepsin B activity was measured in total cell lysates. All cathepsin B measurements are represented as change in RFU per minute corrected to µg of protein (RFU/min/µg). (B) Immunoblot and (C and D) densitometric analysis were performed to examine the protein content of (B, C) TFEB, LAMP-2A and Hsp90, (B, D) Beclin, and calcineurin normalized to protein stain in total cell lysates and actin was used as a loading control. Graph represents mean ± S.E.M., *P<0.05 vs glucose and +P<0.05 vs palmitate; one-way ANOVA, n = 3, A.U.; arbitrary unit. **Note:** all the presented lanes are from the same membranes. Non-adjacent lanes from the same membranes are separated by a black line between the lanes. All the experiments were repeated three times. First two times experiments were performed with n=1 and the final experiment was performed with n=3 technical replicates on which statistical analysis was performed.

lysosomal proteolytic activity, was observed in H9C2 cells incubated with palmitate (P) when compared to glucose alone **(Figure 3.11. A)**. The decrease in cathepsin B activity was further potentiated when palmitate was co-incubated with glucose (GP) **(Figure 3.11. A)**. Lysosomal biogenesis and function is governed by TFEB, a master transcriptional regulator of MiTF family of proteins (Settembre, Di Malta et al. 2011). TFEB positively (Sardiello, Palmieri et al. 2009, Settembre, Di Malta et al. 2011) encode expression of genes, which are part of the regulatory network known as CLEAR network, which augment cellular autophagy. Indeed, palmitate exposure triggered a strong decline in TFEB content **(Figure 3.11. B-C)** when compared to glucose (G) alone in H9C2 cells, an effect further exacerbated when palmitate was incubated in combination with glucose. The decrease in TFEB level in response to both palmitate and a combination of glucose/palmitate, was also correlated with a reduction in lysosome content and proteolytic activity. Interestingly, in H9C2 cells exposed to a combination of glucose/palmitate (GP) decreases in TFEB level also paralleled with a reduction in the content of lysosome resident protein LAMP-2A and Hsp90, **(Figure 3.11. B-C),** highlighting that TFEB levels likely influences lysosomal number and content of lysosomal membrane proteins. TFEB not only regulates lysosome function, but is also responsible for induction of genes facilitating macroautophagy (Sardiello, Palmieri et al. 2009, Settembre and Ballabio 2011) such as Beclin. Indeed, in H9C2 cells subjected to combination of glucose/palmitate (GP) decreases in TFEB content coincided with decrease in Beclin protein levels **(Figure 3.11. B and D)**. To explain the loss of TFEB in our model, we examined the level of the Ca^{2+} activated TFEB phosphatase, calcineurin, since changes in TFEB action was recently attributed to changes in calcineurin (Medina, Di Paola et al. 2015). Lysosomal Ca^{2+} release through mucolipin 1 (MCOLN1) activates calcineurin, which binds and dephosphorylates TFEB, thus promoting its nuclear translocation and activation (Medina and Ballabio 2015, Medina, Di Paola et al. 2015). Indeed, a combination of high glucose/palmitate (GP), significantly reduced calcineurin protein levels **(Figure 3.11. B and D),** indicating hyperphosphorylation of TFEB and loss of TFEB action in H9C2 cells following nutrient overload. Consistent with our H9C2 data, exposure to high palmitate or a combination of high glucose/palmitate (GP) in NRCM cells, blunted lysosome abundance compared to high glucose (G) **(Figure 3.12. C-E),** as indicated by loss of fluorescence staining. The decline in lysosome content in NRCM cells

was associated with a suppression of cathepsin B activity in response to palmitate (P) and combination of glucose/palmitate (GP) **(Figure 3.13. A)**. Furthermore, high palmitate (P) or a combination of glucose/palmitate (GP) depleted cellular TFEB content and decreased lysosomal membrane protein such as LAMP-2A and Hsp90 **(Figure 3.13. B-C)**. Notably, the observed decreased in LC3B-I level in response to high palmitate or in combination with glucose paralleled by strong reduction in TFEB level in these cells. Additionally, level of TFEB's downstream target, Beclin and TFEB activator, calcineurin, were also suppressed **(Figure 3.13. B-D)** in NRCMs when incubated with high palmitate or a combination of high glucose/palmitate (GP). Unlike H9C2 cells, NRCM cells exposed to high oleate (O), showed a decrease in LAMP-2A, TFEB, Beclin and calcineurin protein levels compared to glucose **(Figure 3.13. C-D)**, suggesting that the FA specific regulation of lysosome signalling. To confirm that nutrient overload can induce an inhibition of autophagic flux, suppression of TFEB and CMA proteins leading to a decline in lysosomal proteolysis, we also verified H9C2 and NRCM data in adult rat ventricular cardiomyocytes, a physiologically relevant model. In agreement with our H9C2 and NRCM data, cardiomyocytes exposed to palmitate (P) or glucose/palmitate (G/P) demonstrated a robust decline in cathepsin B activity followed by decreases in protein content of TFEB, LAMP-2A, Hsp90, Beclin and calcineurin **(Figure. 3.14. A-D)**. This experiment supports the argument that data obtained are not cell type specific rather an active underlying mechanism of nutrient overload pathology. Overall, these data demonstrate that palmitate overloading (lipotoxicity) alone or in presence of glucose (glucolipotoxicity) is sufficient to decrease cellular TFEB in the cardiomyocyte likely responsible for suppressing macroautophagy, lysosomal CMA and proteolysis. Furthermore, the data from NRCM and ARCM suggest that the observed effect was contribution of myocyte cells and not from non-myocytes cells that are routinely found in the whole heart.

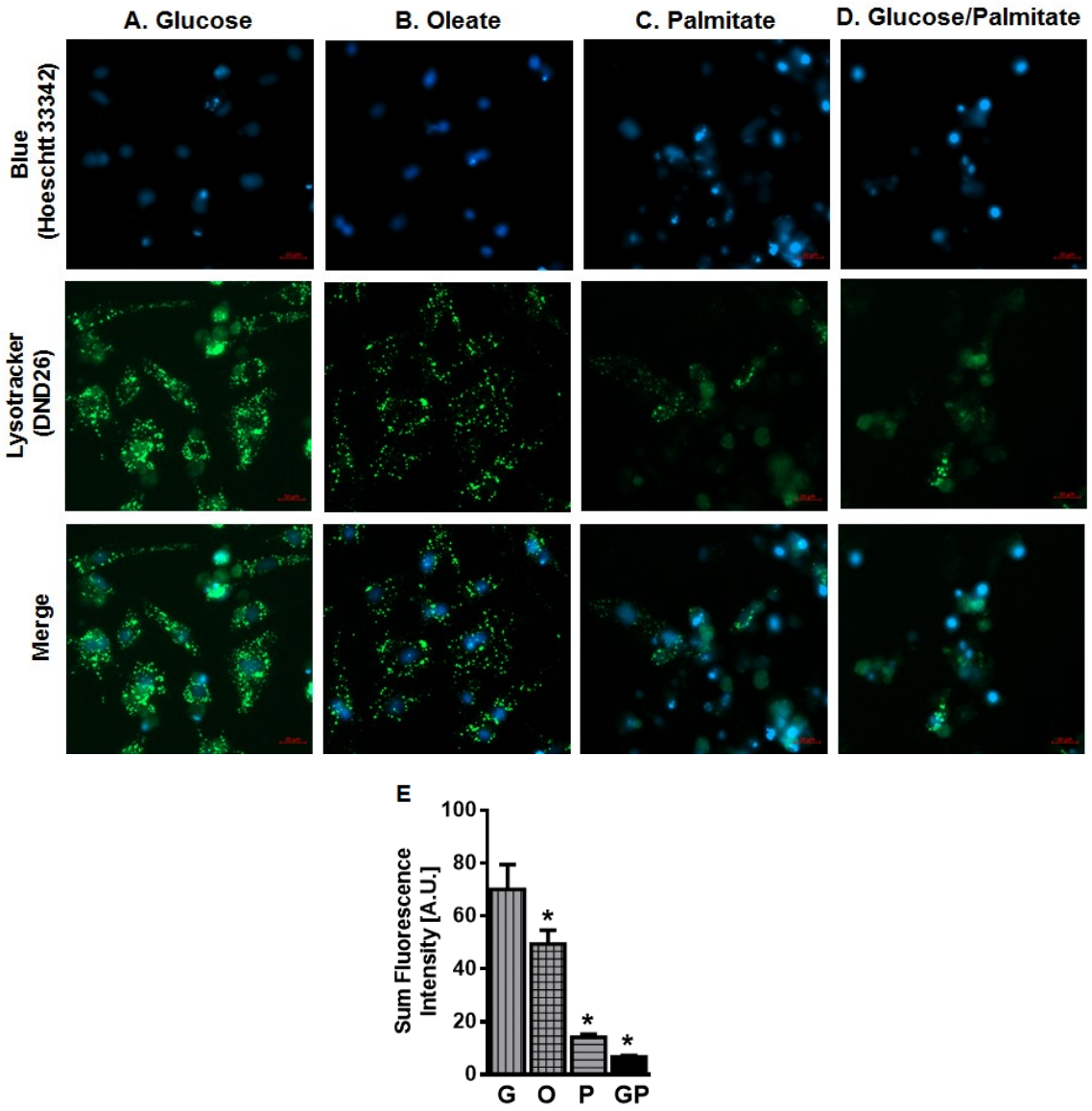

Figure 3.12. NRCMs exposed to high palmitate and combination of high glucose/palmitate treatment, decreases lysosome density. NRCMs were exposed to (A) glucose (30 mM), (B) oleate (1.2 mM), (C) palmitate (1.2 mM) and (D) glucose/palmitate (30/1.2 mM) for 17 h. After 17 h, cells were incubated with lysotracker DND-26 dye in the presence of nutrient deprivation medium, EBSS for 3 h. (A-D) Fluorescence image showing GFP (Green) and nuclei stained with Hoechst 33342 (Blue). (E) Graphical representation of fluorescence intensity measured from 7 to 8 images per group. Graph represents mean ± S.E.M., *P<0.05 vs glucose, +P<0.05 vs palmitate; one-way ANOVA, A.U.; arbitrary unit.

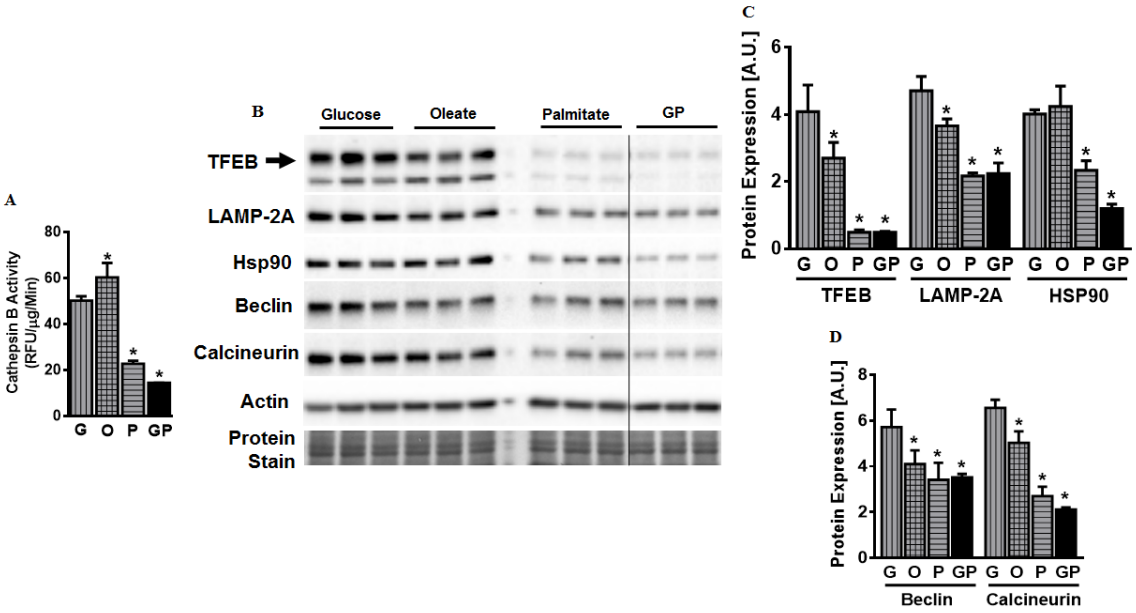

Figure 3.13. NRCMs exposed to high palmitate alone or in combination with glucose suppresses cathepsin B activity and CMA protein levels, with corresponding decline in TFEB protein. NRCM cells were incubated with glucose (G; 30 mM), oleate (O; 1.2 mM), palmitate (P; 1.2 mM) or glucose/palmitate (G/P; 30/1.2 mM) for 17 h, followed by 3 h starvation in the presence of EBSS medium prior to cell harvest. (A) Cathepsin B activity was measured in total cell lysates. All cathepsin B measurements are represented as change in RFU per minute corrected to µg of protein (RFU/min/µg). (B) Immunoblot and (C and D) densitometric analysis were performed to examine the protein levels of (B, C) TFEB, LAMP-2A and Hsp90, (B, D) Beclin, and calcineurin normalized to protein stain in total cell lysates and actin was used as a loading control. Graph represents mean ± S.E.M., *P<0.05 vs glucose and +P<0.05 vs palmitate; one-way ANOVA, n = 3, A.U.; arbitrary unit. **Note:** all the presented lanes are from the same membranes. Non-adjacent lanes from the same membranes are separated by a black line between the lanes. All the experiments were repeated three times. First two times experiments were performed with n=1 and the final experiment was performed with n=3 technical replicates on which statistical analysis was performed.

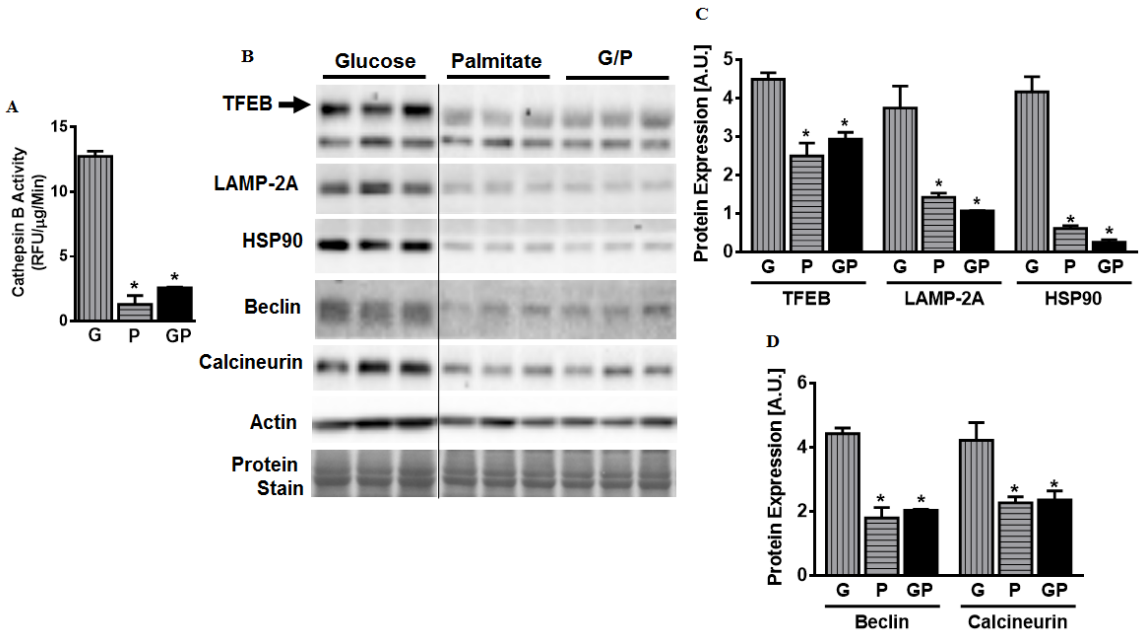

Figure 3.14. In ARCMs glucolipotoxicity mediated suppression in proteolytic activity is associated with low CMA proteins and depletion of myocyte TFEB content. ARCMs were incubated with glucose (G; 30 mM), palmitate (P; 1.2 mM) and glucose/palmitate (GP; 30/1.2 mM) for 17 h, followed by 3 h starvation in the presence of EBSS media prior to cell harvest. (A) Cathepsin B activity was measured in total cell lysates. All cathepsin B measurements are represented as change in RFU per minute corrected to µg of protein (RFU/min/µg). (B) Immunoblot and (C and D) densitometric analysis were performed to examine the protein levels of (B, C) TFEB, LAMP-2A and Hsp90, (B, D) Beclin, and calcineurin normalized to protein stain in total cell lysates and actin was used as a loading control. Graph represents mean ± S.E.M., *P<0.05 vs glucose and +P<0.05 vs palmitate; one-way ANOVA, n = 3, A.U.; arbitrary unit. **Note:** all the presented lanes are from the same membranes. Non-adjacent lanes from the same membranes are separated by a black line between the lanes. All the experiments were repeated three times. First two times experiments were performed with n=1 and the final experiment was performed with n=3 technical replicates on which statistical analysis was performed.

3.5. Diet-induced obese mice display glucose intolerance, insulin resistance and moderate cardiac hypertrophy

After having characterized the inhibitory effect of nutrient overloading on myocytes ex vivo, we further recapitulated these findings in-vivo using mouse models of obesity and diabetes, which are more clinically more relevant to human health and disease. To examine the impact of obesity and diabetes on cardiac autophagy, we fed C57BL6J mice a HFHS diet with 45% kcal from fat for 16 weeks to simulate glucolipotoxicity. This type of diet and length of feeding is reported to cause mild to moderate glucolipotoxicity in multiple tissues including the heart (Pulinilkunnil, Kienesberger et al. 2014). Consistent with previous diet-induced obesity studies (Pulinilkunnil, Kienesberger et al. 2014), our mice fed HFHS diet exhibited increases in body weight **(Figure 3.15 A)** and fed blood glucose levels **(Figure 3.15 B)**. Metabolic inflexibility in HFHS fed mice was evident from systemic glucose intolerance **(Figure 3.15. C)** and insulin resistance **(Figure 3.15. D),** when compared to chow fed controls as assessed by intraperitoneal glucose tolerance test (GTT) and insulin tolerance test (ITT), respectively. Systemic changes were also associated with early signs of cardiac hypertrophy in mice fed HFHS diet as indicated by an increased ratio of ventricle weight to tibia length **(Figure 3.15. E)**. Taken together, our data are in agreement with previous studies (Xu, Hua et al. 2013, Zhang, Xu et al. 2013, Pulinilkunnil, Kienesberger et al. 2014), demonstrating that mice fed HFHS diet exhibit obesity, pre-diabetes, glucose intolerance, insulin resistance.

3.6. Dysregulated mitochondrial protein levels, ER stress and ATP insufficiency in the obese myocardium is associated with upregulation of mTOR signaling

We further examined if HFHS diet feeding for 16 weeks impaired myocardial health. Indeed, hearts from HFHS diet fed mice when compared to chow control showed decreased level of MTCO1 (complex IV subunit of mitochondrial electron transport chain), and increased content of CCAAT-enhancer-binding protein homologous protein (CHOP; transcriptional inducer of cell death), and calreticulin (ER stress marker) (**Figure 3.16. A-B)**, suggesting that nutrient overload is sufficient to induce mitochondrial, nuclear and ER distress in cardiac tissue.

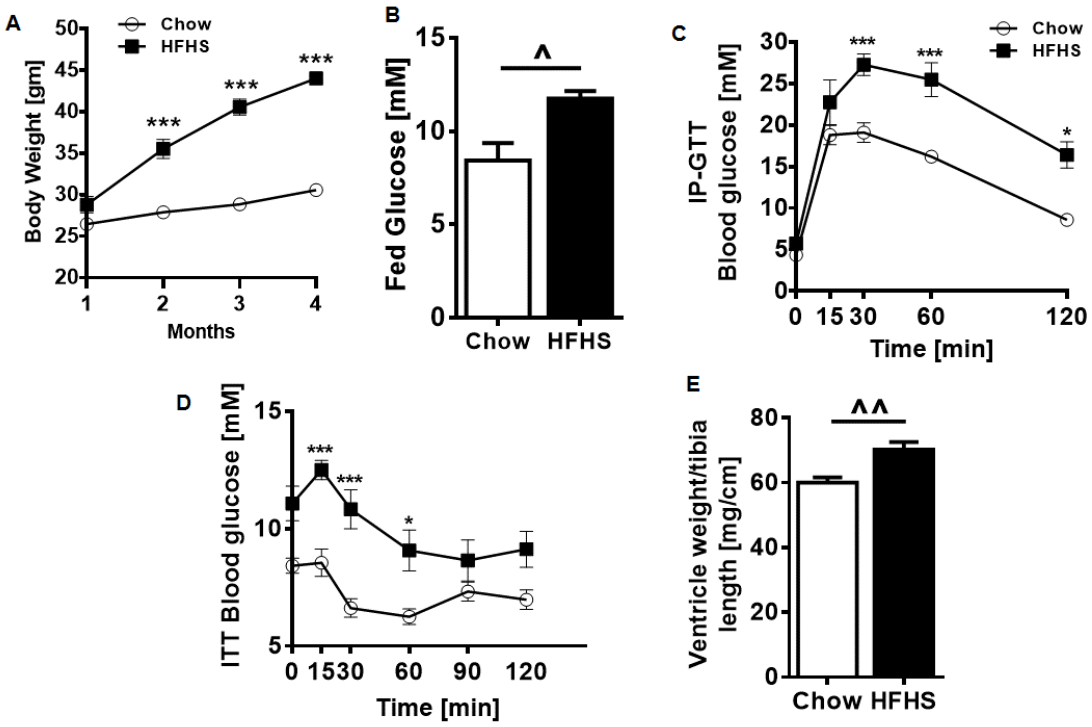

Figure 3.15. Mice fed HFHS diet for 16 weeks are obese, diabetic and exhibit early sign of cardiac dysfunction. (A) Body weight, (B) fed blood glucose, (D) intraperitoneal glucose tolerance test (n = 6-8, ***P<0.001; two way ANOVA), (E) insulin tolerance test (n = 6-8, ***P<0.001; two way ANOVA) and (E) ratio of ventricular weight to tibia length in mice fed either chow or HFHS diet for 16 weeks (n = 8-10, ^P<0.05, ^^P<0.01, ^^^P<0.001; Student's t-test). A.U.; arbitrary unit.

We next investigated whether HFHS diet feeding alters mTOR signaling in mice hearts, since the activation of the mTOR pathway induces insulin resistance (Ginion, Auquier et al. 2011, Blagosklonny 2013) and inhibits autophagy (Xu, Hua et al. 2013, Zhang, Xu et al. 2013). Notably, obese mice hearts exhibited increases in activating phosphorylation of mTOR at Ser^{2448} and total mTOR levels **(Figure 3.16. C-D)**. The two downstream substrates of mTOR, P70S6 kinase (p70S6K) and ribosomal S6, were also upregulated in obese mice hearts compared to chow fed control mice **(Figure 3.16. C-D)**. In addition, we examined the level of AMPK α, a master regulator and sensor of cellular energy that is activated in response to low ATP levels and activates autophagy (Kim, Kundu et al. 2011) by inhibiting mTOR signaling. We found that hearts from mice fed HFHS diet demonstrated a decrease in the phosphorylated AMPK (Thr^{172}) to total AMPK ratio compared to chow fed mice **(Figure 3.16. C-D),** suggesting a loss of AMPK activation. Consistent with prior findings (Xu, Hua et al. 2013, Zhang, Xu et al. 2013) our data from HFHS died fed mice show a loss of AMPK activation, relieving its inhibition on mTOR, rendering mTOR more active to plausibly supress autophagy.

3.7. Autophagic flux is impaired in the obese myocardium

Prior studies have demonstrated that diet induced obesity remodels the macroautophagy pathway in the heart (Li, Woollard et al. 2012, Cui, Yu et al. 2013, Guo, Zhang et al. 2013, Xu, Hua et al. 2013, Jaishy, Zhang et al. 2015). Our data show that in the heart of mice fed HFHS diet, there were higher LC3B-I and lower LC3B-II protein levels, indicating reduction in the rate of autophagosome formation as normal rate of autophagosome formation would result in equal level of both LC3B-I and LC3B-II proteins **(Figure 3.17. A-B)**. Furthermore, the ratio of LC3B-II to its non-lipidated form LC3B-I was also significantly decreased when compared to chow control mice **(Figure 3.17. A-B)**, signifying impaired autophagosome formation. To explain the underlying cause for decline in LC3B-II, we examined the content of autophagy adaptor protein p62/SQSTM1 (Bjorkoy, Lamark et al. 2005). There was a significant increase in p62/SQSTM1 protein content in obese mouse heart when compared to chow control mice **(Figure 3.17. A-B)**, likely indicating a reduced rate of autophagosome formation as free form of p62/SQSTM1 or

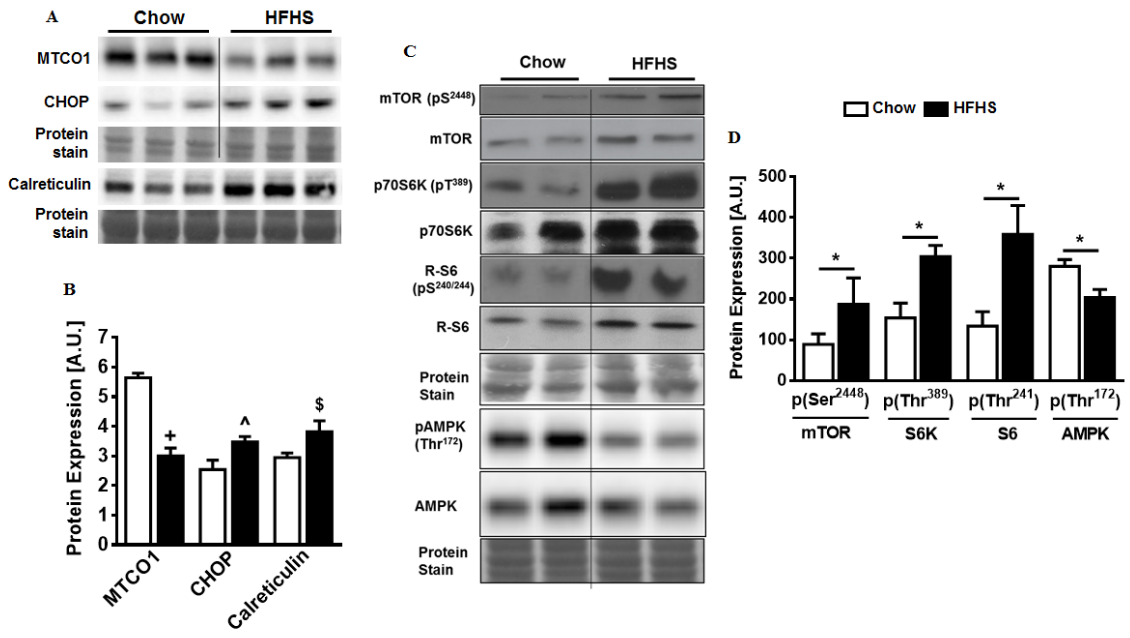

Figure 3.16. Mice fed HFHS diet for 16 weeks exhibit early sign of ER stress and cell death pathway. (A) Immunoblot and (B) densitometric analysis of protein levels of (A, B) MTCOI, CHOP and calreticulin, (C, D) mTOR phosphorylated at Ser^{2448}, ribosomal S6 phosphorylated at $Ser^{240/244}$ and S6 kinase (P70S6K) phosphorylated at Thr^{389} in hearts of mice fed either chow or HFHS diet. (n = 8-10, $P<0.05, ^P<0.01, +P<0.001; Student's t-test). A.U.; arbitrary unit. **Note:** all the presented lanes are from the same membranes. Non-adjacent lanes from the same membranes are separated by black line between the lanes.

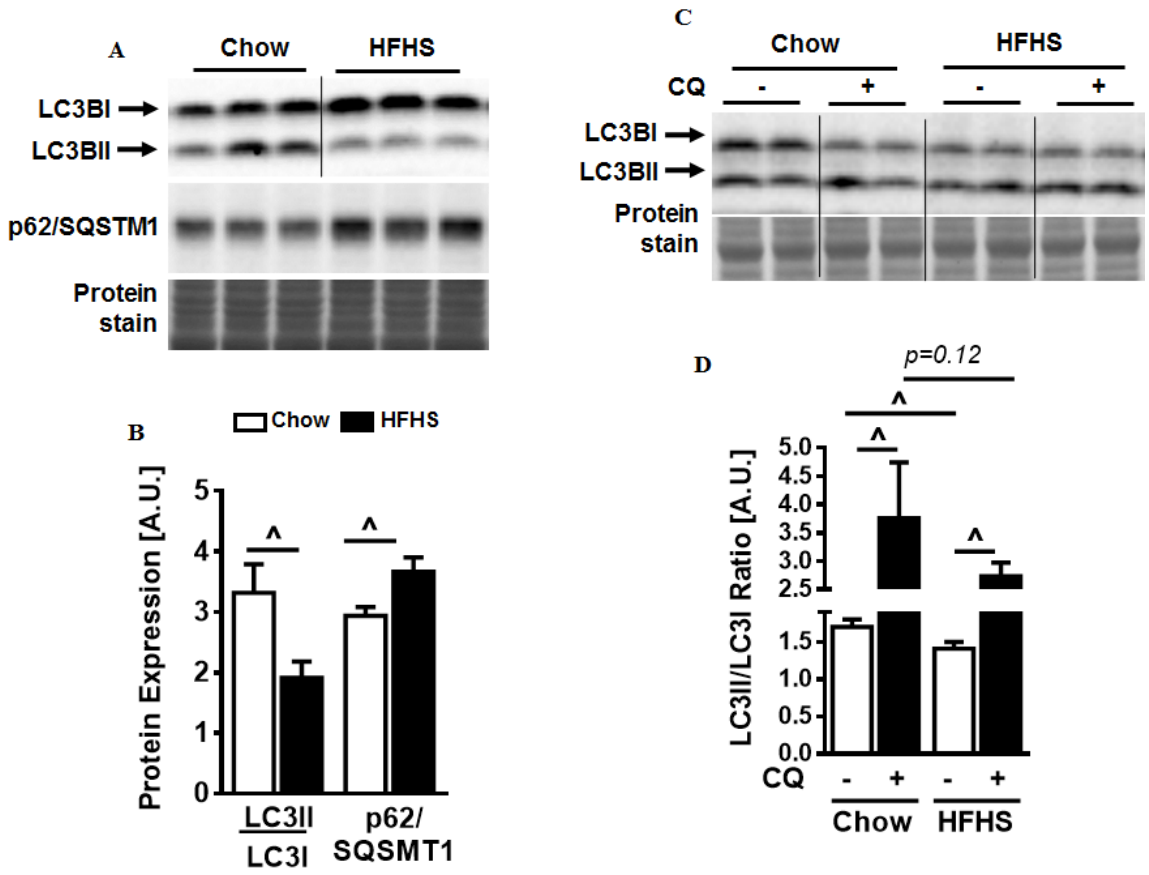

Figure 3.17. Autophagosome turnover is impaired in obese mice heart. (A) Immunoblot and (B) densitometric analysis of protein levels of (A, B) LC3B and (A, B) p62/SQSTM1 in hearts of mice fed either chow or HFHS diet for 16 weeks. (C) Immunoblot and (D) densitometric analysis of protein levels of LC3B in hearts of mice fed either chow or HFHS diet for 16 weeks and treated with either saline or CQ at 48 h, 24 h and 3 h prior to euthanasia. (n = 8, ^P<0.05; Student's t-test). A.U.; arbitrary unit. **Note:** all the presented lanes are from the same membranes. Non-adjacent lanes from the same membranes are separated by black line between the lanes.

non-autophagosome bound p62/SQSTM1 gets accumulated in the cytoplasm. The impairment in autophagosome synthesis was further clarified by examining autophagic flux in chow and HFHS diet fed mice injected with CQ. In chow fed hearts, CQ treatment resulted in autophagosome accumulation as measured by a 2.2-fold increase in LC3B-II to LC3B-I ratio when compared to saline control **(Figure 3.17. C-D)**. However compared to chow control group, in hearts from mice fed HFHS diet, CQ induced autophagosome accumulation exhibited a declining trend, which was not statistically significant **(Figure. 3.17. C-D and D)**. Overall, these data suggest that formation of autophagosome is perturbed following diet induced obesity which is likely due to mTOR hyperactivation. We next examined if disruption in autophagosome formation in the obese myocardium could be a compensatory outcome to render lysosome dysfunctional and incapable to be clear autophagosomal load during obesity.

3.8. Reduction in lysosomal proteolytic activity is associated with decreased level of TFEB and signalling effectors of CMA in the obese diabetic heart

To deduce whether the impairment in autophagosome formation and its clearance in HFHS fed mice heart, is a consequence of alteration in lysosomal enzyme activity, we measured lysosomal proteolytic activity. We observed that cathepsin B activity was decreased in obese mice heart compared to chow fed control mice respectively **(Figure 3.18. A)**, suggesting that glucolipotoxic environment in obese heart is sufficient to inhibit lysosomal function by decreasing cathepsin B activity. Decline in lysosomal proteolytic activity was associated with decreased LAMP-2A and Hsc70 content in HFHS diet fed mice heart **(Figure 3.18. B-C)** compared to chow control mice, in the absence of any changes in Hsp90 **(Figure 3.18 B-C)**. Our data demonstrate that diet-induced obesity exert a negative influence on lysosomal protein content which drive the process of chaperone mediated autophagy to facilitate protein degradation in the lysosome (Eskelinen, Illert et al. 2002, Massey, Kaushik et al. 2006). Indeed, we observed a significant reduction in the nuclear TFEB content within the heart of HFHS fed mice **(Figure. 3.18 D-E),** suggesting loss of TFEB action. In nutrient-rich conditions, TFEB is retained on the cytosolic side of the lysosome via inhibitory serine phosphorylation, whereas, upon stimulation such as starvation or stress, TFEB is dephosphorylated, leading to its activation

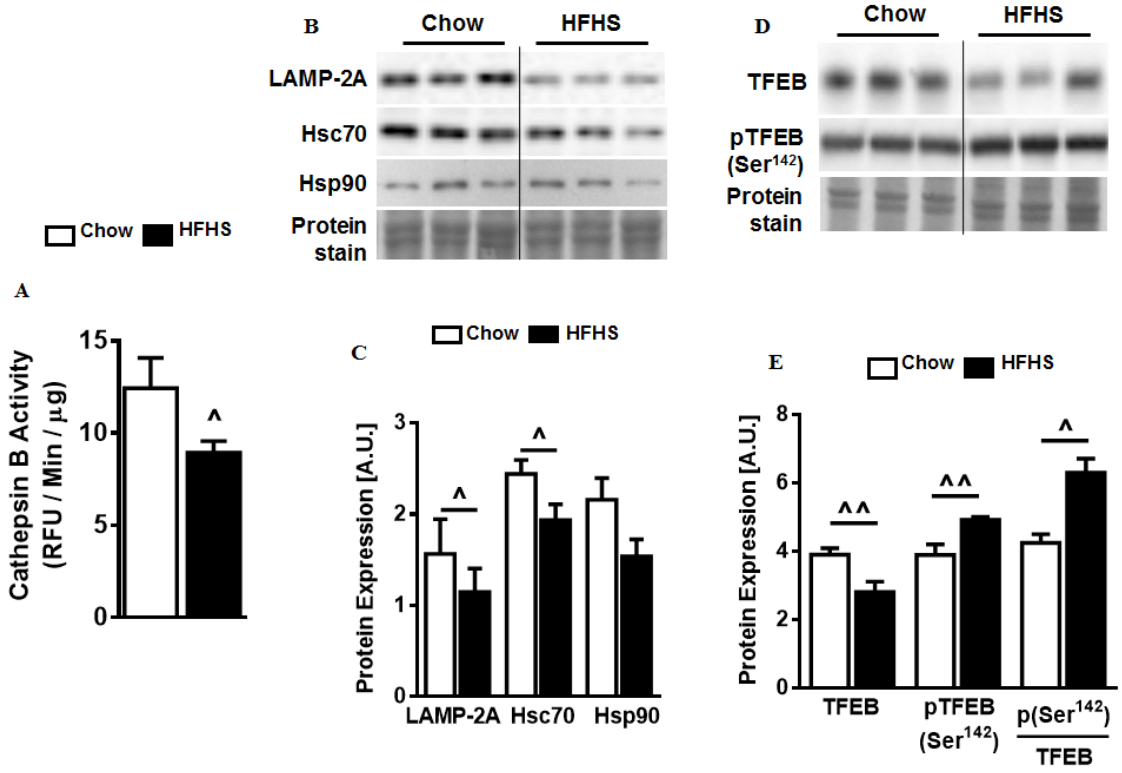

Figure 3.18. Decrease in lysosomal proteolytic activity in the obese heart is associated with suppressed CMA protein content and increased inhibitory phosphorylation of TFEB. (A) Cathepsin B activity in the heart of mice fed either chow or HFHS diet for 16 weeks. All cathepsin B measurements are represented as change in RFU per minute corrected to µg of protein (RFU/min/µg). (B) Immunoblot and (C) densitometric analysis of protein levels of (B-C) LAMP-2A, Hsc70 and Hsp90 from crude lysosomal membrane protein fraction, (D, E) TFEB from nuclear membrane protein fraction and phosphorylated TFEB at Ser^{142} from cytosolic soluble protein fraction in the hearts of mice fed HFHS diet for 16 weeks. (n = 3 to 7, ^P<0.05, ^^P<0.01, ^^P<0.001; Student's t-test). A.U.; arbitrary unit. **Note:** all the presented lanes are from the same membranes. Non-adjacent lanes from the same membranes are separated by black line between the lanes.

and translocation into the nucleus to increase transcription of genes involved in lysosomal autophagy (Sardiello, Palmieri et al. 2009, Settembre, Fraldi et al. 2013, Shen and Mizushima 2014). A significant increase in the stoichiometric ratio of TFEB (Ser^{142}) to total TFEB was observed in the heart of mice fed HFHS diet **(Figure. 3.18. D-E)** when compared to chow fed control mice highlighting the inhibitory effect of glucolipotoxicity on TFEB in obese and diabetic myocardium. Taken together, these data suggest that glucolipotoxic environment in obese and diabetic myocardium augmented inactivating phosphorylation of TFEB and prevent nuclear localization of TFEB resulting in likely decreasing TFEB action on lysosomal autophagy and function in the heart.

3.9. Severe diabetes in the absence of obesity is sufficient to dysregulate macroautophagy, impair lysosome function and TFEB levels in the murine heart

Given that the HFHS diet not only cause insulin resistance and diabetes but also obesity, we sought to distinguish the effects of obesity from diabetes on macroautophagy using a type 1 diabetic (non-obese) mouse model (Akita mice). Consistent with the previous findings (Basu, Oudit et al. 2009), Akita mice demonstrated hyperglycemia (*Ins2*$^{WT/WT}$: 9.2 ± 0.6 mmol/L glucose; *Ins2*$^{WT/C96Y}$: 31.6 ± 1.7 mmol/L glucose: n=3; P<0.0003) and decreased body weight (Ins2$^{WT/WT}$: 28.5 ± 0.43 g; Ins2$^{WT/C96Y}$: 24.4 ± 0.33 g; n=3; P<0.05) compared to their wild type (WT) control mice**.** In the Akita mouse heart, ratio of LC3B-II/LC3B-I was significantly increased when compared to WT mice **(Figure. 3.19 A-B)**. Furthermore, we observed a significant increase in the level of p62/SQSTM1 compared to WT mice **(Figure. 3.19 A-B),** suggesting that autophagosome clearance is impaired in Akita mouse heart. Since proteins participating in macroautophagy such as LC3B-II were reciprocally regulated in two distinct models of metabolic inflexibility and given that these proteins are degraded in the lysosome, we speculated that inefficient lysosomal proteolysis due to impaired CMA process could explain the differential effect on LC3B-II content (Massey, Kaushik et al. 2006). Indeed, we found that cathepsin B activity and content of lysosome proteins such as LAMP-2A, Hsp90 and Hsc70 were suppressed in Akita mice heart compared to their wild type control mice **(Figure. 3.19. D-E)**.

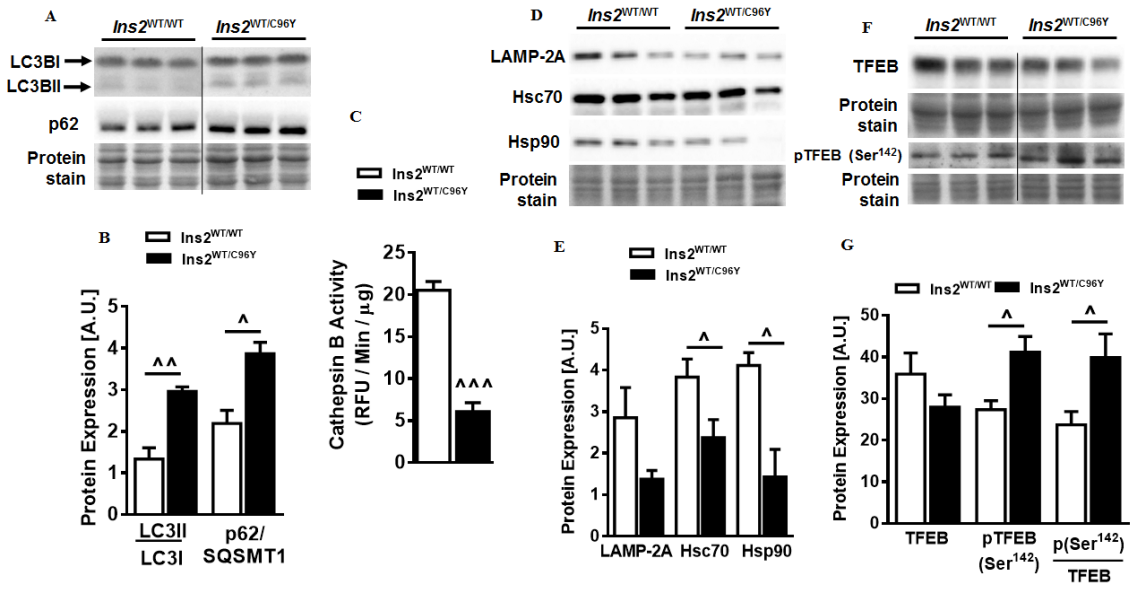

Figure 3.19. Akita mice heart exhibit decrease in proteolytic activity is associated with decrease in CMA proteins and TFEB levels with concomitant increase in inhibitory phosphorylation of TFEB. (A) Cathepsin B activity was measured in 12 weeks old Akita mice heart. (B, D, F) Immunoblot and (C, E, G) densitometric analysis of protein levels of (B, C) LC3B, p62/SQSTM1, (D, E) LAMP-2A, Hsc70 and Hsp90 from crude lysosomal membrane protein fraction, (F, G) TFEB from nuclear membrane protein fraction and phosphorylated TFEB at Ser^{142} from cytosolic soluble protein fraction in 12 week old Akita mice hearts. (n = 3, ^P<0.05, ^^P<0.01, ^^P<0.001; Student's t-test). A.U.; arbitrary unit. **Note:** all the presented lanes are from the same membranes. Non-adjacent lanes from the same membranes are separated by black line between the lanes.

Moreover changes in proteolytic activity and CMA protein levels corresponded with decrease in nuclear TFEB content with concomitant increase in inhibitory phosphorylation of TFEB in Akita hearts **(Figure 3.19 F-G)** signifying the impairment in role of TFEB in regulating lysosome function following severe diabetes.

Taken together, these data suggest that glucolipotoxic environment in obese and diabetic myocardium augmented inactivating phosphorylation of TFEB and prevented nuclear localization of TFEB likely resulting in loss of TFEB action on lysosomal autophagy and function in the heart.

CHAPTER 4: DISCUSSION

Diabetic cardiomyopathy, a disorder of heart muscle in obese and diabetic patients, occurs due to structural abnormalities of cardiomyocytes, eventually leading to systolic and diastolic dysfunction and heart failure (Boudina and Abel 2010, Isfort, Stevens et al. 2014). In experimental obese and diabetic models, altered cardiac energy metabolism is the earliest change observed prior to the onset of cardiomyopathy (Abe, Ohga et al. 2002, An and Rodrigues 2006, Bugger and Abel 2009). However, in human cases of diabetic cardiomyopathy, metabolic changes are underestimated due to rapidity of metabolic transformation, underdiagnoses and delayed detection ((Asghar, Al-Sunni et al. 2009)). During diabetes, insulin deficiency or its functional insufficiency promotes hyperglycemia with concomitant FA overutilization resulting in glucotoxicity (Cai, Li et al. 2002, Ghosh, An et al. 2004, Ghosh, Pulinilkunnil et al. 2005) and lipotoxicity (van der Vusse, van Bilsen et al. 2000, van de Weijer, Schrauwen-Hinderling et al. 2011, Wende, Symons et al. 2012), both conditions collectively referred to as "glucolipotoxicity" (Kim and Yoon 2011, Las, Serada et al. 2011, Karunakaran, Kim et al. 2012). Although metabolic remodeling and glucolipotoxicity in the diabetic heart have been shown to primarily cause mitochondrial dysfunction (Aon, Bhatt et al. 2014) and ER stress (Karunakaran, Kim et al. 2012, Yang, Zhao et al. 2015), pathological effects could also be attributed to dysregulation of other cellular systems. Indeed, lack of insulin function during obesity and diabetes induces dysfunctional proteolysis, which overwhelms the ER and compromises protein quality control (Tsuchiya, Saito et al. 2016). Loss of protein quality control leads to inhibition of protein degradation and promotes build-up of misfolded proteins, accumulation of dysfunctional mitochondrial, ROS overproduction and cell death. Indeed, functional defects in diabetic muscle, liver and islet are strongly associated with impaired ubiquitin-mediated proteasomal protein degradation and cytotoxic protein aggregation termed as "proteotoxicity" (Willis and Patterson 2013). Therefore, it stands to reason that proteotoxic stress secondary to glucolipotoxicity could be an early maladaptation in the diabetic heart, progressing to cardiomyopathy. Reduction of proteotoxic load not only occurs in proteasomes (Tsukamoto, Minamino et al. 2006) but also within lysosomes by a process known as autophagy. Protein degradation by autophagy within the lysosome is a coordinated action of macroautophagy (pre-lysosomal), chaperone-mediated autophagy (at

the lysosome level) and proteases (post-lysosomal) (Tanida 2011). Aberrations in autophagy processes results in impaired proteostasis leading to proteotoxicity. Significant accumulation of amylin oligomers, fibrillar tangles and plaques were observed in failing lipid-laden hearts of obese patients, which was further exacerbated with diabetes (Despa, Margulies et al. 2012) suggesting proteotoxic buildup in early stages of diabetes. Therefore, it is plausible that changes in lysosome function and abundance could significantly impact cellular metabolism in the setting of glucolipotoxicity observed during obesity and diabetes. My thesis work uncovered one of the mechanisms by which glucolipotoxicity contributes to cellular proteotoxic load in the heart. Data from my thesis suggest that 1) ex-vivo H9C2 rat cardiomyofibroblasts and neonatal rat cardiomyocytes exposed to high palmitate alone or in combination with high glucose exhibited impaired autophagic flux with concomitant decline in cellular TFEB and CMA proteins LAMP-2A, Hsc70, and Hsp90, which facilitate initiation of CMA; 2) In ex-vivo studies loss of TFEB is likely due to decreased calcineurin protein levels reflected in decreases in CMA, lysosomal content and proteolytic activity; 3) During diet-induced obesity, in-vivo suppression of myocardial autophagic flux was secondary to increased mTOR signaling and decreased AMPK phosphorylation, effects which persisted in diabetes in the absence of obesity; 4) Lack of autophagosome maturation, fusion and turnover in the obese and diabetic heart was associated with decreased lysosomal proteolytic activity and TFEB content; 5) Both in-vivo models (diet-induced obesity and obesity-independent diabetes) increased inhibitory phosphorylation of TFEB at serine residue 142 in the heart, likely preventing nuclear localization of TFEB and inhibiting induction of lysosomal autophagy.

In experimental models of obesity and diabetes, “glucolipotoxic” effects are observed prior to the onset of diabetic cardiomyopathy (Ghosh, An et al. 2004, Sharma, Adrogue et al. 2004, Buchanan, Mazumder et al. 2005, Pulinilkunnil, Kienesberger et al. 2013, Pulinilkunnil, Kienesberger et al. 2014), suggesting that the glucolipotoxic milieu in the heart may precipitate cardiomyocyte dysfunction. Although full-state glucolipotoxicity is known to modulate protein degradation pathway (Las, Serada et al. 2011), it was not entirely clear whether glucolipotoxic-induced dysregulation of proteolytic pathways was due to individual glucolipotoxic substrates or substrates in combination. Since in-vivo models of obesity and diabetes are limited in their ability to uncover precise effects of

individual substrates on lysosomal signaling, we sought to dissect the role of individual or combinations of glucolipotoxic substrates on cardiac health and autophagy using ex-vivo models of H9C2 rat cardiomyoblast and NRCM cells. Two different fatty acids were utilized due to their natural abundance in human blood and tissues; palmitic acid (saturated fatty acid) and oleic acid (mono unsaturated fatty acid), either alone or in combination with glucose to create a glucolipotoxic environment within the cells in order to mimic physiologically relevant substrate exposure. Consistent with prior research, we found that H9C2 and NRCMs cells exposed a combination of glucose/palmitate elevated the LC3B-II/LC3B-I ratio. This increase in LC3B-II/LC3B-I ratio suggested decreases in autophagosome clearance within the lysosome or increases in autophagosome formation. Since autophagosome accumulation is indicative of impaired lysosomal clearance of autophagic load, we assessed autophagic flux in the presence or absence of chloroquine, a lysosome de-acidifier which inhibits autophagosome-lysosome fusion resulting in autophagosome accumulation. Indeed, H9C2 and NRCM cells exposed to excess palmitate and a combination of glucose/palmitate did not elicit additional increases in LC3B-II content when treated with chloroquine signifying impaired autophagic flux, which is in agreement with previous studies (Jaishy, Zhang et al. 2015, Kanamori, Takemura et al. 2015). Indeed, our immunoblot data was also consistent with imaging data which showed increased yellow fluorescent autophagosomal puncta in H9C2 cells treated with palmitate alone or a combination of glucose/palmitate. Therefore, a combination of glucose and palmitate profoundly inhibited macroautophagic function, and this suppression was associated with augmented cleavage of caspase-3, a surrogate marker for cell death. Notably, it has been demonstrated in pancreatic islet cells that glucolipotoxicity-induced impairment of autophagosome turnover is associated with cell death (Las, Serada et al. 2011). Interestingly, upon examining individual substrate effects, palmitate (saturated FA) but not oleate (unsaturated FA) was found to induce greater suppression of autophagic flux in both cardiomyoblasts (H9C2) and primary cardiomyocytes (NRCMs). Importantly, glucose/palmitate-induced macroautophagic dysregulation and cell death/glucolipotoxicity was reversed when glucose/palmitate was incubated in a combination with oleate. We hypothesize that distinct effects of oleate and palmitate on autophagic flux might be an outcome of fatty acid specific targeting of distinct arms of the autophagy pathway, since a

recent study demonstrated that oleate stimulates non-canonical autophagy distinct from palmitate and independent of classical autophagy regulators (Bankaitis 2015).

Extrapolating ex-vivo data to an in-vivo setting is important due to the metabolically complex nature of development and maintenance of diabetic cardiomyopathy. Furthermore, the confounding influence of non-cardiomyocyte cells on macroautophagy are not present in primary culture and cell lines. We therefore examined the status of autophagy in whole heart from mice subjected to diet-induced obesity. Following 16 weeks of HFHS diet, mice were found to be pre-diabetic, which is consistent with much prior research (Cui, Yu et al. 2013, Guo, Zhang et al. 2013, Xu, Hua et al. 2013, Jaishy, Zhang et al. 2015). Interestingly, although animals did not exhibit an overt diabetic phenotype, we observed decreased mitochondrial electron transport chain protein level (Pulinilkunnil, Kienesberger et al. 2013, Pulinilkunnil, Kienesberger et al. 2014) and increased ER stress (calreticulin) and cell death (CHOP) markers leading to cellular injury in the hearts of these pre-diabetic animals, consistent with similar findings found in animal models of obese and diabetic cardiomyopathy (Cai, Li et al. 2002, Varga, Giricz et al. 2015). Furthermore, these mice also exhibited early signs of ventricular hypertrophy evidenced by increased ratio of ventricle weight/tibia length, suggesting that even in a pre-diabetic state, characteristic signs of diabetic cardiomyopathy are being observed. Therefore, it appears that our in-vivo model of diet-induced obesity represents an intermediate time-frame, which allowed us to assess whether mild-to-moderate glucolipotoxic damage leads to the progression and development of diabetic cardiomyopathy. In line with prior reports (Prause, Christensen et al. 2014), a glucolipotoxic milieu in the obese myocardium reduced LC3B-II content in response to CQ challenge that paralleled increases in p62/SQSTM1, signifying reduced biosynthesis of autophagosomes. This inhibition of macroautophagy in the obese heart was associated with augmented mTOR signaling and activation of cell death pathways, consistent with prior findings, (Xu, Hua et al. 2013, Zhang, Xu et al. 2013, Jaishy, Zhang et al. 2015). However, unlike obese hearts, LC3B-II levels were upregulated in type-1 diabetic Akita hearts, indicating a distinct regulation of obesity and diabetes on autophagosome clearance and macroautophagy. Indeed, distinct effects of obesity and diabetes are observed in OVE26 type-1 diabetic mouse hearts, wherein macroautophagy is inhibited indicated by decrease in LC3B-II level in diabetic mice (Xie, Lau et al. 2011),

while macroautophagy is elevated in hearts from fructose-fed insulin-resistant rats evidenced by increase in LC3B-II/LC3B-I ratio (Mellor, Bell et al. 2011). It is plausible that dissimilar regulation of LC3B-II content is influenced by the alteration in autophagic flux which is governed by the rate of fusion between autophagosome and lysosome. In agreement with previous reports, blockade of lysosomal autophagy by chloroquine failed to elicit accumulation of LC3B-II in obese hearts suggesting impairment in autophagosome synthesis and hence autophagic flux (Barth, Glick et al. 2010), recapitulating our observation of glucolipotoxicity-mediated inhibition of autophagosome turnover in H9C2 and NRCM cells. Interestingly, LC3B-II levels usually correlate with changes in p62/SQSTM1, a surrogate marker for detecting macroautophagy process (Yang, Carra et al. 2013). However, p62/SQSTM1 levels were augmented in the heart in both models of obesity and diabetes, highlighting a dissociation between p62/SQSTM1 and LC3B-II, and suggesting that increases in p62 content correlates better with impaired lysosomal function.

Since autophagosomes are eventually processed within the lysosome, the reported disparity in macroautophagy data within the heart between models of obesity and diabetes may be attributed to the absence of data on the molecular mechanisms regulating lysosome signaling, biogenesis and function in metabolic disorders. Furthermore, individual or combination of substrates may induce distinct alterations of autophagic processes and failing to examine these contributions may also yield disparate results. We therefore addressed the question whether glucolipotoxic environments alter the levels of proteins driving autophagic signaling in the lysosome and of proteins that regulate lysosomal cargo trafficking and function using in-vivo and ex-vivo models. Since numerous proteins participating in macroautophagy undergo lysosomal degradation, diminished autophagic flux could be a direct consequence of impaired lysosomal signaling and CMA function (Nishino, Fu et al. 2000, Sugimoto, Shiomi et al. 2007). Disruptions in CMA are commonly observed in chronic pathologies such as aging, neurodegeneration, cancer and obesity (Nishino, Fu et al. 2000, Kaushik and Cuervo 2012, Rodriguez-Navarro, Kaushik et al. 2012, Schneider, Villarroya et al. 2015). Disturbances in lysosomal homeostasis can precipitate defects in CMA through effects on cytosolic chaperones, Hsc70 and Hsp90 and CMA receptor, LAMP-2A (Cuervo 2004, Orenstein and Cuervo 2010). Notably, heart from patients with Danon's disease carry mutations in genes that encode for LAMP-2, resulting

in toxic accumulation of autophagic vacuoles and cardiomyopathy (Nishino, Fu et al. 2000, Sugimoto, Shiomi et al. 2007). Consistently in H9C2, NRCMs and ARCM, it was observed that when myocytes were exposed to either high palmitate or a combination of high glucose and palmitate, the levels of key CMA proteins such as LAMP-2A and Hsp90 were suppressed. This observation was further recapitulated in-vivo in murine models of obesity and diabetes, wherein we observed that lysosomal LAMP-2A, Hsc70 and Hsp90 protein content in the heart were decreased at a time when mice exhibit cardiac dysfunction (Pulinilkunnil, Kienesberger et al. 2014). A likely mechanism by which glucolipotoxic moieties perturb CMA protein stability is by altering the lipid composition of lysosomal microdomains causing LAMP-2A degradation. This mechanism was demonstrated in liver from mice fed high-cholesterol diet (Koga, Kaushik et al. 2010, Rodriguez-Navarro, Kaushik et al. 2012). Moreover, during ischemic injury, diminished LAMP-2A content sensitizes myocardium to protein aggregation and ROS-induced cell death (Ma, Liu et al. 2012). Whether glucolipotoxicity could alter the lipid composition of lysosomal microdomains in the heart and influence CMA signaling and cardiac function remains to be examined. Changes in CMA protein content correlated with decreases in cathepsin B activity, a surrogate marker for lysosomal proteolysis in all tested models; NRCMs, H9C2, ARCM, diet-induced obesity and in a model of severe type 1 diabetes (Akita). Indeed, 16 h exposure to glucolipotoxic milieu has been found to impair LAMP activity and CMA in macrophages (Schilling, Machkovech et al. 2013) and hepatocytes (Rodriguez-Navarro, Kaushik et al. 2012, Schneider, Suh et al. 2014), data consistent with our studies. Lysosomal proteolytic activity is an indicator of lysosome function and content within the myocyte. Our observation that exposure to palmitate and glucose-palmitate combination decreased lysosomal staining in H9C2 and NRCM cells, suggesting that lysosomal content and/or function is suppressed following exposure to these substrates, which is in agreement with prior studies. Notably, ROS production increases following glucolipotoxicity-induced lysosomal dysfunction in pancreatic β cells, which could be likely occurring in our model (Barlow and Affourtit 2013).

Lysosomal CMA protein dysregulation could be secondary to defects in lysosomal biogenesis and function (Sardiello 2016). Lysosomal content and function is transcriptionally regulated by bHLH/LZ TFEB. Activation of TFEB induces transcription

of CLEAR network genes involved in autophagosome formation, autophagosome-lysosome fusion and lysosomal biogenesis and function. During obesity and diabetes, decreases in the level of proteins driving lysosomal CMA corresponded with a decrease in nuclear TFEB levels. A crucial finding in this study was the observation that palmitate alone downregulated TFEB in cardiomyoblasts and cardiomyocytes, an affect that was not observed with exposure to oleate or glucose alone. These data point to a nutrient (FA) specific regulation of TFEB levels in the heart. Moreover, nutrient overload with palmitate alone or in combination with glucose resulted in loss of TFEB and CMA protein content, thereby clarifying the mechanism by which glucolipotoxicity suppresses lysosomal autophagy in-vivo. Not only lack of TFEB but also changes in phosphorylation and localization of TFEB is reported to influence TFEB action (Martina, Chen et al. 2012). During nutrient overload, TFEB is phosphorylated on serine residues by mTOR and ERK and rendered inactive, blocking entry of TFEB into the nucleus (Settembre, Zoncu et al. 2012, 2015). However, during fasting, mTOR inhibition enables TFEB to be dephosphorylated by calcium-activated phosphatase calcineurin (Medina, Di Paola et al. 2015), promoting TFEB translocation into the nucleus. Indeed, in our studies, following obesity and diabetes, TFEB Ser^{142} phosphorylation was increased in the heart explaining the decreases in nuclear TFEB. Furthermore, in our ex-vivo model of glucolipotoxicity, the decreases in cellular TFEB was accompanied by a robust decline in calcineurin protein levels signifying yet another mechanism by which TFEB content in the heart is targeted by glucolipotoxicity. Our data on TFEB regulation is in agreement with a prior report confirming the role of TFEB in autophagic dysregulation observed during the pathogenesis of amyloid induced cardiac proteotoxicity (Guan, Mishra et al. 2015). In this model, dysregulation of autophagy lead to the accumulation of depolarized mitochondria, subsequent generation of ROS, and eventual cellular dysfunction and cell death that was rescued by transient overexpression of TFEB (Guan, Mishra et al. 2015). Our study suggests that loss of TFEB and lysosomal insufficiency are among the earliest insults to cardiomyocytes following glucolipotoxicity, which results in dysregulation of autophagy, mitochondrial dysfunction, ROS production, ER stress and ultimately cellular death and myocyte dysfunction.

CHAPTER 5: CONCLUSION

Role of proteasomal degradation pathway in the heart have been known from the prior research (Weekes, Morrison et al. 2003, Willis and Patterson 2013). However, it is still unknown whether non-proteasomal degradation pathways modulate functional outcomes of metabolic cardiomyopathy. Physiological reduction of proteotoxic load also occurs within lysosomes by macroautophagy, and CMA, processes that are critical for maintaining energetic balance (Settembre, Fraldi et al. 2013) and organelle homeostasis (Kaushik and Cuervo 2012). Dysfunctional lysosomes are observed in the pathologies of aging (Kaushik and Cuervo 2012), neurodegeneration, cancer, lipid overload, ischemia and metabolic syndrome. Lysosomal proteins are also transcriptionally regulated by bHLH-leucine zipper TFEB which induces lysosomal biogenesis by activating genes part of the CLEAR network. Since TFEB alterations influence autophagy, it is plausible that decrease in TFEB levels during obesity and diabetes could impact lysosome function and proteolytic activity, thereby impairing macroautophagy and CMA mediated proteostasis. Plausibly glucolipotoxicity alters TFEB levels and inhibits lysosomal autophagy and function thereby rendering the obese and diabetic heart susceptible to proteotoxicity, ER and mitochondrial dysfunction and cardiomyopathy. Our studies in ex-vivo models of glucolipotoxicity demonstrated that 1) palmitate alone or in combination with glucose induces "gluco-palmitotoxic" milieu with concomitant cell death in H9C2 and NRCM cells; 2) H9C2 and NRCM cells exposed to glucolipotoxic substrates, impairs autophagosome turnover; 3) glucolipotoxicity-induced cellular TFEB loss is associated with decrease in lysosome abundance, proteolytic activity and content of key CMA proteins in H9C2, NRCM and ARCM cells. Furthermore, using in-vivo models, we definitively confirmed that; 1) obese and diabetic heart distinctly impair autophagic flux; 2) loss of proteolytic activity and decrease in CMA protein content in both obese and diabetic heart, is possibly due to decrease in nuclear TFEB content and 3) both types of metabolic distress (obesity and diabetes) increased inhibitory phosphorylation of TFEB at Serine^{142} in the heart likely preventing nuclear localization of TFEB **(Figure 5.1).**

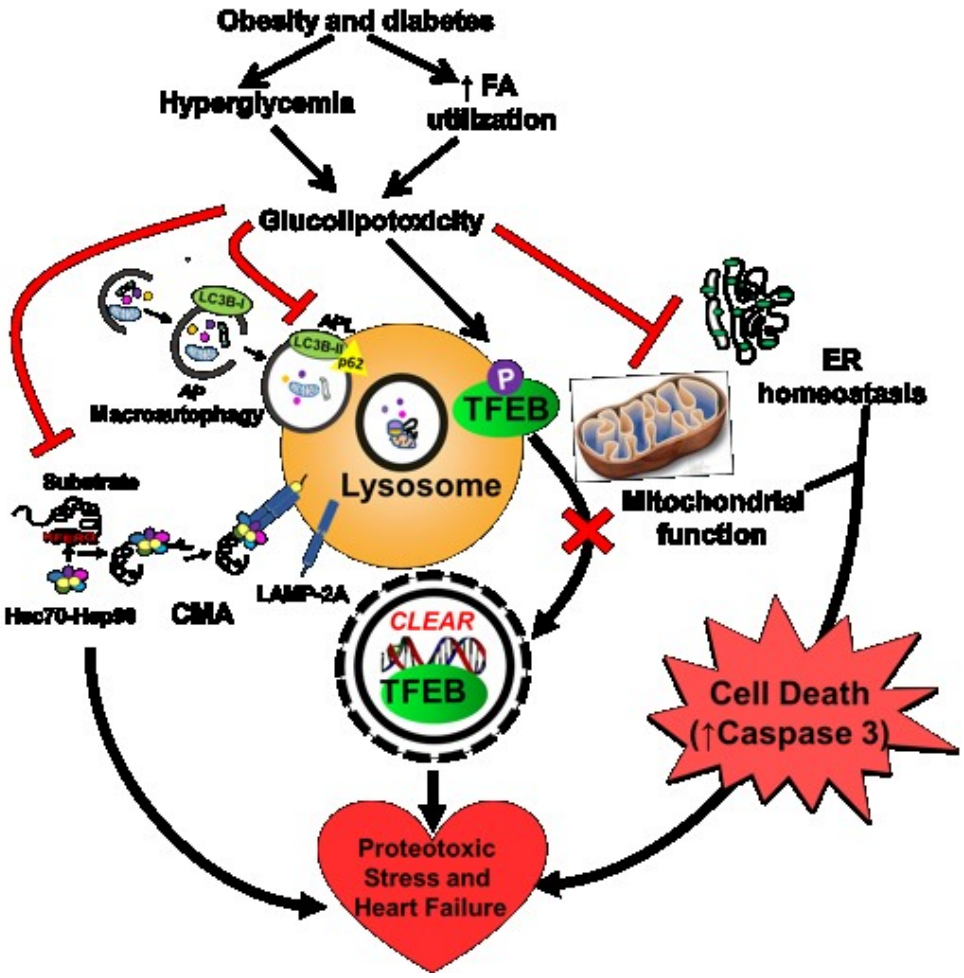

Figure 5.1. During obesity and diabetes, glucolipotoxicity causes cardiomyocyte injury by decreasing TFEB and inhibiting lysosomal autophagy. This study highlights a novel mechanism by which glucolipotoxicity causes myocyte injury. Glucolipotoxicity in the obese and diabetic heart impairs macroautophagy and chaperone mediated autophagy, which is associated with loss of transcriptional regulation by TFEB. Glucolipotoxicity induced loss of TFEB content is likely due to increases in inhibitory phosphorylation of TFEB which will prevent TFEB translocation into the nucleus to promote activation of CLEAR genes to maintain lysosomal autophagy and function. TFEB inhibition compromises lysosome function causing proteotoxicity, ER stress, mitochondrial dysfunction and cell death rendering the obese diabetic heart susceptible to cardiomyopathic failure. AP; autophagosome, APL; autophagosome lysosome fusion.

In summary, our data signify that with increasing severity of glucolipotoxcity there is progressive decline in lysosomal CMA protein content which reduces lysosomal proteolytic activity. Saturated FA per se affect regulation of TFEB and this effect is exacerbated in the presence of high glucose. Since, TFEB activation increases lysosome number and autophagy (Settembre and Ballabio 2011, Settembre, Di Malta et al. 2011) and given that TFEB is a central player of lysosome nutrient sensing machinery (Settembre, Fraldi et al. 2013), the inactivation and loss of TFEB content during obesity and diabetes is expected to impair lysosomal protein degradation and disrupt cardiomyocyte proteostasis. Given that lysosomal autophagy enables cellular waste clearance (Cuervo 2004, Settembre, Di Malta et al. 2011, Singh and Cuervo 2011, Settembre, Fraldi et al. 2013, Shen and Mizushima 2014), selective targeting of cellular TFEB in the obese diabetic heart could prevent or ameliorate cardiomyopathy. In this regard, recent studies have demonstrated that overexpression of TFEB during kidney cysts and neurodegeneration rescues impairment in CMA and restores cellular proteastasis (Martini-Stoica, Xu et al. 2016, Rega, Polishchuk et al. 2016). Indeed, the current study highlights a novel mechanism by which glucolipotoxicity causes cardiomyocyte injury attesting the paradigm that TFEB induced regulation of lysosomal autophagy is vital for cellular homeostasis during obesity and diabetes.

In future, our studies will decipher whether molecular mechanisms regulating TFEB are indispensable for lysosome function and how glucolipotoxicity depletes cellular TFEB content and whether this change is physiologically important for maintaining cardiac function. To address the physiological importance of TFEB in-vivo and ex-vivo, I have already developed and validated adenoviruses overexpressing wild type TFEB **(Figure 5.2.)**. In my doctoral program with Dr. Pulinilkunnil I aim to examine whether TFEB could rescue glucolipotoxicity mediated cardiomyocyte injury. Indeed, my preliminary data demonstrated that we were successful in genetically manipulating TFEB in NRCM cells. To further clarify the central role of TFEB in cardiac energy metabolism, we have developed an inducible cardiac-specific TFEB knockout mouse by utilizing TFEB-floxed mice provided by Dr. Andrea Ballabio. The current view in the field is that macroautophagy and CMA could interchangeably protect cells under normal physiological conditions. We believe that when myocardium is exposed to glucolipotoxicity for a prolonged period,

lysosomal function and CMA is impaired and in this pathological milieu macroautophagy is insufficient to offer adequate cellular protection against glucolipotoxic injury. A recent study showed that when cardiac mitochondrial DNA increasingly evades autophagy, inflammation and dilated cardiomyopathy ensues. My thesis findings concurs with this paradigm wherein normal lysosomal protein degradation is vital for cardiac function during obesity and diabetes. Since lysosomal autophagy enables cellular waste clearance and nutrient catabolism selective targeting of lysosomal proteins in the obese and diabetic heart could attenuate complications and mortality associated with cardiomyopathy.

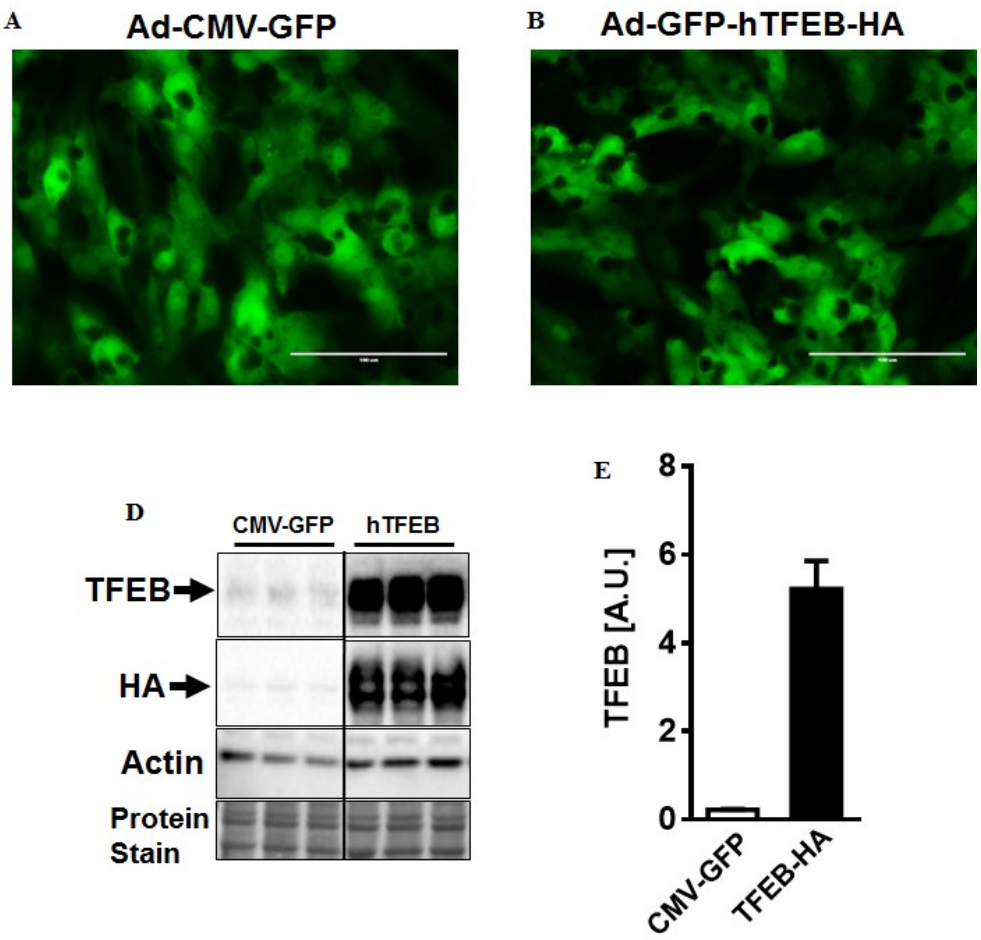

Figure 5.2. Adenovirally mediated overexpression of TFEB in NRCM cells. NRCM cells were infected with adenoviruses overexpresses wild type human TFEB tagged with HA and CMV-GFP was used as a control for 24 hr. (A, B and C) Microscopic images of adenovirally infected cells overexpressed (A) Ad-CMV-GFP and (B) Ad-GFP-hTFEB-HA. (D) Immunoblot and (E) densitometric analysis of protein levels of (D) TFEB and HA from total cell lysates.

REFERENCES:

1. Abe, T., Y. Ohga, N. Tabayashi, S. Kobayashi, S. Sakata, H. Misawa, T. Tsuji, H. Kohzuki, H. Suga, S. Taniguchi and M. Takaki (2002). "Left ventricular diastolic dysfunction in type 2 diabetes mellitus model rats." Am J Physiol Heart Circ Physiol **282**(1): H138-148.
2. Alers, S., A. S. Loffler, S. Wesselborg and B. Stork (2012). "Role of AMPK-mTOR-Ulk1/2 in the regulation of autophagy: cross talk, shortcuts, and feedbacks." Mol Cell Biol **32**(1): 2-11.
3. An, D. and B. Rodrigues (2006). "Role of changes in cardiac metabolism in development of diabetic cardiomyopathy." Am J Physiol Heart Circ Physiol **291**(4): H1489-1506.
4. Aon, M. A., N. Bhatt and S. C. Cortassa (2014). "Mitochondrial and cellular mechanisms for managing lipid excess." Front Physiol **5**: 282.
5. Appelqvist, H., P. Waster, K. Kagedal and K. Ollinger (2013). "The lysosome: from waste bag to potential therapeutic target." J Mol Cell Biol **5**(4): 214-226.
6. Asghar, O., A. Al-Sunni, K. Khavandi, A. Khavandi, S. Withers, A. Greenstein, A. M. Heagerty and R. A. Malik (2009). "Diabetic cardiomyopathy." Clin Sci (Lond) **116**(10): 741-760.
7. Augustus, A., H. Yagyu, G. Haemmerle, A. Bensadoun, R. K. Vikramadithyan, S. Y. Park, J. K. Kim, R. Zechner and I. J. Goldberg (2004). "Cardiac-specific knock-out of lipoprotein lipase alters plasma lipoprotein triglyceride metabolism and cardiac gene expression." J Biol Chem **279**(24): 25050-25057.
8. Balasubramanyam, M., R. Sampathkumar and V. Mohan (2005). "Is insulin signaling molecules misguided in diabetes for ubiquitin-proteasome mediated degradation?" Mol Cell Biochem **275**(1-2): 117-125.
9. Bankaitis, V. A. (2015). "Unsaturated fatty acid-induced non-canonical autophagy: unusual? Or unappreciated?" EMBO J **34**(8): 978-980.
10. Bao, J., L. Zheng, Q. Zhang, X. Li, X. Zhang, Z. Li, X. Bai, Z. Zhang, W. Huo, X. Zhao, S. Shang, Q. Wang, C. Zhang and J. Ji (2016). "Deacetylation of TFEB promotes fibrillar Abeta degradation by upregulating lysosomal biogenesis in microglia." Protein Cell **7**(6): 417-433.

11. Barlow, J. and C. Affourtit (2013). "Novel insights into pancreatic beta-cell glucolipotoxicity from real-time functional analysis of mitochondrial energy metabolism in INS-1E insulinoma cells." Biochem J **456**(3): 417-426.
12. Barth, S., D. Glick and K. F. Macleod (2010). "Autophagy: assays and artifacts." J Pathol **221**(2): 117-124.
13. Basu, R., G. Y. Oudit, X. Wang, L. Zhang, J. R. Ussher, G. D. Lopaschuk and Z. Kassiri (2009). "Type 1 diabetic cardiomyopathy in the Akita (Ins2WT/C96Y) mouse model is characterized by lipotoxicity and diastolic dysfunction with preserved systolic function." Am J Physiol Heart Circ Physiol **297**(6): H2096-2108.
14. Bellot, G., R. Garcia-Medina, P. Gounon, J. Chiche, D. Roux, J. Pouyssegur and N. M. Mazure (2009). "Hypoxia-induced autophagy is mediated through hypoxia-inducible factor induction of BNIP3 and BNIP3L via their BH3 domains." Mol Cell Biol **29**(10): 2570-2581.
15. Benbrook, D. M. and A. Long (2012). "Integration of autophagy, proteasomal degradation, unfolded protein response and apoptosis." Exp Oncol **34**(3): 286-297.
16. Bertrand, L., S. Horman, C. Beauloye and J. L. Vanoverschelde (2008). "Insulin signalling in the heart." Cardiovasc Res **79**(2): 238-248.
17. Bjorkoy, G., T. Lamark, A. Brech, H. Outzen, M. Perander, A. Overvatn, H. Stenmark and T. Johansen (2005). "p62/SQSTM1 forms protein aggregates degraded by autophagy and has a protective effect on huntingtin-induced cell death." J Cell Biol **171**(4): 603-614.
18. Blagosklonny, M. V. (2013). "TOR-centric view on insulin resistance and diabetic complications: perspective for endocrinologists and gerontologists." Cell Death Dis **4**: e964.
19. Borradaile, N. M., X. Han, J. D. Harp, S. E. Gale, D. S. Ory and J. E. Schaffer (2006). "Disruption of endoplasmic reticulum structure and integrity in lipotoxic cell death." J Lipid Res **47**(12): 2726-2737.
20. Boudina, S. and E. D. Abel (2010). "Diabetic cardiomyopathy, causes and effects." Rev Endocr Metab Disord **11**(1): 31-39.

21. Brindley, D. N., B. P. Kok, P. C. Kienesberger, R. Lehner and J. R. Dyck (2010). "Shedding light on the enigma of myocardial lipotoxicity: the involvement of known and putative regulators of fatty acid storage and mobilization." Am J Physiol Endocrinol Metab **298**(5): E897-908.
22. Brownsey, R. W., A. N. Boone, J. E. Elliott, J. E. Kulpa and W. M. Lee (2006). "Regulation of acetyl-CoA carboxylase." Biochem Soc Trans **34**(Pt 2): 223-227.
23. Buchanan, J., P. K. Mazumder, P. Hu, G. Chakrabarti, M. W. Roberts, U. J. Yun, R. C. Cooksey, S. E. Litwin and E. D. Abel (2005). "Reduced cardiac efficiency and altered substrate metabolism precedes the onset of hyperglycemia and contractile dysfunction in two mouse models of insulin resistance and obesity." Endocrinology **146**(12): 5341-5349.
24. Bugger, H. and E. D. Abel (2009). "Rodent models of diabetic cardiomyopathy." Dis Model Mech **2**(9-10): 454-466.
25. Cai, L. and Y. J. Kang (2001). "Oxidative stress and diabetic cardiomyopathy: a brief review." Cardiovasc Toxicol **1**(3): 181-193.
26. Cai, L., W. Li, G. Wang, L. Guo, Y. Jiang and Y. J. Kang (2002). "Hyperglycemia-induced apoptosis in mouse myocardium: mitochondrial cytochrome C-mediated caspase-3 activation pathway." Diabetes **51**(6): 1938-1948.
27. Carr, C. S. and P. A. Sharp (1990). "A helix-loop-helix protein related to the immunoglobulin E box-binding proteins." Mol Cell Biol **10**(8): 4384-4388.
28. Carroll, R., A. N. Carley, J. R. Dyck and D. L. Severson (2005). "Metabolic effects of insulin on cardiomyocytes from control and diabetic db/db mouse hearts." Am J Physiol Endocrinol Metab **288**(5): E900-906.
29. Cerf, M. E. (2013). "Beta cell dysfunction and insulin resistance." Front Endocrinol (Lausanne) **4**: 37.
30. Chauhan, S., J. G. Goodwin, S. Chauhan, G. Manyam, J. Wang, A. M. Kamat and D. D. Boyd (2013). "ZKSCAN3 is a master transcriptional repressor of autophagy." Mol Cell **50**(1): 16-28.
31. Cheng, X. W., G. P. Shi, M. Kuzuya, T. Sasaki, K. Okumura and T. Murohara (2012). "Role for cysteine protease cathepsins in heart disease: focus on biology and mechanisms with clinical implication." Circulation **125**(12): 1551-1562.

32. Choi, A. M., S. W. Ryter and B. Levine (2013). "Autophagy in human health and disease." N Engl J Med **368**(19): 1845-1846.
33. Cnop, M., N. Welsh, J. C. Jonas, A. Jorns, S. Lenzen and D. L. Eizirik (2005). "Mechanisms of pancreatic beta-cell death in type 1 and type 2 diabetes: many differences, few similarities." Diabetes **54 Suppl 2**: S97-107.
34. Costes, S., C. J. Huang, T. Gurlo, M. Daval, A. V. Matveyenko, R. A. Rizza, A. E. Butler and P. C. Butler (2011). "beta-cell dysfunctional ERAD/ubiquitin/proteasome system in type 2 diabetes mediated by islet amyloid polypeptide-induced UCH-L1 deficiency." Diabetes **60**(1): 227-238.
35. Cuervo, A. M. (2004). "Autophagy: in sickness and in health." Trends Cell Biol **14**(2): 70-77.
36. Cuervo, A. M. and J. F. Dice (2000). "Unique properties of lamp2a compared to other lamp2 isoforms." J Cell Sci **113 Pt 24**: 4441-4450.
37. Cui, M., H. Yu, J. Wang, J. Gao and J. Li (2013). "Chronic caloric restriction and exercise improve metabolic conditions of dietary-induced obese mice in autophagy correlated manner without involving AMPK." J Diabetes Res **2013**: 852754.
38. Czaja, M. J. (2010). "Autophagy in health and disease. 2. Regulation of lipid metabolism and storage by autophagy: pathophysiological implications." Am J Physiol Cell Physiol **298**(5): C973-978.
39. De Duve, C. (1958). "[Lysosomes]." Bull Acad R Med Belg **23**(8): 608-618.
40. de Simone, G., R. B. Devereux, M. Chinali, E. T. Lee, J. M. Galloway, A. Barac, J. A. Panza and B. V. Howard (2010). "Diabetes and incident heart failure in hypertensive and normotensive participants of the Strong Heart Study." J Hypertens **28**(2): 353-360.
41. de Vries, J. E., M. M. Vork, T. H. Roemen, Y. F. de Jong, J. P. Cleutjens, G. J. van der Vusse and M. van Bilsen (1997). "Saturated but not mono-unsaturated fatty acids induce apoptotic cell death in neonatal rat ventricular myocytes." J Lipid Res **38**(7): 1384-1394.

42. Decressac, M., B. Mattsson, P. Weikop, M. Lundblad, J. Jakobsson and A. Bjorklund (2013). "TFEB-mediated autophagy rescues midbrain dopamine neurons from alpha-synuclein toxicity." Proc Natl Acad Sci U S A **110**(19): E1817-1826.
43. Despa, S., K. B. Margulies, L. Chen, A. A. Knowlton, P. J. Havel, H. Taegtmeyer, D. M. Bers and F. Despa (2012). "Hyperamylinemia contributes to cardiac dysfunction in obesity and diabetes: a study in humans and rats." Circ Res **110**(4): 598-608.
44. Donthi, R. V., G. Ye, C. Wu, D. A. McClain, A. J. Lange and P. N. Epstein (2004). "Cardiac expression of kinase-deficient 6-phosphofructo-2-kinase/fructose-2,6-bisphosphatase inhibits glycolysis, promotes hypertrophy, impairs myocyte function, and reduces insulin sensitivity." J Biol Chem **279**(46): 48085-48090.
45. Du Bois, P., C. Pablo Tortola, D. Lodka, M. Kny, F. Schmidt, K. Song, S. Schmidt, R. Bassel-Duby, E. N. Olson and J. Fielitz (2015). "Angiotensin II Induces Skeletal Muscle Atrophy by Activating TFEB-Mediated MuRF1 Expression." Circ Res **117**(5): 424-436.
46. Du, X., T. Matsumura, D. Edelstein, L. Rossetti, Z. Zsengeller, C. Szabo and M. Brownlee (2003). "Inhibition of GAPDH activity by poly(ADP-ribose) polymerase activates three major pathways of hyperglycemic damage in endothelial cells." J Clin Invest **112**(7): 1049-1057.
47. Eguchi, K. and I. Manabe (2014). "Toll-like receptor, lipotoxicity and chronic inflammation: the pathological link between obesity and cardiometabolic disease." J Atheroscler Thromb **21**(7): 629-639.
48. Eskelinen, E. L. (2006). "Roles of LAMP-1 and LAMP-2 in lysosome biogenesis and autophagy." Mol Aspects Med **27**(5-6): 495-502.
49. Eskelinen, E. L., A. L. Illert, Y. Tanaka, G. Schwarzmann, J. Blanz, K. Von Figura and P. Saftig (2002). "Role of LAMP-2 in lysosome biogenesis and autophagy." Mol Biol Cell **13**(9): 3355-3368.
50. Eskelinen, E. L. and P. Saftig (2009). "Autophagy: a lysosomal degradation pathway with a central role in health and disease." Biochim Biophys Acta **1793**(4): 664-673.

51. Finck, B. N., X. Han, M. Courtois, F. Aimond, J. M. Nerbonne, A. Kovacs, R. W. Gross and D. P. Kelly (2003). "A critical role for PPARalpha-mediated lipotoxicity in the pathogenesis of diabetic cardiomyopathy: modulation by dietary fat content." Proc Natl Acad Sci U S A **100**(3): 1226-1231.
52. Frojdo, S., H. Vidal and L. Pirola (2009). "Alterations of insulin signaling in type 2 diabetes: a review of the current evidence from humans." Biochim Biophys Acta **1792**(2): 83-92.
53. Gavaghan, M. (1998). "Cardiac anatomy and physiology: a review." AORN J **67**(4): 802-822; quiz 824-808.
54. Ghosh, S., D. An, T. Pulinilkunnil, D. Qi, H. C. Lau, A. Abrahani, S. M. Innis and B. Rodrigues (2004). "Role of dietary fatty acids and acute hyperglycemia in modulating cardiac cell death." Nutrition **20**(10): 916-923.
55. Ghosh, S., T. Pulinilkunnil, G. Yuen, G. Kewalramani, D. An, D. Qi, A. Abrahani and B. Rodrigues (2005). "Cardiomyocyte apoptosis induced by short-term diabetes requires mitochondrial GSH depletion." Am J Physiol Heart Circ Physiol **289**(2): H768-776.
56. Ginion, A., J. Auquier, C. R. Benton, C. Mouton, J. L. Vanoverschelde, L. Hue, S. Horman, C. Beauloye and L. Bertrand (2011). "Inhibition of the mTOR/p70S6K pathway is not involved in the insulin-sensitizing effect of AMPK on cardiac glucose uptake." Am J Physiol Heart Circ Physiol **301**(2): H469-477.
57. Godar, R. J., X. Ma, H. Liu, J. T. Murphy, C. J. Weinheimer, A. Kovacs, S. D. Crosby, P. Saftig and A. Diwan (2015). "Repetitive stimulation of autophagy-lysosome machinery by intermittent fasting preconditions the myocardium to ischemia-reperfusion injury." Autophagy **11**(9): 1537-1560.
58. Goldberg, A. L. (2003). "Protein degradation and protection against misfolded or damaged proteins." Nature **426**(6968): 895-899.
59. Groenendyk, J., P. K. Sreenivasaiah, H. Kim do, L. B. Agellon and M. Michalak (2010). "Biology of endoplasmic reticulum stress in the heart." Circ Res **107**(10): 1185-1197.

60. Guan, J., S. Mishra, Y. Qiu, J. Shi, K. Trudeau, G. Las, M. Liesa, O. S. Shirihai, L. H. Connors, D. C. Seldin, R. H. Falk, C. A. MacRae and R. Liao (2014). "Lysosomal dysfunction and impaired autophagy underlie the pathogenesis of amyloidogenic light chain-mediated cardiotoxicity." EMBO Mol Med **6**(11): 1493-1507.
61. Guan, J., S. Mishra, Y. Qiu, J. Shi, K. Trudeau, G. Las, M. Liesa, O. S. Shirihai, L. H. Connors, D. C. Seldin, R. H. Falk, C. A. MacRae and R. Liao (2015). "Lysosomal dysfunction and impaired autophagy underlie the pathogenesis of amyloidogenic light chain-mediated cardiotoxicity." EMBO Mol Med **7**(5): 688.
62. Guo, R., Y. Zhang, S. Turdi and J. Ren (2013). "Adiponectin knockout accentuates high fat diet-induced obesity and cardiac dysfunction: role of autophagy." Biochim Biophys Acta **1832**(8): 1136-1148.
63. Hippisley-Cox, J. and C. Coupland (2016). "Diabetes treatments and risk of heart failure, cardiovascular disease, and all cause mortality: cohort study in primary care." BMJ **354**: i3477.
64. Isfort, M., S. C. Stevens, S. Schaffer, C. J. Jong and L. E. Wold (2014). "Metabolic dysfunction in diabetic cardiomyopathy." Heart Fail Rev **19**(1): 35-48.
65. Jaacks, L. M., K. R. Siegel, U. P. Gujral and K. M. Narayan (2016). "Type 2 diabetes: A 21st century epidemic." Best Pract Res Clin Endocrinol Metab **30**(3): 331-343.
66. Jaishy, B., Q. Zhang, H. S. Chung, C. Riehle, J. Soto, S. Jenkins, P. Abel, L. A. Cowart, J. E. Van Eyk and E. D. Abel (2015). "Lipid-induced NOX2 activation inhibits autophagic flux by impairing lysosomal enzyme activity." J Lipid Res **56**(3): 546-561.
67. Jiang, T., B. Harder, M. Rojo de la Vega, P. K. Wong, E. Chapman and D. D. Zhang (2015). "p62 links autophagy and Nrf2 signaling." Free Radic Biol Med **88**(Pt B): 199-204.
68. Jin, S. M. and R. J. Youle (2012). "PINK1- and Parkin-mediated mitophagy at a glance." J Cell Sci **125**(Pt 4): 795-799.
69. Jung, C. H., C. B. Jun, S. H. Ro, Y. M. Kim, N. M. Otto, J. Cao, M. Kundu and D. H. Kim (2009). "ULK-Atg13-FIP200 complexes mediate mTOR signaling to the autophagy machinery." Mol Biol Cell **20**(7): 1992-2003.

70. Kanamori, H., G. Takemura, K. Goto, A. Tsujimoto, A. Mikami, A. Ogino, T. Watanabe, K. Morishita, H. Okada, M. Kawasaki, M. Seishima and S. Minatoguchi (2015). "Autophagic adaptations in diabetic cardiomyopathy differ between type 1 and type 2 diabetes." Autophagy **11**(7): 1146-1160.
71. Kannel, W. B., M. Hjortland and W. P. Castelli (1974). "Role of diabetes in congestive heart failure: the Framingham study." Am J Cardiol **34**(1): 29-34.
72. Karunakaran, U., H. J. Kim, J. Y. Kim and I. K. Lee (2012). "Guards and culprits in the endoplasmic reticulum: glucolipotoxicity and beta-cell failure in type II diabetes." Exp Diabetes Res **2012**: 639762.
73. Kaushik, S. and A. M. Cuervo (2012). "Chaperone-mediated autophagy: a unique way to enter the lysosome world." Trends Cell Biol **22**(8): 407-417.
74. Kaushik, S. and A. M. Cuervo (2012). "Chaperones in autophagy." Pharmacol Res **66**(6): 484-493.
75. Kienesberger, P. C., T. Pulinilkunnil, J. Nagendran and J. R. Dyck (2013). "Myocardial triacylglycerol metabolism." J Mol Cell Cardiol **55**: 101-110.
76. Kim, J., M. Kundu, B. Viollet and K. L. Guan (2011). "AMPK and mTOR regulate autophagy through direct phosphorylation of Ulk1." Nat Cell Biol **13**(2): 132-141.
77. Kim, J. W. and K. H. Yoon (2011). "Glucolipotoxicity in Pancreatic beta-Cells." Diabetes Metab J **35**(5): 444-450.
78. Koga, H., S. Kaushik and A. M. Cuervo (2010). "Altered lipid content inhibits autophagic vesicular fusion." FASEB J **24**(8): 3052-3065.
79. Kolb, R., F. S. Sutterwala and W. Zhang (2016). "Obesity and cancer: inflammation bridges the two." Curr Opin Pharmacol **29**: 77-89.
80. Kuma, A., M. Hatano, M. Matsui, A. Yamamoto, H. Nakaya, T. Yoshimori, Y. Ohsumi, T. Tokuhisa and N. Mizushima (2004). "The role of autophagy during the early neonatal starvation period." Nature **432**(7020): 1032-1036.
81. Kwak, S. J., C. S. Kim, M. S. Choi, T. Park, M. K. Sung, J. W. Yun, H. Yoo, Y. Mine and R. Yu (2016). "The Soy Peptide Phe-Leu-Val Reduces TNFalpha-Induced Inflammatory Response and Insulin Resistance in Adipocytes." J Med Food **19**(7): 678-685.

82. Larsen, T. S. and E. Aasum (2008). "Metabolic (in)flexibility of the diabetic heart." Cardiovasc Drugs Ther **22**(2): 91-95.
83. Las, G., S. B. Serada, J. D. Wikstrom, G. Twig and O. S. Shirihai (2011). "Fatty acids suppress autophagic turnover in beta-cells." J Biol Chem **286**(49): 42534-42544.
84. Lecker, S. H., A. L. Goldberg and W. E. Mitch (2006). "Protein degradation by the ubiquitin-proteasome pathway in normal and disease states." J Am Soc Nephrol **17**(7): 1807-1819.
85. Lee, F. N., L. Zhang, D. Zheng, W. S. Choi and J. H. Youn (2004). "Insulin suppresses PDK-4 expression in skeletal muscle independently of plasma FFA." Am J Physiol Endocrinol Metab **287**(1): E69-74.
86. Lee, W. S. and J. Kim (2015). "Peroxisome Proliferator-Activated Receptors and the Heart: Lessons from the Past and Future Directions." PPAR Res **2015**: 271983.
87. Li, Z. L., J. R. Woollard, B. Ebrahimi, J. A. Crane, K. L. Jordan, A. Lerman, S. M. Wang and L. O. Lerman (2012). "Transition from obesity to metabolic syndrome is associated with altered myocardial autophagy and apoptosis." Arterioscler Thromb Vasc Biol **32**(5): 1132-1141.
88. Listenberger, L. L., X. Han, S. E. Lewis, S. Cases, R. V. Farese, Jr., D. S. Ory and J. E. Schaffer (2003). "Triglyceride accumulation protects against fatty acid-induced lipotoxicity." Proc Natl Acad Sci U S A **100**(6): 3077-3082.
89. Liu, M. and S. C. Dudley, Jr. (2014). "Targeting the unfolded protein response in heart diseases." Expert Opin Ther Targets **18**(7): 719-723.
90. Lopaschuk, G. D., J. R. Ussher, C. D. Folmes, J. S. Jaswal and W. C. Stanley (2010). "Myocardial fatty acid metabolism in health and disease." Physiol Rev **90**(1): 207-258.
91. Luzio, J. P., S. R. Gray and N. A. Bright (2010). "Endosome-lysosome fusion." Biochem Soc Trans **38**(6): 1413-1416.
92. Ma, X., H. Liu, S. R. Foyil, R. J. Godar, C. J. Weinheimer, J. A. Hill and A. Diwan (2012). "Impaired autophagosome clearance contributes to cardiomyocyte death in ischemia/reperfusion injury." Circulation **125**(25): 3170-3181.

93. Ma, X., H. Liu, J. T. Murphy, S. R. Foyil, R. J. Godar, H. Abuirqeba, C. J. Weinheimer, P. M. Barger and A. Diwan (2015). "Regulation of the transcription factor EB-PGC1alpha axis by beclin-1 controls mitochondrial quality and cardiomyocyte death under stress." Mol Cell Biol **35**(6): 956-976.
94. Markou, T., T. E. Cullingford, A. Giraldo, S. C. Weiss, A. Alsafi, S. J. Fuller, A. Clerk and P. H. Sugden (2008). "Glycogen synthase kinases 3alpha and 3beta in cardiac myocytes: regulation and consequences of their inhibition." Cell Signal **20**(1): 206-218.
95. Martina, J. A., Y. Chen, M. Gucek and R. Puertollano (2012). "MTORC1 functions as a transcriptional regulator of autophagy by preventing nuclear transport of TFEB." Autophagy **8**(6): 903-914.
96. Martina, J. A., H. I. Diab, H. Li and R. Puertollano (2014). "Novel roles for the MiTF/TFE family of transcription factors in organelle biogenesis, nutrient sensing, and energy homeostasis." Cell Mol Life Sci **71**(13): 2483-2497.
97. Martini-Stoica, H., Y. Xu, A. Ballabio and H. Zheng (2016). "The Autophagy-Lysosomal Pathway in Neurodegeneration: A TFEB Perspective." Trends Neurosci **39**(4): 221-234.
98. Mashek, D. G., L. O. Li and R. A. Coleman (2007). "Long-chain acyl-CoA synthetases and fatty acid channeling." Future Lipidol **2**(4): 465-476.
99. Massey, A. C., S. Kaushik, G. Sovak, R. Kiffin and A. M. Cuervo (2006). "Consequences of the selective blockage of chaperone-mediated autophagy." Proc Natl Acad Sci U S A **103**(15): 5805-5810.
100. Medina, D. L. and A. Ballabio (2015). "Lysosomal calcium regulates autophagy." Autophagy **11**(6): 970-971.
101. Medina, D. L., S. Di Paola, I. Peluso, A. Armani, D. De Stefani, R. Venditti, S. Montefusco, A. Scotto-Rosato, C. Prezioso, A. Forrester, C. Settembre, W. Wang, Q. Gao, H. Xu, M. Sandri, R. Rizzuto, M. A. De Matteis and A. Ballabio (2015). "Lysosomal calcium signalling regulates autophagy through calcineurin and TFEB." Nat Cell Biol **17**(3): 288-299.

102. Mellor, K. M., J. R. Bell, M. J. Young, R. H. Ritchie and L. M. Delbridge (2011). "Myocardial autophagy activation and suppressed survival signaling is associated with insulin resistance in fructose-fed mice." J Mol Cell Cardiol **50**(6): 1035-1043.
103. Miki, T., S. Yuda, H. Kouzu and T. Miura (2013). "Diabetic cardiomyopathy: pathophysiology and clinical features." Heart Fail Rev **18**(2): 149-166.
104. Mindell, J. A. (2012). "Lysosomal acidification mechanisms." Annu Rev Physiol **74**: 69-86.
105. Mizushima, N. (2009). "Physiological functions of autophagy." Curr Top Microbiol Immunol **335**: 71-84.
106. Mizushima, N. and D. J. Klionsky (2007). "Protein turnover via autophagy: implications for metabolism." Annu Rev Nutr **27**: 19-40.
107. Mizushima, N., B. Levine, A. M. Cuervo and D. J. Klionsky (2008). "Autophagy fights disease through cellular self-digestion." Nature **451**(7182): 1069-1075.
108. Mony, V. K., S. Benjamin and E. J. O'Rourke (2016). "A lysosome-centered view of nutrient homeostasis." Autophagy **12**(4): 619-631.
109. Moyzis, A. G., J. Sadoshima and A. B. Gustafsson (2015). "Mending a broken heart: the role of mitophagy in cardioprotection." Am J Physiol Heart Circ Physiol **308**(3): H183-192.
110. Muoio, D. M. (2014). "Metabolic inflexibility: when mitochondrial indecision leads to metabolic gridlock." Cell **159**(6): 1253-1262.
111. Must, A. and N. M. McKeown (2000). The Disease Burden Associated with Overweight and Obesity. Endotext. L. J. De Groot, P. Beck-Peccoz, G. Chrousos et al. South Dartmouth (MA).
112. Nakatogawa, H. and K. Mochida (2015). "Reticulophagy and nucleophagy: New findings and unsolved issues." Autophagy **11**(12): 2377-2378.
113. Ni, Y., L. Zhao, H. Yu, X. Ma, Y. Bao, C. Rajani, L. W. Loo, Y. B. Shvetsov, H. Yu, T. Chen, Y. Zhang, C. Wang, C. Hu, M. Su, G. Xie, A. Zhao, W. Jia and W. Jia (2015). "Circulating Unsaturated Fatty Acids Delineate the Metabolic Status of Obese Individuals." EBioMedicine **2**(10): 1513-1522.

114. Nishino, I., J. Fu, K. Tanji, T. Yamada, S. Shimojo, T. Koori, M. Mora, J. E. Riggs, S. J. Oh, Y. Koga, C. M. Sue, A. Yamamoto, N. Murakami, S. Shanske, E. Byrne, E. Bonilla, I. Nonaka, S. DiMauro and M. Hirano (2000). "Primary LAMP-2 deficiency causes X-linked vacuolar cardiomyopathy and myopathy (Danon disease)." Nature **406**(6798): 906-910.

115. Obacz, J., S. Pastorekova, B. Vojtesek and R. Hrstka (2013). "Cross-talk between HIF and p53 as mediators of molecular responses to physiological and genotoxic stresses." Mol Cancer **12**(1): 93.

116. Oku, M. and Y. Sakai (2010). "Peroxisomes as dynamic organelles: autophagic degradation." FEBS J **277**(16): 3289-3294.

117. Orenstein, S. J. and A. M. Cuervo (2010). "Chaperone-mediated autophagy: molecular mechanisms and physiological relevance." Semin Cell Dev Biol **21**(7): 719-726.

118. Orrenius, S., B. Zhivotovsky and P. Nicotera (2003). "Regulation of cell death: the calcium-apoptosis link." Nat Rev Mol Cell Biol **4**(7): 552-565.

119. Pagan, J., T. Seto, M. Pagano and A. Cittadini (2013). "Role of the ubiquitin proteasome system in the heart." Circ Res **112**(7): 1046-1058.

120. Pagano, M., S. Naviglio, A. Spina, E. Chiosi, G. Castoria, M. Romano, A. Sorrentino, F. Illiano and G. Illiano (2004). "Differentiation of H9c2 cardiomyoblasts: The role of adenylate cyclase system." J Cell Physiol **198**(3): 408-416.

121. Palmieri, M., S. Impey, H. Kang, A. di Ronza, C. Pelz, M. Sardiello and A. Ballabio (2011). "Characterization of the CLEAR network reveals an integrated control of cellular clearance pathways." Hum Mol Genet **20**(19): 3852-3866.

122. Parameswaran, S., S. Kumar, R. S. Verma and R. K. Sharma (2013). "Cardiomyocyte culture - an update on the in vitro cardiovascular model and future challenges." Can J Physiol Pharmacol **91**(12): 985-998.

123. Patterson, C., A. L. Portbury, J. C. Schisler and M. S. Willis (2011). "Tear me down: role of calpain in the development of cardiac ventricular hypertrophy." Circ Res **109**(4): 453-462.

124. Pepin, J. L., J. F. Timsit, R. Tamisier, J. C. Borel, P. Levy and S. Jaber (2016). "Prevention and care of respiratory failure in obese patients." Lancet Respir Med **4**(5): 407-418.

125. Petit, C. S., A. Roczniak-Ferguson and S. M. Ferguson (2013). "Recruitment of folliculin to lysosomes supports the amino acid-dependent activation of Rag GTPases." J Cell Biol **202**(7): 1107-1122.

126. Platt, F. M., B. Boland and A. C. van der Spoel (2012). "The cell biology of disease: lysosomal storage disorders: the cellular impact of lysosomal dysfunction." J Cell Biol **199**(5): 723-734.

127. Pociot, F. and A. Lernmark (2016). "Genetic risk factors for type 1 diabetes." Lancet **387**(10035): 2331-2339.

128. Poornima, I. G., P. Parikh and R. P. Shannon (2006). "Diabetic cardiomyopathy: the search for a unifying hypothesis." Circ Res **98**(5): 596-605.

129. Powell, S. R., J. Herrmann, A. Lerman, C. Patterson and X. Wang (2012). "The ubiquitin-proteasome system and cardiovascular disease." Prog Mol Biol Transl Sci **109**: 295-346.

130. Prause, M., D. P. Christensen, N. Billestrup and T. Mandrup-Poulsen (2014). "JNK1 protects against glucolipotoxicity-mediated beta-cell apoptosis." PLoS One **9**(1): e87067.

131. Pulinilkunnil, T., D. An, P. Yip, N. Chan, D. Qi, S. Ghosh, A. Abrahani and B. Rodrigues (2004). "Palmitoyl lysophosphatidylcholine mediated mobilization of LPL to the coronary luminal surface requires PKC activation." J Mol Cell Cardiol **37**(5): 931-938.

132. Pulinilkunnil, T., P. C. Kienesberger, J. Nagendran, N. Sharma, M. E. Young and J. R. Dyck (2014). "Cardiac-specific adipose triglyceride lipase overexpression protects from cardiac steatosis and dilated cardiomyopathy following diet-induced obesity." Int J Obes (Lond) **38**(2): 205-215.

133. Pulinilkunnil, T., P. C. Kienesberger, J. Nagendran, T. J. Waller, M. E. Young, E. E. Kershaw, G. Korbutt, G. Haemmerle, R. Zechner and J. R. Dyck (2013). "Myocardial adipose triglyceride lipase overexpression protects diabetic mice from the development of lipotoxic cardiomyopathy." Diabetes **62**(5): 1464-1477.

134. Pulinilkunnil, T. and B. Rodrigues (2006). "Cardiac lipoprotein lipase: metabolic basis for diabetic heart disease." Cardiovasc Res **69**(2): 329-340.

135. Raben, N. and R. Puertollano (2016). "TFEB and TFE3: Linking Lysosomes to Cellular Adaptation to Stress." Annu Rev Cell Dev Biol.

136. Randle, P. J. (1980). "The biochemical basis of the relation between glucose and fatty acid metabolism." Acta Chir Scand Suppl **498**: 111-114.

137. Rebsamen, M., L. Pochini, T. Stasyk, M. E. de Araujo, M. Galluccio, R. K. Kandasamy, B. Snijder, A. Fauster, E. L. Rudashevskaya, M. Bruckner, S. Scorzoni, P. A. Filipek, K. V. Huber, J. W. Bigenzahn, L. X. Heinz, C. Kraft, K. L. Bennett, C. Indiveri, L. A. Huber and G. Superti-Furga (2015). "SLC38A9 is a component of the lysosomal amino acid sensing machinery that controls mTORC1." Nature **519**(7544): 477-481.

138. Rega, L. R., E. Polishchuk, S. Montefusco, G. Napolitano, G. Tozzi, J. Zhang, F. Bellomo, A. Taranta, A. Pastore, R. Polishchuk, F. Piemonte, D. L. Medina, S. D. Catz, A. Ballabio and F. Emma (2016). "Activation of the transcription factor EB rescues lysosomal abnormalities in cystinotic kidney cells." Kidney Int **89**(4): 862-873.

139. Rodrigues, B., M. C. Cam and J. H. McNeill (1995). "Myocardial substrate metabolism: implications for diabetic cardiomyopathy." J Mol Cell Cardiol **27**(1): 169-179.

140. Rodriguez-Navarro, J. A., S. Kaushik, H. Koga, C. Dall'Armi, G. Shui, M. R. Wenk, G. Di Paolo and A. M. Cuervo (2012). "Inhibitory effect of dietary lipids on chaperone-mediated autophagy." Proc Natl Acad Sci U S A **109**(12): E705-714.

141. Rubler, S., J. Dlugash, Y. Z. Yuceoglu, T. Kumral, A. W. Branwood and A. Grishman (1972). "New type of cardiomyopathy associated with diabetic glomerulosclerosis." Am J Cardiol **30**(6): 595-602.

142. Saftig, P., B. Schroder and J. Blanz (2010). "Lysosomal membrane proteins: life between acid and neutral conditions." Biochem Soc Trans **38**(6): 1420-1423.

143. Saito, T. and J. Sadoshima (2015). "Molecular mechanisms of mitochondrial autophagy/mitophagy in the heart." Circ Res **116**(8): 1477-1490.

144. Samovski, D., X. Su, Y. Xu, N. A. Abumrad and P. D. Stahl (2012). "Insulin and AMPK regulate FA translocase/CD36 plasma membrane recruitment in cardiomyocytes via Rab GAP AS160 and Rab8a Rab GTPase." J Lipid Res **53**(4): 709-717.

145. Sano, R. and J. C. Reed (2013). "ER stress-induced cell death mechanisms." Biochim Biophys Acta **1833**(12): 3460-3470.

146. Sardiello, M. (2016). "Transcription factor EB: from master coordinator of lysosomal pathways to candidate therapeutic target in degenerative storage diseases." Ann N Y Acad Sci **1371**(1): 3-14.

147. Sardiello, M., M. Palmieri, A. di Ronza, D. L. Medina, M. Valenza, V. A. Gennarino, C. Di Malta, F. Donaudy, V. Embrione, R. S. Polishchuk, S. Banfi, G. Parenti, E. Cattaneo and A. Ballabio (2009). "A gene network regulating lysosomal biogenesis and function." Science **325**(5939): 473-477.

148. Schilling, J. D., H. M. Machkovech, L. He, A. Diwan and J. E. Schaffer (2013). "TLR4 activation under lipotoxic conditions leads to synergistic macrophage cell death through a TRIF-dependent pathway." J Immunol **190**(3): 1285-1296.

149. Schneider, J. L., Y. Suh and A. M. Cuervo (2014). "Deficient chaperone-mediated autophagy in liver leads to metabolic dysregulation." Cell Metab **20**(3): 417-432.

150. Schneider, J. L., J. Villarroya, A. Diaz-Carretero, B. Patel, A. M. Urbanska, M. M. Thi, F. Villarroya, L. Santambrogio and A. M. Cuervo (2015). "Loss of hepatic chaperone-mediated autophagy accelerates proteostasis failure in aging." Aging Cell **14**(2): 249-264.

151. Settembre, C. and A. Ballabio (2011). "TFEB regulates autophagy: an integrated coordination of cellular degradation and recycling processes." Autophagy **7**(11): 1379-1381.

152. Settembre, C. and A. Ballabio (2014). "Lysosome: regulator of lipid degradation pathways." Trends Cell Biol **24**(12): 743-750.

153. Settembre, C., C. Di Malta, V. A. Polito, M. Garcia Arencibia, F. Vetrini, S. Erdin, S. U. Erdin, T. Huynh, D. Medina, P. Colella, M. Sardiello, D. C. Rubinsztein and A. Ballabio (2011). "TFEB links autophagy to lysosomal biogenesis." Science **332**(6036): 1429-1433.

154. Settembre, C., A. Fraldi, D. L. Medina and A. Ballabio (2013). "Signals from the lysosome: a control centre for cellular clearance and energy metabolism." Nat Rev Mol Cell Biol **14**(5): 283-296.

155. Settembre, C., R. Zoncu, D. L. Medina, F. Vetrini, S. Erdin, S. Erdin, T. Huynh, M. Ferron, G. Karsenty, M. C. Vellard, V. Facchinetti, D. M. Sabatini and A. Ballabio (2012). "A lysosome-to-nucleus signalling mechanism senses and regulates the lysosome via mTOR and TFEB." EMBO J **31**(5): 1095-1108.

156. Sharma, S., J. V. Adrogue, L. Golfman, I. Uray, J. Lemm, K. Youker, G. P. Noon, O. H. Frazier and H. Taegtmeyer (2004). "Intramyocardial lipid accumulation in the failing human heart resembles the lipotoxic rat heart." FASEB J **18**(14): 1692-1700.

157. Sharma, V. and J. H. McNeill (2006). "Diabetic cardiomyopathy: where are we 40 years later?" Can J Cardiol **22**(4): 305-308.

158. Shen, H. M. and N. Mizushima (2014). "At the end of the autophagic road: an emerging understanding of lysosomal functions in autophagy." Trends Biochem Sci **39**(2): 61-71.

159. Shindler, D. M., J. B. Kostis, S. Yusuf, M. A. Quinones, B. Pitt, D. Stewart, T. Pinkett, J. K. Ghali and A. C. Wilson (1996). "Diabetes mellitus, a predictor of morbidity and mortality in the Studies of Left Ventricular Dysfunction (SOLVD) Trials and Registry." Am J Cardiol **77**(11): 1017-1020.

160. Shulman, R. G., G. Bloch and D. L. Rothman (1995). "In vivo regulation of muscle glycogen synthase and the control of glycogen synthesis." Proc Natl Acad Sci U S A **92**(19): 8535-8542.

161. Singh, R. and A. M. Cuervo (2011). "Autophagy in the cellular energetic balance." Cell Metab **13**(5): 495-504.

162. Singh, R. and A. M. Cuervo (2012). "Lipophagy: connecting autophagy and lipid metabolism." Int J Cell Biol **2012**: 282041.

163. Stanley, W. C., F. A. Recchia and G. D. Lopaschuk (2005). "Myocardial substrate metabolism in the normal and failing heart." Physiol Rev **85**(3): 1093-1129.

164. Steinberg, G. R. and B. E. Kemp (2009). "AMPK in Health and Disease." Physiol Rev **89**(3): 1025-1078.

165. Stypmann, J., P. M. Janssen, J. Prestle, M. A. Engelen, H. Kogler, R. Lullmann-Rauch, L. Eckardt, K. von Figura, J. Landgrebe, A. Mleczko and P. Saftig (2006). "LAMP-2 deficient mice show depressed cardiac contractile function without significant changes in calcium handling." Basic Res Cardiol **101**(4): 281-291.

166. Sugimoto, S., K. Shiomi, A. Yamamoto, I. Nishino, I. Nonaka and T. Ohi (2007). "LAMP-2 positive vacuolar myopathy with dilated cardiomyopathy." Intern Med **46**(11): 757-760.

167. Tanida, I. (2011). "Autophagosome formation and molecular mechanism of autophagy." Antioxid Redox Signal **14**(11): 2201-2214.

168. Tong, M. and J. Sadoshima (2016). "Mitochondrial autophagy in cardiomyopathy." Curr Opin Genet Dev **38**: 8-15.

169. Tsuchiya, Y., M. Saito and K. Kohno (2016). "Pathogenic Mechanism of Diabetes Development Due to Dysfunction of Unfolded Protein Response." Yakugaku Zasshi **136**(6): 817-825.

170. Tsukamoto, O., T. Minamino, K. Okada, Y. Shintani, S. Takashima, H. Kato, Y. Liao, H. Okazaki, M. Asai, A. Hirata, M. Fujita, Y. Asano, S. Yamazaki, H. Asanuma, M. Hori and M. Kitakaze (2006). "Depression of proteasome activities during the progression of cardiac dysfunction in pressure-overloaded heart of mice." Biochem Biophys Res Commun **340**(4): 1125-1133.

171. Twells, L. K., D. M. Gregory, J. Reddigan and W. K. Midodzi (2014). "Current and predicted prevalence of obesity in Canada: a trend analysis." CMAJ Open **2**(1): E18-26.

172. van de Weijer, T., V. B. Schrauwen-Hinderling and P. Schrauwen (2011). "Lipotoxicity in type 2 diabetic cardiomyopathy." Cardiovasc Res **92**(1): 10-18.

173. van der Vusse, G. J., M. van Bilsen and J. F. Glatz (2000). "Cardiac fatty acid uptake and transport in health and disease." Cardiovasc Res **45**(2): 279-293.

174. Varga, T., Z. Czimmerer and L. Nagy (2011). "PPARs are a unique set of fatty acid regulated transcription factors controlling both lipid metabolism and inflammation." Biochim Biophys Acta **1812**(8): 1007-1022.

175. Varga, Z. V., Z. Giricz, L. Liaudet, G. Hasko, P. Ferdinandy and P. Pacher (2015). "Interplay of oxidative, nitrosative/nitrative stress, inflammation, cell death and autophagy in diabetic cardiomyopathy." Biochim Biophys Acta **1852**(2): 232-242.

176. Wakasaki, H., D. Koya, F. J. Schoen, M. R. Jirousek, D. K. Ways, B. D. Hoit, R. A. Walsh and G. L. King (1997). "Targeted overexpression of protein kinase C beta2 isoform in myocardium causes cardiomyopathy." Proc Natl Acad Sci U S A **94**(17): 9320-9325.

177. Weekes, J., K. Morrison, A. Mullen, R. Wait, P. Barton and M. J. Dunn (2003). "Hyperubiquitination of proteins in dilated cardiomyopathy." Proteomics **3**(2): 208-216.

178. Wende, A. R., J. D. Symons and E. D. Abel (2012). "Mechanisms of lipotoxicity in the cardiovascular system." Curr Hypertens Rep **14**(6): 517-531.

179. Willis, M. S. and C. Patterson (2013). "Proteotoxicity and cardiac dysfunction--Alzheimer's disease of the heart?" N Engl J Med **368**(5): 455-464.

180. Xie, Z., K. Lau, B. Eby, P. Lozano, C. He, B. Pennington, H. Li, S. Rathi, Y. Dong, R. Tian, D. Kem and M. H. Zou (2011). "Improvement of cardiac functions by chronic metformin treatment is associated with enhanced cardiac autophagy in diabetic OVE26 mice." Diabetes **60**(6): 1770-1778.

181. Xin, M., E. N. Olson and R. Bassel-Duby (2013). "Mending broken hearts: cardiac development as a basis for adult heart regeneration and repair." Nat Rev Mol Cell Biol **14**(8): 529-541.

182. Xu, H. and D. Ren (2015). "Lysosomal physiology." Annu Rev Physiol **77**: 57-80.

183. Xu, X., Y. Hua, S. Nair, Y. Zhang and J. Ren (2013). "Akt2 knockout preserves cardiac function in high-fat diet-induced obesity by rescuing cardiac autophagosome maturation." J Mol Cell Biol **5**(1): 61-63.

184. Yagyu, H., G. Chen, M. Yokoyama, K. Hirata, A. Augustus, Y. Kako, T. Seo, Y. Hu, E. P. Lutz, M. Merkel, A. Bensadoun, S. Homma and I. J. Goldberg (2003). "Lipoprotein lipase (LpL) on the surface of cardiomyocytes increases lipid uptake and produces a cardiomyopathy." J Clin Invest **111**(3): 419-426.

185. Yamada, E. and R. Singh (2012). "Mapping autophagy on to your metabolic radar." Diabetes **61**(2): 272-280.

186. Yang, J., S. Carra, W. G. Zhu and H. H. Kampinga (2013). "The regulation of the autophagic network and its implications for human disease." Int J Biol Sci **9**(10): 1121-1133.

187. Yang, L., P. Li, S. Fu, E. S. Calay and G. S. Hotamisligil (2010). "Defective hepatic autophagy in obesity promotes ER stress and causes insulin resistance." Cell Metab **11**(6): 467-478.

188. Yang, L., D. Zhao, J. Ren and J. Yang (2015). "Endoplasmic reticulum stress and protein quality control in diabetic cardiomyopathy." Biochim Biophys Acta **1852**(2): 209-218.

189. Yonekawa, T., G. Gamez, J. Kim, A. C. Tan, J. Thorburn, J. Gump, A. Thorburn and M. J. Morgan (2015). "RIP1 negatively regulates basal autophagic flux through TFEB to control sensitivity to apoptosis." EMBO Rep **16**(6): 700-708.

190. Young, M. E., P. H. Guthrie, P. Razeghi, B. Leighton, S. Abbasi, S. Patil, K. A. Youker and H. Taegtmeyer (2002). "Impaired long-chain fatty acid oxidation and contractile dysfunction in the obese Zucker rat heart." Diabetes **51**(8): 2587-2595.

191. Zechner, R., P. C. Kienesberger, G. Haemmerle, R. Zimmermann and A. Lass (2009). "Adipose triglyceride lipase and the lipolytic catabolism of cellular fat stores." J Lipid Res **50**(1): 3-21.

192. Zhang, Y., X. Xu and J. Ren (2013). "MTOR overactivation and interrupted autophagy flux in obese hearts: a dicey assembly?" Autophagy **9**(6): 939-941.